Uniwersytet
Jana Kochanowskiego
w Kielcach

JAN KOCHANOWSKI UNIVERSITY
DOCTORAL SCHOOL
FACULTY OF NATURAL SCIENCES
PHYSICAL SCIENCES

Arthur Vereijken

Phenomenology of Glueballs in Effective Hadronic Models

Doctoral dissertation written under the supervision of
prof. dr. hab. Francesco Giacosa and dr. Leonardo Tinti

January 2026, Kielce

This doctoral thesis was supported by the Polish National Science Centre (NCN) OPUS project No. 2019/33/B/ST2/00613. and the Polish National Science Centre NCN Grant SONATA project No. 2020/39/D/ST2/02054

Abstract

Because QCD is strongly coupled at low energies, standard perturbative techniques are no longer applicable at this energy scale. In this thesis, we use effective models that have hadronic degrees of freedom. The guiding principle throughout is the implementation of the global symmetries of QCD and their anomalous, explicit, and spontaneous breaking patterns, notably chiral symmetry and dilatation symmetry.

First, the theory of a free scalar field coupled to a time-independent classical source is studied as a simplified model for dilaton production in a medium. We show that the time evolution in the theory is non-trivial, contrary to historical expectations. The theory exhibits nonperturbative particle production similar to the Schwinger mechanism, with interesting features such as non-exponential decay and the quantum Zeno effect.

Next, we introduce the extended Linear Sigma Model (eLSM) and apply it to (axial) tensor mesons, the tensor glueball, and charmonium states mixing with the vector glueball.

We confirm the quark-antiquark assignment of the standard tensor meson nonet by fitting their decays to data. Using chiral symmetry, we derive predictions for the masses and decays of axial tensor mesons which can be tested by experiments. The axial tensor mesons are predicted to be very broad states.

The eLSM is used to calculate decay ratios of the tensor glueball. We then compare these to experimental data on known candidates for the tensor glueball. This comparison shows that the $f_2(1950)$ is the most likely tensor glueball candidate in this framework. A rough estimate of the decay widths also indicates that the tensor glueball could be a relatively broad state.

Finally, the decays of the charmonium states J/ψ and $\psi(3686)$ into vector–pseudoscalar final states are investigated. These channels exhibit significant violations of the perturbative QCD "13% rule", most prominently in the $\rho\pi$ channel. We apply the eLSM, including electromagnetic effects and mixing with the vector glueball. It is shown that these ingredients allow for a successful phenomenological description of the observed ratios $\mathcal{B}(\psi(3686) \to h)/\mathcal{B}(J/\psi \to h)$.

Streszczenie
Fenomenologia kuł gluonowych w efektywnych modelach hadronowych

Ponieważ QCD jest teorią silnie oddziałującą w reżimie niskich energii, standardowe techniki perturbacyjne nie znajdują w tym zakresie zastosowania. W niniejszej rozprawie wykorzystujemy modele efektywne, w których stopnie swobody mają charakter hadronowy. Zasadą przewodnią jest konsekwentna implementacja globalnych symetrii QCD oraz wzorców ich łamania – anomalnego, jawnego i spontanicznego – ze szczególnym uwzględnieniem symetrii chiralnej oraz dylatacyjnej.

W pierwszej części badana jest teoria swobodnego pola skalarnego oddziałującego z klasycznym, niezależnym od czasu źródłem, traktowana jako uproszczony model produkcji dylatonu w ośrodku. Pokazujemy, że ewolucja czasowa w tej teorii jest nietrywialna, wbrew wcześniejszym oczekiwaniom. Teoria wykazuje nieperturbacyjną produkcję cząstek, analogiczną do mechanizmu Schwingera, z interesującymi własnościami, takimi jak nieeksponencjalny rozpad oraz kwantowy efekt Zeno.

Następnie wprowadzamy extended Linear Sigma Model (eLSM) i stosujemy go do opisu mezonów (aksjalno-)tensorowych, tensorowej kuli gluonowej oraz stanów charmonium mieszających się z wektorową kulą gluonową. Potwierdzamy standardowe przypisanie mezonów tensorowych do nonetu kwark–antykwark poprzez dopasowanie ich szerokości rozpadów do danych doświadczalnych. Wykorzystując symetrię chiralną, wyprowadzamy przewidywania dotyczące mas oraz rozpadów mezonów aksjalno-tensorowych, które mogą zostać zweryfikowane eksperymentalnie. Przewiduje się, że mezony aksjalno-tensorowe są stanami bardzo szerokimi.

Model eLSM jest następnie wykorzystywany do obliczenia stosunków rozpadów tensorowej kuli gluonowej. Otrzymane wyniki porównujemy z danymi doświadczalnymi dotyczącymi znanych kandydatów na tensorową kulę gluonową. Porównanie to wskazuje, że rezonans $f_2(1950)$ jest w tych ramach teoretycznych najbardziej prawdopodobnym kandydatem na tensorową kulę gluonową. Przybliżone oszacowania szerokości rozpadu sugerują ponadto, że tensorowa kula gluonowa może być stanem relatywnie szerokim.

W końcowej części analizowane są rozpady stanów charmonium J/ψ oraz $\psi(3686)$ do stanów końcowych typu wektor–pseudoskalar. Kanały te wykazują istotne naruszenia perturbacyjnej reguły QCD „13%", szczególnie wyraźne w kanale $\rho\pi$. Stosujemy model eLSM, uwzględniając efekty elektromagnetyczne oraz mieszanie z wektorową kulą gluonową. Pokazujemy, że uwzględnienie tych składników umożliwia udany fenomenologiczny opis obserwowanych stosunków $\mathcal{B}(\psi(3686) \to h)/\mathcal{B}(J/\psi \to h)$.

Contents

List of Figures

List of Tables

Chapter 1

Introduction

In the 1970s, the Standard Model (SM) of particle physics was finalized, and it has since described our current knowledge of the fundamental particles and their interactions. Although certain large-scale phenomena such as dark matter, dark energy, and baryogenesis have not been explained by the SM, the SM has been extremely successful in describing and predicting the results from particle physics experiments to the present day. Notable predictions of the SM include anomalous magnetic dipole moments, and the existence of multiple particles, including the W, Z and Higgs boson. The SM is a quantum field theory (QFT) based on local gauge symmetries – internal symmetries of the fields that do not act on their spacetime coordinates – from which the form of the fundamental interactions can be derived. The gauge symmetries of the SM are described by the group

$$\mathrm{SU}(3) \times \mathrm{SU}(2) \times \mathrm{U}(1). \tag{1.0.1}$$

The $\mathrm{SU}(2) \times \mathrm{U}(1)$ describe the electroweak interactions, which at low energies are spontaneously broken by the Higgs mechanism to just the electromagnetic U(1) gauge symmetry; electromagnetism and the weak nuclear force are no longer unified. By this spontaneous symmetry breaking, mass terms for all the massive fundamental particles are generated. In one of the models studied in this thesis the mechanism of spontaneous symmetry breaking is used in a similar manner to the Higgs mechanism and is a key ingredient of the model, although with some differences, such as the kind of symmetry that is broken; in the Higgs mechanism in the Standard Model a local symmetry is broken while for the effective model is it a global symmetry.

In this thesis we will be primarily interested in the strong nuclear force, which is described by the SU(3) part, which together with the matter fields is called quantum chromodynamics (QCD). The standard method of calculating quantities in QFT is via perturbation theory; the case in the full theory is regarded as a small perturbation on a more simple, solvable theory, usually a free (noninteracting) theory. Quantities are then calculated in a perturbative expansion in a small parameter, the coupling. In doing this it is important that the coupling is small, which is not always the case for QCD. In particular, QCD has a property that is called Asymptotic Freedom, which means that at high energies (small length scales) the coupling becomes weaker and QCD approaches a free field theory at high energies, called the ultraviolet (UV) limit. Conversely, at low energies and larger length scales around the size of hadrons such as the proton, QCD is strongly coupled. In this regime, a perturbative expansion is not a reliable way to calculate observable quantities, and effects which cannot be represented in a perturbative expansion, called nonperturbative effects, become more significant.

While for weakly coupled systems perturbation theory is a very good universal method for computing ob-

servables, for strongly coupled systems there is no approximation that is known to work for all kinds of systems. Indeed there are numerous different methods for approximating QCD observables, each with their own advantages and disadvantages. QCD also has a peculiar feature which is called confinement. Quarks and gluons are the fundamental degrees of freedom (particles) of QCD, and they carry color charge. However, asymptotic states, the ones we can see in detectors, are all color neutral. Experiments do not measure quarks and gluons but composite particles in which the color charges cancel, called hadrons. This is called confinement, and while it is not completely understood yet, a qualitative explanation is the gluon self-interaction which forms a narrow flux tube between two color charged particles, when the particles are separated the energy of the flux tube increases enough to form another quark-antiquark pair, making it so that if we try to break up a hadron we just end up making more hadrons. Due to the self-interactions between gluons, a special case of hadrons is predicted to appear in QCD, which are the glueballs, made up of only gluons. So far they have only been predicted by theory, but are not conclusively found in any experiment. In this thesis we will be especially interested in the behavior of glueballs and how we might detect them.
Given that the physical particles experiments detect are not the quarks and gluons but the hadrons, instead of attempting to calculate observables from the behavior of quarks and gluons, one option is to directly construct a theory of the hadronic degrees of freedom, which are able to be detected in experiments. This is done in effective models, which will be the main focus of the thesis. The symmetries of QCD will be used as a guiding principle in constructing the interactions in the model. For this purpose we will review the basics of QCD in 1.1, with an emphasis on the (breaking of) symmetries. In 1.3 we will give a more detailed overview of the topics of this thesis.

1.1 Quantum Chromodynamics

The QCD Lagrangian is [2]

$$\mathcal{L} = \bar{\psi}^i_m(i(D_\mu)_{mn}\gamma^\mu - m_i)\psi^i_n - \frac{1}{4}G^a_{\mu\nu}G^{a,\mu\nu}. \tag{1.1.1}$$

QCD with only gluon fields is called Yang-Mills theory, whose Lagrangian is

$$\mathcal{L}_{YM} = -\frac{1}{4}G^a_{\mu\nu}G^{a,\mu\nu}. \tag{1.1.2}$$

Here and in the rest of the thesis, repeated indices will be summed over unless stated otherwise. The indices μ, ν are spacetime indices, running from 0 to 3. The index i stands for the quark flavors and runs from 1 to N_f, In Nature there are 6 quark flavors so $N_f = 6$, but usually $N_f = 3$ is taken as we are interested primarily in the light quarks when it comes to creating hadrons. The quark color indices m, n run from 1 to 3 as the quarks are in the fundamental representation of SU(3), and a runs from 1 to 8 as gluons are in the adjoint representation. Suppressing the color indices, the covariant derivative is given by

$$D_\mu = \partial_\mu - igA^a_\mu t^a, \tag{1.1.3}$$

where t^a are the generators of SU(3), g is the coupling, and A^a_μ are the components of the gluon field $A_\mu = A^a_\mu t^a$. One explicit representation of the generators are the Gell-Mann matrices [4]. The field strength

$G^a_{\mu\nu}$ is given by the commutator of the covariant derivative in two different directions:

$$G_{\mu\nu} = \frac{i}{g}[D_\mu, D_\nu] = \partial_\mu A_\nu - \partial_\nu A_\mu - ig[A_\mu, A_\nu], \tag{1.1.4}$$

which leads to the 3-gluon and 4-gluon self interaction vertices by taking its square in the Lagrangian. The Lagrangian (1.1.1) is constructed by taking the Lagrangian for non-interacting fermions and demanding a local SU(3) symmetry. Under this symmetry, the quarks and gluons transform as.

$$\psi \to U(x)\psi, \qquad A_\mu \to U(x)A_\mu - \frac{i}{g}(\partial_\mu U(x))U^\dagger(x). \tag{1.1.5}$$

The matrix $U(x) \in \mathrm{SU}(3)$ can be written in terms of the generators

$$U(x) = \exp[i\theta(x)^a t^a], \tag{1.1.6}$$

where $\theta(x)$ is a real function of spacetime coordinates x making the transformations local.
Aside from the local SU(3) gauge symmetry, QCD contains some additional (broken) symmetries we are interested in in this thesis. Their breaking patterns are a key ingredient to the creation of hadrons and their masses, as only a small fraction of hadron masses is from the Higgs mechanism. The first of these broken symmetries is dilatation symmetry. In the chiral limit $m_i \to 0$ for all flavors the Lagrangian only contains the dimensionless coupling g as a parameter. Consequently, the action is invariant under rescaling of spacetime coordinates

$$x^\mu \to \lambda^{-1}x^\mu, \tag{1.1.7}$$

which also transforms the fields according to their dimension, that is

$$\psi(x) \to \lambda^{3/2}\psi(x), \qquad A_\mu(x) \to \lambda A_\mu(x). \tag{1.1.8}$$

The associated Noether current is

$$J^\mu = x_\nu T^{\mu\nu}, \tag{1.1.9}$$

with $T^{\mu\nu}$ being the stress-energy (energy-momentum) tensor of QCD, defined by

$$T^{\mu\nu} = 2\frac{\delta S}{\delta g_{\mu\nu}}\Big|_{g_{\mu\nu}=\eta_{\mu\nu}}. \tag{1.1.10}$$

Classically, the divergence of the current is zero. However, due to quantum fluctuations of the gluons this dilatation symmetry is broken [5]. In order to correctly deal with divergencies in loops one needs to renormalize QCD. As a result of this, the coupling g becomes a function $g(\mu)$ of the renormalization scale or energy scale μ. In practice this is usually proportional to the center of mass energy. While $g(\mu)$ is still dimensionless, it is now scale dependent and the theory is not anymore fully dilatation symmetric. Consequently the divergence of the Noether current is nonzero even at zero quark masses:

$$\partial_\mu J^\mu = T^\mu_\mu = \frac{\beta(g)}{2g}G^a_{\mu\nu}G^{a,\mu\nu} \neq 0. \tag{1.1.11}$$

The function $\beta(g)$ is called the beta-function of QCD, defined by

$$\beta(g) = \mu \frac{\partial g}{\partial \mu}. \tag{1.1.12}$$

The beta function has been computed to 5 loops [6, 7]. The beta function is negative, with leading term in pertubation theory

$$\beta(g) = -\frac{11N_c - 2N_f}{48\pi^2} g^3 \equiv -b\, g^3, \tag{1.1.13}$$

where $N_c = 3$ is the number of colors, and $N_f = 6$ again the number of quark flavors. In Nature the number of colors $N_c = 3$ is fixed, but it can be useful to consider the theory of a large amount of colors, called the large N_c limit. Some features of the large N_c theory are discussed in Appendix A. Because the beta function is negative, the coupling gets smaller when the energy scale increases, ultimately approaching zero coupling in the UV limit. This is called asymptotic freedom. In the IR however, the coupling grows larger past the point where we can rely on pertubation theory. The solution to (1.1.13) is

$$g^2(\mu) = \frac{g^2(\mu_*)}{1 + 2b\, g^2(\mu_*) \log\left(\frac{\mu}{\mu_*}\right)}, \tag{1.1.14}$$

where μ_* is a reference scale one needs to measure the coupling at for the initial condition. the solution diverges at a specific scale called the Landau pole of QCD:

$$\mu = \Lambda_{\text{Landau}} = \Lambda_{\text{QCD}} = \mu_* \exp\left(\frac{-1}{g^2(\mu_*)}\right), \tag{1.1.15}$$

so that we can express the coupling in terms of the Landau pole:

$$g^2(\mu) = \frac{1}{2b \log \frac{\mu}{\Lambda_{\text{QCD}}}}. \tag{1.1.16}$$

This Landau pole is not interpreted as a physical divergence. Before this Landau pole is reached, the coupling will grow to order 1 and perturbative methods will no longer be reliable. Therefore it signals the approximate energy scale at and below which nonperturbative effects such as confinement become highly relevant. In Figure 1.1 the coupling constant is shown as a function of $p = \mu$, obtained from [1] using nonperturbative renormalization group equations[8]. The different curves are the result of determining the coupling from different vertices. As is common in many pieces of literature, the coupling in Fig 1.1 is expressed as $\alpha = g^2/4\pi$. For energies $\gtrsim 1$ GeV the curves agree and follow the behavior of (1.1.14). For low energies the curves are different but all seem to plateau, contrary to the divergence the Landau pole tells us about.
Even if it does not signify a physical divergence, the Landau Pole is important because it means the renormalization procedure has generated an inherent energy scale of a theory for which no energy scale appears in the Lagrangian. The appearance of a dimension from a dimensionless theory is called dimensional transmutation. The numerical value of Λ_{QCD} is about 200 to 300 MeV, but depends on the renormalization scheme [9]. An important aspect for later is that the anomalous breaking of dilatation symmetry is related to the emergence of the gluon condensate, made clear by the fact that the vacuum expectation value (v.e.v.) of the trace anomaly is nonzero

$$\langle T^\mu_\mu \rangle = \frac{\beta(g)}{2g} \langle G^a_{\mu\nu} G^{\mu\nu}_a \rangle \neq 0. \tag{1.1.17}$$

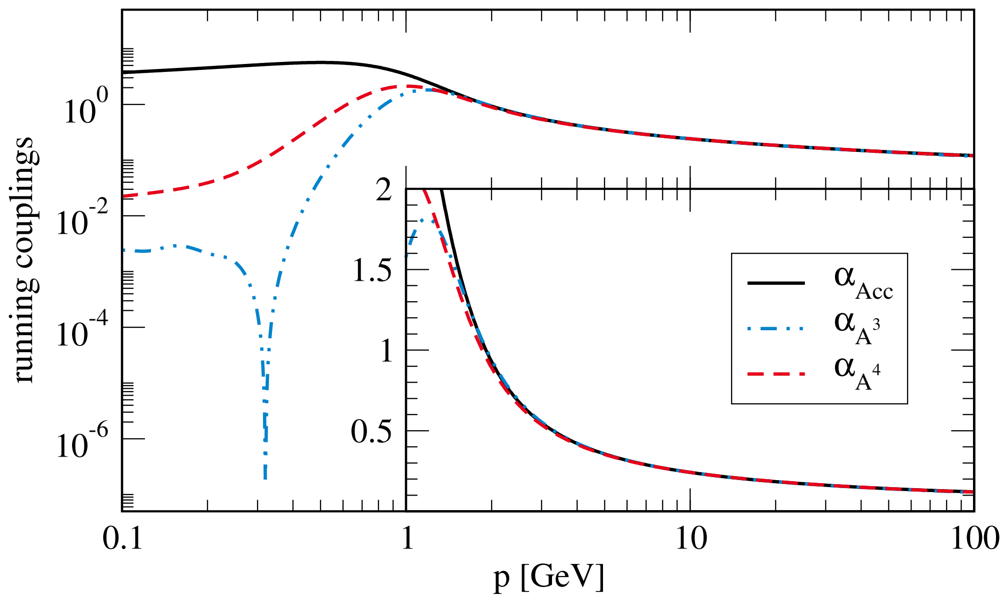

Figure 1.1: Effective running couplings, [1], obtained from different Yang-Mills vertices: three-gluon vertex: α_{A^3}, four-gluon vertex: α_{A^4}, ghost-gluon vertex: $\alpha_{A\bar{c}c}$.

The fluctuations around the gluon condensate in the form of glueballs are then also related to the trace anomaly. We will use this feature to construct a Lagrangian for the dilaton, the lightest scalar glueball, in the Linear Sigma Model.

The next important symmetry is chiral symmetry. Again in the chiral limit $m_i \to 0$, the QCD Lagrangian is invariant under transformations $\mathrm{U}(N_f)_R \times \mathrm{U}(N_f)_L$ acting on the right- and left-handed quarks as

$$\psi^i = \psi^i_R + \psi^i_L \to (U_R)_{ij}\psi_{j,R} + (U_L)_{ij}\psi_{j,L}, \tag{1.1.18}$$

where the left- and right-handed quarks are defined by the projection operators

$$\psi^i_R = P_R\psi^i = \frac{1}{2}(1+\gamma^5)\psi^i, \quad \psi^i_L = P_L\psi^i = \frac{1}{2}(1-\gamma^5)\psi^i. \tag{1.1.19}$$

The symmetry group can be decomposed in the following form

$$\mathrm{U}(N_f)_R \times \mathrm{U}(N_f)_L = \mathrm{SU}(N_f)_R \times \mathrm{SU}(N_f)_L \times \mathrm{U}(1)_V \times \mathrm{U}(1)_A, \tag{1.1.20}$$

in which the axial $\mathrm{U}(1)_A$ transformations have the property $U_A = U_R = U_L^\dagger = e^{i\theta t^0}$ and the $\mathrm{U}(1)_V$ vector transformations with $U_R = U_L$. The $\mathrm{U}(1)_V$ symmetry describes baryon number, which is conserved in QCD. The invariance under axial transformations is also broken by quantum fluctuations [10]. This breaking is called the axial anomaly. The associated Noether current has a nonzero divergence:

$$J^\mu_A = \bar{\psi}^i\gamma^\mu\gamma^5\psi^i, \quad \partial_\mu J^\mu_A = \frac{g^2 N_f}{8\pi^2}\widetilde{G}^a_{\mu\nu}G^{\mu\nu}_a, \tag{1.1.21}$$

where $\widetilde{G}_{\mu\nu} = \frac{1}{2}\epsilon_{\mu\nu\rho\sigma}G^{\rho\sigma}$ is the Hodge dual of the field strength tensor. The breaking of axial symmetry is particularly important for the description of the η and $\eta\prime$ mesons.

Similarly, the $\mathrm{SU}(N_f)_R \times \mathrm{SU}(N_f)_L$ can also be rewritten in terms of vector and axial vector transformations, i.e. $\mathrm{SU}(N_f)_R \times \mathrm{SU}(N_f)_L = \mathrm{SU}(N_f)_V \times \mathrm{SU}(N_f)_A$ with the same construction as before. The $\mathrm{SU}(N_f)_A$ is not a group since its multiplication is not closed, but the elements are well-defined transformations on the fields. While the Noether currents for these are conserved, the vacuum is not invariant under $\mathrm{SU}(N_f)_A$ transformations. This specific mechanism of symmetry breaking is called spontaneous symmetry breaking. According to Goldstone's theorem, Goldstone bosons will appear as a result. Assuming $N_f = 2$ massless quarks, we will end up with the 3 pions as Goldstone bosons. If we take the 3 $N_f = 3$ we have 8 Goldstone bosons: the pions, kaons and η mesons. In reality, the quark masses are not vanishing, so these Goldstone bosons are only approximately massless. They are then called pseudo-Goldstone bosons.

The quark mass terms immediately break most of the aforementioned symmetries. Symmetries broken in this way, at the level of the Lagrangian but controlled by a (small) parameter, are called explicitly broken symmetries. A dilatation of spacetime (1.1.7) gives the following transformation for a mass term:

$$m_i\bar{\psi}^i\psi^i \to \lambda^3 m_i\bar{\psi}^i\psi^i, \tag{1.1.22}$$

which leaves a factor λ^{-1} when integrated over d^4x. Likewise, a mass term mixes left- and right-handed fermions so they cannot be rotated separately:

$$m_i\bar{\psi}^i\psi^i = m_i(\bar{\psi}^i_L\psi^i_R + \bar{\psi}^i_R\psi^i_L). \tag{1.1.23}$$

The chiral symmetry group then breaks to the previously mentioned vector part $\mathrm{U}(N_f)_V = \mathrm{SU}(N_f)_V \times \mathrm{U}(1)_V$, provided all the quark masses are equal. If they are not, we only have a $(\mathrm{U}(1)_V)^{N_f}$ symmetry, which conserves each of the different quark flavor numbers separately. Taking quark masses to zero is a good approximation for the up and down quarks, since their masses are only a few MeV and quite close to one another. These two then have an $\mathrm{SU}(2)_V \times \mathrm{U}(1)_V$, which is called isospin. The third lightest quark s has a mass of about 100 MeV, of the same order as Λ_{QCD}, making it non-negligible. This gives an explanation as to why the pions are the lightest pseudoscalar mesons.

Aside from the mass term directly in the Lagrangian, at low energies the QCD interactions give the quarks and gluons an effective mass, called the constituent mass, as it can be seen as the mass of quarks when they are constituents of hadrons. The constituent quark mass is of the order of one third of the mass of the proton or neutron, approximately 300 MeV.

1.2 Bound states of QCD

Quarks and gluons are not the asymptotic physical states that we detect. While it is not rigorously derived from QCD, we have understood that color charge and by extension color charged particles such as quarks and gluons are confined. In other words, all detected particles are in a color singlet state. The composite particles we can detect are hadrons, and are categorized into mesons and baryons. Mesons are defined by having integer spin and thus being bosons, or equivalently by having vanishing baryon number $B = 0$, where $B = \pm 1/3$ for (anti)quarks and $B = 0$ for gluons. Baryons are defined by being fermions or equivalently by $B = 1$ baryon number.

Mesons can be further split up into conventional and unconventional mesons. Conventional mesons are made up of a quark and antiquark pair, while unconventional mesons are made of every other possibility, examples are tetraquarks, glueballs (made of only gluons), and molecular states (made up by two spatially distinct quark-antiquark pairs). While unconventional mesons have many more possibilities, the vast majority of mesons listed in the PDG are interpreted as a quark-antiquark state. Mesons are classified by a few quantum numbers. These are their spatial angular momentum L, their spin S, their total angular momentum $J = L + S$. From these the parity P and charge conjugation C eigenvales can be calculated as

$$P = (-1)^{L+1}, \quad C = (-1)^{L+S}. \tag{1.2.1}$$

Mesons are then labeled by J^{PC}. For example, the previously mentioned pseudo-Goldstone bosons have $J^{PC} = 0^{-+}$ and are pseudoscalars. Scalar mesons have $J^{PC} = 0^{++}$, and vector mesons have $J^{PC} = 1^{--}$. In conventional mesons with nonrelativistic quarks, the spin of the quark-antiquark pair necessarily sums up to either 1 or 0. When $S = 0$, it follows that $J = L$, $P = -C$ and the only possibilities are $J^{PC} = \text{even}^{-+}, \text{odd}^{+-}$. On the other hand if $S = 1$, we have $P = C$ so only J^{++}, J^{--} (except 0^{--}) are allowed. This means that the discovery of a meson with quantum numbers such as $J^{PC} = 0^{+-}, J^{PC} = 1^{-+}$ immediately confirms that these are nonconventional and their internal structure is not simply quark-antiquark. In table 1.1 the assignments of the ground state ($n = 1$) conventional mesons up to $J = 2$ are listed along with their J^{PC} and spectroscopic notation $n^{2S+1}L_J$.

$n^{2S+1}L_J$	J^{PC}	I=1 $u\bar{d}$, $d\bar{u}$ $\frac{d\bar{d}-u\bar{u}}{\sqrt{2}}$	I=1/2 $u\bar{s}$, $d\bar{s}$ $s\bar{d}$, $s\bar{u}$	I=0 $\approx \frac{u\bar{u}+d\bar{d}}{\sqrt{2}}$	I=0 $\approx s\bar{s}$	Meson names
1^1S_0	0^{-+}	π	K	$\eta(547)$	$\eta'(958)$	Pseudoscalar
1^3P_0	0^{++}	$a_0(1450)$	$K_0^\star(1430)$	$f_0(1370)$	$f_0(1500)/f_0(1710)$	Scalar
1^3S_1	1^{--}	$\rho(770)$	$K^\star(892)$	$\omega(782)$	$\phi(1020)$	Vector
1^3P_1	1^{++}	$a_1(1260)$	K_{1A}	$f_1(1285)$	$f_1'(1420)$	Axial vector
1^1P_1	1^{+-}	$b_1(1235)$	K_{1B}	$h_1(1170)$	$h_1(1415)$	Pseudovector
1^3D_1	1^{--}	$\rho(1700)$	$K^\star(1680)$	$\omega(1650)$	$\phi(?)$	Excited-vector
1^3P_2	2^{++}	$a_2(1320)$	$K_2^\star(1430)$	$f_2(1270)$	$f_2'(1525)$	Tensor
1^3D_2	2^{--}	$\rho_2(?)$	$K_2(1820)$	$\omega_2(?)$	$\phi_2(?)$	Axial tensor
1^1D_2	2^{-+}	$\pi_2(1670)$	$K_2(1770)$	$\eta_2(1645)$	$\eta_2(1870)$	Pseudotensor

Table 1.1: List of conventional $q\bar{q}$ mesons following the quark model review of the PDG [2] up to $J = 2$ and up to the lowest radial excitation.

It is still an open problem whether or not QCD breaks T and therefore CP invariance [11, 12]; the symmetries of QCD allow for a term which breaks this, but experiments have only given an upper bound for the strength of this term thus far. For the current work we can safely ignore this possibility and then C and P are separately conversed in all QCD interactions.

1.3 Outline of the thesis

In this thesis we will study effective models for QCD at the level of hadrons. We phenomenologically describe and predict the behavior of certain hadron. A particular focus is given to glueballs and unconventional hadrons. The thesis is based on the publications [13] (Chapter 2), [14] (Chapter 4), [15, 16, 17] (Chapter 5), [18] (Chapter 6)

In chapter 2 we examine the theory of a free scalar field interacting with a time independent classical source, as a model for the phenomenology of scalar glueballs in a post-collision medium. Historically it was believed that on a time independent source there is no scattering and so the dynamics are trivial. We compute scattering amplitudes exactly and show that this is not the case, but that the absence of scattering was a result of the idea that one can switch off the interaction adiabatically. In fact this assumption does not hold in this case, and particle production from the vacuum, conceptually similar to the Schwinger mechanism, gives rise to scattering.

In chapters 3 we go over the construction of the extended Linear Sigma Model (eLSM), which is an effective hadronic model based on the symmetries of QCD and their anomalous, explicit and spontaneous breaking patterns. In its basic form it contains the dilaton (scalar glueball), pseudoscalars, scalars, vectors, and axial vectors mesons. It can be readily extended to include more mesons such as higher spin mesons or different glueballs. This is done in the following chapters. In chapter 4 we include the tensor and axial tensor mesons. Experimentally, the ground-state tensor mesons are well known, but for the axial tensors the data on most decay modes and masses are still missing. Due to the fact they are chiral partners, both of their interactions can be described in a unified framework in the eLSM. From the eLSM we describe the decays of the tensor mesons and predict some decay channels, and use this to predict the masses and decays of the axial tensor mesons.

In chapter 5, we extend the eLSM to the tensor glueball. No glueball has yet been experimentally identified, but the tensor is the second lightest glueball (after the scalar) according to lattice QCD calculations at around 2 GeV, and therefore likely to be one of the easiest to find. There are a number of potential candidate resonance which could be the tensor glueball, and we compare their known data to predictions we make with the eLSM. From this, we conclude the $f_2(1950)$ is the most likely tensor glueball candidate.

In chapter 6 we study the decays of the J/ψ and $\psi(2S)$ charmonium states in the eLSM. From perturbative calculations in QCD it follows that these states should obey the so-called 13% rule, but for some decay channels this rule is severely violated. The first discovered and biggest offender is the $\rho\pi$ channel, and most vector-pseudoscalar channels do not follow the 13% rule. We use the eLSM along with electromagnetic decay channels, and allow the vector glueball to mix with the $\psi(2S)$. Electromagnetic interactions turn out to be crucial in order to agree with data, and the inclusion of the vector glueball improves the description as well. With both these ingredients we reach a successful phenomenological description of the breaking of the 13% rule of the VP decays of J/ψ and $\psi(2S)$.

1.4 List of Publications

This thesis is based on the works

Chapter 2

1. L. Tinti, A. Vereijken, S. Jafarzade and F. Giacosa, “Scalar field with a time-independent classical source is not trivial after all: From vacuum decay to scattering,” Phys. Rev. D **110** (2024) no.11, 116004 [arXiv:2403.15531 [hep-th]], doi:10.1103/PhysRevD.110.116004.

Chapter 4

2. S. Jafarzade, A. Vereijken, M. Piotrowska and F. Giacosa, “From well-known tensor mesons to yet unknown axial-tensor mesons,” Phys. Rev. D **106** (2022) no.3, 036008 [arXiv:2203.16585 [hep-ph]],

doi:10.1103/PhysRevD.106.036008.

Chapter 5

3. A. Vereijken, S. Jafarzade, M. Piotrowska and F. Giacosa, "Is f2(1950) the tensor glueball?," Phys. Rev. D **108** (2023) no.1, 014023 [arXiv:2304.05225 [hep-ph]], doi:10.1103/PhysRevD.108.014023.

4. A. Vereijken, "Tensor glueball decay into nucleon-antinucleon," Nuovo Cim. C **47** (2024) no.4, 188 [arXiv:2310.10273 [hep-ph]], doi:10.1393/ncc/i2024-24188-6.

5. A. Vereijken, "Decays of the tensor glueball in a chiral approach," EPJ Web Conf. **291** (2024), 02005, [arXiv:2310.09608 [hep-ph]], doi:10.1051/epjconf/202429102005.

Chapter 6

6. A. Vereijken, "The rho-pi puzzle and vector glueball mixing," [arXiv:2502.21042 [hep-ph]], Proceedings of FAIRNESS2024.

Other works by the author

7. Giacosa, F., Kolbus, A., Kyziol, K., Plodowska, M., Piotrowska, M., Szary, K., and Vereijken, A. (2026). Two-Exponential Decay of Acridine Orange. Acta Physica Polonica A, 148(6), S110, [arXiv:2511.04185 [quant-ph]], https://doi.org/10.12693/APhysPolA.148.S110

8. F. Giacosa, A. Kolbus, K. Kyziol, M. Plodowska, M. Piotrowska, K. Szary and A. Vereijken, "Quantum Late-Time Decay and Channel Dependence," [arXiv:2509.17163 [quant-ph]], doi:10.48550/arXiv.2509.17163.

Chapter 2

The scalar glueball with a time independent classical source

2.1 Introduction

In the previous chapter we have seen that the gluons have a nonzero vacuum expectation value due to the trace anomaly. In the presence of a medium, such as in matter or heavy-ion collisions, this expectation value will pick up a spacetime dependence. This can then be modeled as a classical source of these particles, which can form a scalar glueball. For example, particle production of a scalar field ϕ can manifest from a self-interaction as follows

$$\phi^4(x) \to \langle\phi\rangle_x^4 + 4\,\langle\phi\rangle_x^3\,\phi(x) + ... \tag{2.1.1}$$

One of these terms describes a ϕ field being created or annihilated by a source $\langle\phi\rangle_x^3$. This is the model we will study in depth in this chapter. This theory, which describes an uncharged free scalar particle coupled to an external classical source, has received much attention during the early stages of the development of quantum field theory. This is very natural given it is one of the simpler QFTs one can write down, and it has become a textbook example illustrating concepts in quantum field theory [19, 20, 21, 22].

The common belief that was held in the past is that if the classical source is static in time, the theory has no scattering and the time evolution is trivial. We will take a close look at the arguments used for this claim and give reasoning as to why it can be disputed. Namely, in this chapter we calculate the exact time evolution of quantum states, in particular states with definite particle number (and momentum). It turns out that in the specific case of a time-independent source, the scattering is not trivial, but caused by particle production from the (particle) vacuum. This vacuum decays in a similar fashion as in the Schwinger mechanism. In fact, this vacuum decay, together with absorption of incoming particles by the source, is the key element to solve all the dynamics of the system, whatever the initial state.

Vacuum decay is often described in terms of a metastable or false vacuum, which is a state at a local minimum of the Hamiltonian[1], which then decays due to tunneling. In this context, vacuum decay of scalar fields has been studied extensively for example by using thin wall approximations [23, 24, 25, 26, 27, 28, 29], which in certain situations is analogous to quantum mechanical tunneling [30]. A possible experimental test

[1] This local minimum energy is a complex number, hence the metastable vacuum is not a true eigenstate of the Hamiltonian which is why it decays.

of false vacuum decay is proposed in [31, 32]. One important application is the study of the electroweak vacuum of the Higgs potential [33, 34, 35, 36, 37, 38]. Quantum corrections to the Higgs self-interaction can turn the minimum, which classically is a global one, to just a local minimum. Whether or not this happens and the electroweak vacuum is a false vacuum depends on the parameters, in particular, the Higgs mass and the top quark mass. According to current measurements and calculations it is indeed metastable [34, 35, 36] with a lifetime longer than the age of the universe. It is however close enough to stability that further studies and precise measurements are required. The presence of gravity also has interesting effects on vacuum stability and vice versa, see e.g. [24, 39, 40, 41]. Recently it has been shown that also in the non-interacting case nontrivial vacua can be necessary to properly renormalize the expectation values of observables in flat [42, 43], as well as curved spacetimes and cosmologies [44, 45]. Non-trivial vacuum effects have also been shown to be a relevant source of particles in heavy-ion collisions [42, 46].

Aside from serving as an effective description for dilaton production in the presence of a medium such as a quark-gluon plasma in heavy-ion collisions, the perturbation of a ground state by a (temporary) classical external field can be a convenient way to approximate various physical phenomena. Besides the many scalar fields in hadron physics, beyond the Standard Model physics often have new scalar particles as well, such as the inflaton in cosmology.

This vacuum decay process for scalar fields is conceptually analogous to the Schwinger mechanism [47, 48, 49, 30], in which particle-antiparticle pairs are created nonperturbatively from the vacuum in the presence of a strong static electric field. Past the conceptual similarity, the methods and results in this chapter are different. While the Schwinger mechanism is a nonperturbative effect, is it still based on further approximations, beyond the classical source, while we will have a class of exact solutions instead. In the Schwinger mechanism there is particle-antiparticle pair production, in contrast to our case, in which a single particle production, and by extension any number of particles, is possible. Whereas in the Schwinger mechanism the vacuum decay is exponential, in this chapter we will see the The vacuum decay does not follow an exponential. In fact, the vacuum survival probability eventually saturates at large times, so that the final particle number expectation is constant. In particular, the survival probability is quadratic at short times, thus allowing for the quantum Zeno effect if repeated measurements are performed. The quantum Zeno effect is realized when the time evolution of a system can frozen by repeated measurements at short time intervals and occurs when the decay law at short times is slower than an exponential, see e.g. [50, 51, 52, 53, 54]. It is an important effect in cavity QED [55, 56] and potentially even in large systems when gravity is involved [57]. In the case of the anti Zeno effect [54, 58, 59] the decay is accelerated by repeated measurements with longer time intervals. They are both generic results of quantum mechanics and quantum field theory, but in most cases - for example the decay of muons - an exponential decay is an extremely good approximation. In many systems an exponential is such a good approximation that it is experimentally indistinguishable from the full decay law. In the vacuum decay studied in this chapter this is not the case; there is no time scale where an exponential decay is a good approximation for the full decay formula.

We start off with describing the system in subsection 2.2. In subsection 2.3 we derive exact scattering amplitudes and probabilities of the vacuum decaying to n particles. In subsection 2.4 we focus on the vacuum decay, and look at the small time and large time behaviors. Some specific forms of the external sources are taken as examples and we calculate the vacuum decay probability distribution for these, and find the behavior for large volume. In subsection 2.5 We compare the findings to previous work and discuss phenomenological applications. Finally, we conclude in subsection 2.6.

2.2 Setup of the model

We are interested in a free scalar field interacting with a static external field, as in the second term in (2.1.1). The simplicity of this model allows us to do exact calculations, with no need for a perturbative expansion in Wick or Feynman diagrams, and contrary to many perturbative calculations, we can stay in the Heisenberg picture, and all quantities will be in this picture unless explicitly stated otherwise. The action of this theory is given by

$$\mathcal{S} = \int d^4x\, \mathcal{L} = \int d^4x \left(\frac{1}{2}\partial_\mu \phi(x) \partial^\mu \phi(x) - \frac{1}{2} m^2 \phi^2(x) + g\rho(\mathbf{x})\phi(x) \right). \tag{2.2.1}$$

Here $\rho(\mathbf{x})$ is a time independent, classical source of the field operator ϕ that carries dimensions Energy^3, and $\mathbf{x}$ is the spatial coordinate vector. In the interpretation with the dilaton, $\rho(\mathbf{x})$ is essentially proportional to $\langle \phi \rangle^3(\mathbf{x})$, under the assumption that it does not change in time. The constant g is a dimensionless coupling constant. The only further assumption about the source we will need is that it is Fourier transformable in space. It is not Fourier transformable in time due to its time-independence. The equation of motion for the system reads

$$\Box\, \phi(x) + m^2 \phi(x) = g\rho(\mathbf{x}). \tag{2.2.2}$$

As with many ordinary differential equations, solutions to this equation of motion consist of two parts. The first is a solution $\phi_0(x)$ to the homogeneous part of the equation, i.e. the Klein-Gordon equation:

$$\Box\, \phi_0(x) + m^2 \phi_0(x) = 0. \tag{2.2.3}$$

The homogeneous part $\phi_0(x)$ can be solved by a decomposition into positive and negative energy plane waves as:

$$\phi_0(x) = \int \frac{d^3p}{(2\pi)^3 \sqrt{2E_{\mathbf{p}}}} \left[a_{\mathbf{p}} e^{-ip\cdot x} + a^\dagger_{\mathbf{p}} e^{ip\cdot x} \right], \tag{2.2.4}$$

where $a_{\mathbf{p}}, a^\dagger_{\mathbf{p}}$ are the particle creation and annihilation operators. The second part is the particular solution. It can be thought of as an advanced Green's function for $t < t_0$ and a retarded Green's function for $t > t_0$, and zero for $t = t_0$. We will just give the solution and verify it explicitly. The full solution is then

$$\phi(x) = \phi_0(x) + i\, g \int_{t_0}^{t} dy_0 \int d^3y \int \frac{d^3p}{(2\pi)^3 2E_{\mathbf{p}}} \left[e^{-ip\cdot(x-y)} - e^{ip\cdot(x-y)} \right] \rho(\mathbf{y}). \tag{2.2.5}$$

Here $t = x^0$ is the time coordinate and t_0 is an initial time. Without loss of generality, we can set this initial time $t_0 = 0$, which we will do from here on out. This solution encompasses both situations $t > 0$ and $t < 0$, by a sign difference due to the integral boundaries. Because the integral vanishes for $t = 0$, the initial condition is then that at $t = 0$, the full solution is equal to a free field: $\phi(0, \mathbf{x}) = \phi_0(0, \mathbf{x})$ We can see it is a solution by explicitly applying the Klein-Gordon operator:

$$\begin{aligned}
(\Box + m^2)\phi(x) &= 0 + i\, g \int_0^t dy_0 \int d^3y \int \frac{d^3p}{(2\pi)^3 2E_{\mathbf{p}}} \left[(-p^2 + m^2) e^{-ip\cdot(x-y)} - (-p^2 + m^2) e^{ip\cdot(x-y)} \right] \rho(\mathbf{y}) \\
&\quad + i\, g \int d^3y \int \frac{d^3p}{(2\pi)^3 2E_{\mathbf{p}}} \left[(-iE_{\mathbf{p}}) e^{i\mathbf{p}\cdot(\mathbf{x}-\mathbf{y})} - (iE_{\mathbf{p}}) e^{-i\mathbf{p}\cdot(\mathbf{x}-\mathbf{y})} \right] \rho(\mathbf{y}) \\
&= g \int \frac{d^3p}{(2\pi)^3} e^{i\mathbf{p}\cdot\mathbf{x}} \int d^3y\, e^{-i\mathbf{p}\cdot\mathbf{y}}\, \rho(\mathbf{y}) = g\rho(\mathbf{x}).
\end{aligned} \tag{2.2.6}$$

In the second passage we use that the integrals are invariant under $\mathbf{p} \to -\mathbf{p}$, and in the final passage we use the requirement of Fourier transformability of ρ mentioned earlier to apply the Fourier and the inverse Fourier transform. Evaluating the y_0 integral in (2.2.5) and using the homogeneous solution (2.2.4), the exact form of the field for $t > 0$ can be written in the explicit form

$$\begin{aligned}\phi(x) = \int \frac{d^3p}{(2\pi)^3\sqrt{2E_{\mathbf{p}}}} \Bigg[&\left(a_{\mathbf{p}} + g\frac{e^{iE_{\mathbf{p}}t} - 1}{\sqrt{2E_{\mathbf{p}}^3}} \int d^3y \, e^{-i\mathbf{p}\cdot\mathbf{y}} \rho(\mathbf{y}) \right) e^{-ip\cdot x} \\ &+ \left(a_{\mathbf{p}}^\dagger + g\frac{e^{-iE_{\mathbf{p}}t} - 1}{\sqrt{2E_{\mathbf{p}}^3}} \int d^3y \, e^{i\mathbf{p}\cdot\mathbf{y}} \rho(\mathbf{y}) \right) e^{ip\cdot x} \Bigg] .\end{aligned} \tag{2.2.7}$$

The time dependence of the in-homogeneous part can also be written as $\sin(E_{\mathbf{p}}t)/E_{\mathbf{p}}$, which is a nascent delta function. For $t \to \infty$ it approaches the Dirac delta function $\delta(E_{\mathbf{p}})$. Because the on-shell energy is strictly larger than zero due to the mass, this then approaches a free field. But just because it approaches a free field at asymptotically late times, does not mean that the time evolution, even for very large time intervals, is trivial. For any finite t we can calculate this integral explicitly and we can take the infinite time limit at a later point, after inner products are taken and we are dealing again with expectation values, this will leave us with nontrivial dynamics.

In order to ease the notation, we define the functions h and f by

$$\begin{aligned} h(\mathbf{p}) &= g\,\frac{-1}{\sqrt{2E_{\mathbf{p}}^3}} \int d^3y \, e^{-i\mathbf{p}\cdot\mathbf{y}} \rho(\mathbf{y}), \\ f(t,\mathbf{p}) &= g\,\frac{e^{iE_{\mathbf{p}}t} - 1}{\sqrt{2E_{\mathbf{p}}^3}} \int d^3y \, e^{-i\mathbf{p}\cdot\mathbf{y}} \rho(\mathbf{y}). \end{aligned} \tag{2.2.8}$$

Using this notation, the field solution (2.2.7) can be written in the compact way

$$\phi(x) = \int \frac{d^3p}{(2\pi)^3\sqrt{2E_{\mathbf{p}}}} \left[\Big(a_{\mathbf{p}} + f(t,\mathbf{p}) \Big) e^{-ip\cdot x} + \Big(a_{\mathbf{p}}^\dagger + f^*(t,\mathbf{p}) \Big) e^{ip\cdot x} \right], \tag{2.2.9}$$

so it is more clearly in a form similar to (2.2.4), but with time dependent creation and annihilation operators. From (2.2.9) we can immediately see the form of these time dependent ladder operators

$$a_{\mathbf{p}}(t) = a_{\mathbf{p}} + f(t,\mathbf{p}) = a_{\mathbf{p}} + (1 - e^{iE_{\mathbf{p}}t})h(\mathbf{p}) \ . \tag{2.2.10}$$

To avoid confusion, we note that the operators $a_{\mathbf{p}}(t)$, despite their explicit time dependence, do not evolve with the Heisenberg equation: $a_{\mathbf{p}}(t) \neq U^\dagger(t,0)a_{\mathbf{p}}(0)U(t,0)$. This is necessary to be consistent with the convention used for the free case (2.2.4). In the limit $g \to 0$ the $a_{\mathbf{p}}(t)$ reduce to the free $a_{\mathbf{p}}$, which have nontrivial commutation relations with the free Hamiltonian, but importantly they are constant. Therefore even in the Heisenberg picture they are defined to be time independent in the free case. One might then expect that they evolve with the interaction picture propagator $U_I = U_0^\dagger U$. This is indeed the case, and will be shown and used extensively in subsection 2.3.

From this relation we have, by construction, that $a_{\mathbf{p}}(0)$ is just $a_{\mathbf{p}}$ which is the initial condition, so we will omit the time argument at $t = 0$. The fact that the field can be written in terms of time dependent creation and annihilation operators is a general feature of quantum field theories. With these new time dependent for the interacting field, we can construct the particle number operator and calculate its expectation value with respect to the (free) particle vacuum. Since the ladder operators are just the free field operators shifted by a function, this expectation value is simply

$$N_0(t) = \langle 0| N(t) |0\rangle = \int \frac{d^3p}{(2\pi)^3} \langle 0| a^\dagger_{\mathbf{p}}(t) a_{\mathbf{p}}(t) |0\rangle = \int \frac{d^3p}{(2\pi)^3} |f(t,\mathbf{p})|^2 = 2\int \frac{d^3p}{(2\pi)^3} \Big(1-\cos(E_{\mathbf{p}}t)\Big) |h(\mathbf{p})|^2 . \tag{2.2.11}$$

Even though the creation and annihilation operators do not evolve according to the Heisenberg equation the number operator $N(t)$ does, as is normal for observables. The combination $a^\dagger_{\mathbf{p}}(t)a_{\mathbf{p}}(t) = U_I^\dagger\, a^\dagger_{\mathbf{p}}\, U_I U_I^\dagger\, a_{\mathbf{p}}\, U_I = U_I^\dagger\, a^\dagger_{\mathbf{p}} a_{\mathbf{p}}\, U_I = U^\dagger\, (U_0\, a^\dagger_{\mathbf{p}}\, U_0^\dagger)\, (U_0\, a_{\mathbf{p}}\, U_0^\dagger)\, U$. The commutation relations between the ladder operators and the free Hamiltonian are the standard ones, and so the phases for the free evolution $U_0\, a_{\mathbf{p}}\, U_0^\dagger = e^{iE_{\mathbf{p}}t} a_{\mathbf{p}}$ and its Hermitian conjugate cancel exactly. The calculation of the normal-ordered Hamiltonian can be done with standard methods. Here we will do it specifically for a time independent source, in the appendix of [13] a derivation for any type of source can be found. The Lagrangian (2.2.1) has no derivatives in its interaction term, so the stress tensor has the standard form

$$T^{\mu\nu}(x) = \partial^\mu\phi(x)\partial^\nu\phi(x) - g^{\mu\nu}\mathcal{L}, \tag{2.2.12}$$

the $(0,0)$th component of which is the Hamiltonian density:

$$H = \int d^3x\, T^{00} = \int d^3x \left(\frac{1}{2}\left[(\partial_t\phi(x))^2 + (\nabla\phi(x))^2 + m^2\phi(x)^2\right] - g\rho(\mathbf{x})\phi(x)\right). \tag{2.2.13}$$

The first part of which has the same form as the stress tensor of the free theory, but with the field (2.2.9). This term will give the standard result of the Klein-Gordon Hamiltonian but expressed in the time dependent ladder operators (2.2.10). We then just need to solve the additional term

$$\begin{aligned}
\int d^3x\, g\rho(\mathbf{x})\phi(x) &= \int \frac{d^3p}{(2\pi)^3\sqrt{2E_{\mathbf{p}}}} \left(a_{\mathbf{p}}(t)\, e^{-iE_{\mathbf{p}}t} \int d^3x\, \rho(\mathbf{x})\, e^{i\mathbf{p}\cdot\mathbf{x}} + h.c.\right) \\
&= \int \frac{d^3p}{(2\pi)^3\sqrt{2E_{\mathbf{p}}}} \left(a_{\mathbf{p}}(t)\, e^{-iE_{\mathbf{p}}t} \left(-\sqrt{2E^3_{\mathbf{p}}}\right) h^*(\mathbf{p}) + h.c.\right) \\
&= \int \frac{d^3p}{(2\pi)^3} (-E_{\mathbf{p}}) \Big(a_{\mathbf{p}}(t)\, e^{-iE_{\mathbf{p}}t}\, h^*(\mathbf{p}) + a^\dagger_{\mathbf{p}}(t) e^{iE_{\mathbf{p}}t}\, h(\mathbf{p})\Big).
\end{aligned} \tag{2.2.14}$$

Combining this with the "free-like" part for the full Hamiltonian:

$$\begin{aligned}
H &= \int \frac{d^3p}{(2\pi)^3} E_{\mathbf{p}} \Big[a^\dagger_{\mathbf{p}}(t) a_{\mathbf{p}}(t) + a_{\mathbf{p}}(t) h^*(\mathbf{p})\, e^{-iE_{\mathbf{p}}t} + a^\dagger_{\mathbf{p}}(t) h(\mathbf{p})\, e^{iE_{\mathbf{p}}t}\Big] \\
&= \int \frac{d^3p}{(2\pi)^3} E_{\mathbf{p}} \Big[\left(a^\dagger_{\mathbf{p}}(t) + h^*(\mathbf{p})\, e^{-iE_{\mathbf{p}}t}\right)\left(a_{\mathbf{p}}(t) + h(\mathbf{p})\, e^{iE_{\mathbf{p}}t}\right)\Big] - \int \frac{d^3p}{(2\pi)^3} E_{\mathbf{p}} |h(\mathbf{p})|^2.
\end{aligned} \tag{2.2.15}$$

Finally we use the relation between h and f also shown in (2.2.10), rewritten as $a_{\mathbf{p}}(t) + h(\mathbf{p})\, e^{iE_{\mathbf{p}}t} = a_{\mathbf{p}} + h(\mathbf{p})$ for the final form of the Hamiltonian

$$H = \int \frac{d^3p}{(2\pi)^3} E_{\mathbf{p}} \left[\Big(a^\dagger_{\mathbf{p}} + h^*(\mathbf{p})\Big)\Big(a_{\mathbf{p}} + h(\mathbf{p})\Big) - |h(\mathbf{p})|^2\right] . \tag{2.2.16}$$

It turns out that when the source is time independent, the Hamiltonian is also time independent. This is as expected, because it means there is time translation symmetry. As long as the integral

$$\int \frac{d^3p}{(2\pi)^3}\, E_{\mathbf{p}} |h(\mathbf{p})|^2 = \int \frac{d^3p}{(2\pi)^3 2E_{\mathbf{p}}^2} \left| \int d^3x \; e^{i\mathbf{p}\cdot\mathbf{x}} \rho(\mathbf{x}) \right|^2 \tag{2.2.17}$$

converges, the full interacting Hamiltonian corresponds to a finite off-set plus a "free-like" term. The Hamiltonian has the same spectrum as a free Hamiltonian but with the creation and annihilation operators shifted by a function. The final Hamiltonian is then not diagonal for the basis that diagonalizes the free Hamiltonian. This is to be expected, since it is necessary in order to have nontrivial time evolution of the observables, i.e. have nontrivial scattering. However, this shift by a function is different from the shift seen in the ladder operators in the field (2.2.10). After all, the fields are time dependent through the creation and annihilation operators $a_{\mathbf{p}}(t)$, while the Hamiltonian is time independent. This is already a first indication that the Hamiltonian does not have a basis of mutual eigenstates with the momentum or the particle number operator. Concretely, we can show this by looking at the commutator. It is clear from (2.2.12) that in the components of the momentum operator, the external source does not show up explicitly:

$$P^i = \int d^3x \; T^{0i} = \int \frac{d^3p}{(2\pi)^3}\; p^i a_{\mathbf{p}}^\dagger(t) a_{\mathbf{p}}(t), \tag{2.2.18}$$

that is, similarly to the "free-like" part of the Hamiltonian, one can go through the usual computation for free fields where only the ladder operators are defined differently. The commutator of the Hamiltonian with the ladder operators is slightly modified compared to the free case:

$$[H, a_{\mathbf{p}}(t)] = [H, a_{\mathbf{p}}] = -E_{\mathbf{p}}(a_{\mathbf{p}} + h(\mathbf{p})). \tag{2.2.19}$$

The commutator of the Hamiltonian and the momentum operator then follows from a straightforward calculation similar to the one for the Hamiltonian:

$$[H, \mathbf{P}] = \int \frac{d^3p}{(2\pi)^3} \mathbf{p} [H, a_{\mathbf{p}}^\dagger(t) a_{\mathbf{p}}(t)] = \int \frac{d^3p}{(2\pi)^3} \mathbf{p} E_{\mathbf{p}} \Big(a_{\mathbf{p}}^\dagger(t) \big(f(t,\mathbf{p}) - h(\mathbf{p}) \big) - a_{\mathbf{p}}(t) \big(f^*(t,\mathbf{p}) - h^*(\mathbf{p}) \big) \Big). \tag{2.2.20}$$

Consequently, there is no basis of simultaneous eigenstates of both the Hamiltonian and the momentum operator. This is also expected, since momentum conservation is violated because there is no space translation symmetry in the Lagrangian. From another point of view. the interaction term describes an external source creating or destroying a single particle, so it is not surprising momentum is not conserved.

2.3 Scattering amplitudes

2.3.1 General expressions

Given a generic initial state of the system $|\psi_i\rangle$ measured or prepared at time $t_i = 0$, the probability amplitude and probability to measure the state $|\psi_f\rangle$ at a later time $t > 0$ are given by the time-evolution operator of the theory $U(t, 0)$ by

$$a_{i\to f}(t) = \langle \psi_f | U(t,0) | \psi_i \rangle \; , \quad P_{i\to f}(t) = |a_{i\to f}(t)|^2 \; . \tag{2.3.1}$$

The operator $U(t,0)$ is also referred to as the 'propagator' [19, 60], but this should not be confused with the Feynman propagator or similar quantities. These other quantities will not be as relevant for this chapter and so we will use the names evolution-time operator or propagator interchangeably in this chapter.
The probability amplitude simplifies significantly when the Hamiltonian is time independent. For a time independent source, the Hamiltonian is also time independent. When the source depends on time then so will the Hamiltonian, and solving (2.3.1) becomes a nontrivial task. Before focusing on the case for the static source, we will solve the dynamics for an arbitrary source, and simplify to a static source later on. One way to tackle this problem is to fully calculate the Dyson series. However, since we have the full solutions to the equation of motion at all time (2.2.9), it is possible to avoid solving for the propagator $U(t,0)$, by taking a small detour into some unphysical states. Any uncharged scalar field can be decomposed in terms of time-dependent ladder operators in the form (2.2.9). This allows us to use all the free-field concepts of normal ordering and build the particle number eigenstates. Since the field coincides with a free field at $t=0$, the particle number eigenstates built with the free field are the particle number eigenstates of the interacting scalar field at $t=0$. In the Heisenberg picture the physical states do not evolve in time, therefore the states at time $t_0=0$ are the physical states at all times.
It is now possible to use this freedom of choice of basis to solve the exact dynamics of this system, while bypassing the need to solve for the time-evolution operator $U(t,0)$. The key ingredient is to notice that the time-dependent ladder operators evolve with the interaction propagator. In general for quantum field theories of real valued scalar fields we can write the annihilation operator as:

$$a_{\mathbf{p}}(t) = \frac{i}{\sqrt{2E_{\mathbf{p}}}} \int d^3x \, e^{iE_{\mathbf{p}}t} \, e^{-i\mathbf{p}\cdot\mathbf{x}} \left[\Pi(t,\mathbf{x}) - iE_{\mathbf{p}} \, \phi(t,\mathbf{x}) \right] , \tag{2.3.2}$$

where $\Pi(t,x) = \partial\mathcal{L}/\partial\dot{\phi}$ is the conjugate momentum, and the creation is the complex conjugate. These have the same (equal time) commutation relations as the free ladder operators $a_{\mathbf{p}}, a^\dagger_{\mathbf{p}}$, and are consistent with writing the field in the form (2.2.9). The interacting (Heisenberg picture) fields evolve according with the full propagator $U(t,0)$ of the theory, therefore

$$\begin{aligned}
a_{\mathbf{p}}(t) &= \frac{i}{\sqrt{2E_{\mathbf{p}}}} \int d^3x \, e^{iE_{\mathbf{p}}t} \, e^{-i\mathbf{p}\cdot\mathbf{x}} \left[U^{-1}(t,0) \, \Pi(0,\mathbf{x}) \, U(t,0) - iE_{\mathbf{p}} \, U^{-1}(t,0) \, \phi(0,\mathbf{x}) \, U(t,0) \right] \\
&= U^{-1}(t,0) \left\{ \frac{i}{\sqrt{2E_{\mathbf{p}}}} \int d^3x \, e^{iE_{\mathbf{p}}t} \, e^{-i\mathbf{p}\cdot\mathbf{x}} \left[\Pi(0,\mathbf{x}) - iE_{\mathbf{p}} \, \phi(0,\mathbf{x}) \right] \right\} U(t,0) \\
&= U^{-1}(t,0) \left\{ e^{iE_{\mathbf{p}}t} \, a_{\mathbf{p}} \right\} U(t,0) \ .
\end{aligned} \tag{2.3.3}$$

On the other hand, the ladder operators have the same commutation relations with the free Hamiltonian H_0 as the free field. Using the commutation relation (2.2.19), the additional phase $e^{iE_{\mathbf{p}}t}$ can be written[2] in terms of the free propagator $U_0(t,0) = \exp\{-iH_0t\}$, leading to

$$\begin{aligned}
a_{\mathbf{p}}(t) &= U^{-1}(t,0) \left\{ e^{iE_{\mathbf{p}}t} \, a_{\mathbf{p}} \right\} U(t,0) \\
&= U^{-1}(t,0) \left\{ U_0(t,0) \, a_{\mathbf{p}} \, U_0^{-1}(t,0) \right\} U(t,0) = U_I^{-1}(t,0) \, a_{\mathbf{p}} \, U_I(t,0) \ ,
\end{aligned} \tag{2.3.4}$$

[2] In a different convention, this phase with opposite sign describes the time dependence of the free ladder operators in the Heisenberg picture, derived in the same way.

where we recognize the propagator in the interaction picture $U_I = U_0^{-1}U$. The very same argument holds for the creation operator, since the numerical phase in the phase has the opposite sign, following from the opposite sign of the commutation relations with H_0. Using the fact that the creation and annihilation operators evolve with the interaction picture propagator, we can define a continuous set of states labeled by t:

$$\begin{aligned}
|0\rangle_t = U_I^{-1}(t,0)|0\rangle \quad &\Rightarrow \quad a_{\mathbf{p}}(t)|0\rangle_t = \left(U_I^{-1}(t,0)\, a_{\mathbf{p}}\, U_I(t,0)\right) U_I^{-1}(t,0)|0\rangle \\
&\qquad\qquad\qquad = U_I^{-1}(t,0)\left(a_{\mathbf{p}}|0\rangle\right) = 0, \\
|\mathbf{p_1},\cdots,\mathbf{p}_n\rangle_t = U_I^{-1}(t,0)|\mathbf{p_1},\cdots,\mathbf{p}_n\rangle \quad &\Rightarrow \\
a^\dagger_{\mathbf{p}}(t)\, a_{\mathbf{p}}(t)\, |\mathbf{p_1},\cdots,\mathbf{p}_n\rangle_t &= U_I^{-1}(t,0)\left(a^\dagger_{\mathbf{p}}\, a_{\mathbf{p}}\, |\mathbf{p_1},\cdots,\mathbf{p}_n\rangle\right).
\end{aligned} \tag{2.3.5}$$

At every time t, the states with subscript t are eigenstates of the number operator $N(t)$, and the states without subscript t are just the regular Heisenberg states, eigenstates of the number operator at time $t = 0$. It is important to note that these states are not physical states[3], nor are they the states described by the interaction picture, since their time evolution is given by U_I^{-1} instead of the regular U_I. They are also not energy eigenstates, as there are no simultaneous eigenstates of the Hamiltonian and the number operator (or equivalently of the Hamiltonian and the momentum operator). Even though these states are defined by the interaction picture propagator, we are still working in the Heisenberg picture. These states are just a useful tool for the calculation. By construction we have

$${}_t\langle\mathbf{p}_1,\cdots,\mathbf{p}_n|\mathbf{k}_1,\cdots\mathbf{k}_n\rangle = \langle\mathbf{p}_1,\cdots,\mathbf{p}_n|\, U_I(t,0)\, |\mathbf{k}_1,\cdots\mathbf{k}_n\rangle. \tag{2.3.6}$$

To avoid confusion it is useful to recall which states to project on. It might be intuitive to think that, since the basis of particle number eigenstates changes over time, one has to sandwich the propagator between the initial time n particle state and an m particle state at final time. Why this should not be done is most easily seen in the Schrödinger picture, where the basis of eigenstates of an operator does not change over time, and one has to sandwich in between two states of the same basis. Matrix elements are equivalent between pictures, so it is correct to sandwich the operator between two $t = 0$ eigenstates[4]. The regular matrix elements of the full propagator then read

$$\begin{aligned}
\langle\mathbf{p}_1,\cdots,\mathbf{p}_n|\, U(t,0)\, |\mathbf{k}_1,\cdots\mathbf{k}_l\rangle &= \langle\mathbf{p}_1,\cdots,\mathbf{p}_n|\, U_0(t,0)\, U_0^{-1}(t,0)\, U(t,0)\, |\mathbf{k}_1,\cdots\mathbf{k}_l\rangle \\
= \langle\mathbf{p}_1,\cdots,\mathbf{p}_n|\, U_0(t,0)\, U_I(t,0)\, |\mathbf{k}_1,\cdots\mathbf{k}_l\rangle &= \left[\prod_{j=1}^{n} e^{-iE_{\mathbf{p}_j}t}\right] {}_t\langle\mathbf{p}_1,\cdots,\mathbf{p}_n|\mathbf{k}_1,\cdots\mathbf{k}_l\rangle.
\end{aligned} \tag{2.3.7}$$

Here we see more clearly the benefit of using the time dependent particle number eigenstates; the matrix elements are given by a projection without the propagator and with some additional phases. It is possible to use this result to solve for the scattering exactly. Namely, from the definition (2.3.5), we recognize that the t states are built just like the regular n particle states, but with the t vacuum and time dependent creation

[3]They are not normalized to one. However they are a basis for the physical states in the usual way.

[4]Or between two eigenstates for some other time $t = t'$ as long as they are taken at the same time, since the basis spans the Hilbert space for all times all the information is still present in these inner products.

operators:

$$|\mathbf{p}_1,\cdots,\mathbf{p}_n\rangle_t = \sqrt{\frac{\prod_{j=1}^{n}(2E_{\mathbf{p}_j})}{n!}}\; a^\dagger_{\mathbf{p}_1}(t)\cdots a^\dagger_{\mathbf{p}_n}(t)\,|0\rangle_t\ . \tag{2.3.8}$$

The explicit form of the $a_{\mathbf{p}}(t)$ in terms of the $a_{\mathbf{p}}$ is known exactly from Eq. (2.2.9), which was a shift by a function. In particular, the mixed commutators still give a Dirac delta

$$a_{\mathbf{p}}(t) = a_{\mathbf{p}} + f(t,\mathbf{p}) \qquad \Rightarrow \qquad \left[a_{\mathbf{p}}(t), a^\dagger_{\mathbf{p}}\right] = (2\pi)^3\delta^3(\mathbf{p}-\mathbf{q}), \tag{2.3.9}$$

and the vacua are proportional to a coherent state of each other (a quick overview of coherent states is given in appendix B)

$$\begin{aligned} &a_{\mathbf{p}}(t)\,|0\rangle_t = 0 \quad \Rightarrow \quad 0 = \Big(a_{\mathbf{p}} + f(t,\mathbf{p})\Big)\,|0\rangle_t \quad \Rightarrow \quad a_{\mathbf{p}}|0\rangle_t = -f(t,\mathbf{p})|0\rangle_t,\\ &a_{\mathbf{p}}\,|0\rangle = 0 \quad \Rightarrow \quad 0 = \Big(a_{\mathbf{p}}(t) - f(t,\mathbf{p})\Big)\,|0\rangle \quad \Rightarrow \quad a_{\mathbf{p}}(t)|0\rangle = f(t,\mathbf{p})|0\rangle. \end{aligned} \tag{2.3.10}$$

Applying (2.3.10) and the commutators (2.3.9) to (2.3.7) we quickly find the propagator matrix element

$$\begin{aligned} \langle\mathbf{p}_1,\cdots,\mathbf{p}_n|\,U(t,0)\,|\mathbf{k}_1,\cdots\mathbf{k}_l\rangle &= \left[\prod_{j=1}^{n} e^{-iE_{\mathbf{p}_j}t}\right]\ {}_t\langle\mathbf{p}_1,\cdots,\mathbf{p}_n|\mathbf{k}_1,\cdots\mathbf{k}_l\rangle \\ &= \sqrt{\frac{\prod_{j=1}^{n}(2E_{\mathbf{p}_j})}{n!}}\sqrt{\frac{\prod_{s=1}^{l}(2E_{\mathbf{k}_s})}{l!}}\left[\prod_{j=1}^{n} e^{-iE_{\mathbf{p}_j}t}\right]\ {}_t\langle 0|\,a_{\mathbf{p}_1}(t)\cdots a_{\mathbf{p}_n}(t)\,a^\dagger_{\mathbf{k}_1}\cdots a^\dagger_{\mathbf{k}_l}|0\rangle \\ &= \frac{{}_t\langle 0|0\rangle}{\sqrt{n!l!}}\Bigg\{\prod_{j=1}^{n}\left[e^{-iE_{\mathbf{p}_j}t}f(t,\mathbf{p}_j)\sqrt{2E_{\mathbf{p}_j}}\right]\prod_{s=1}^{l}\left[-f^*(t,\mathbf{k}_s)\sqrt{2E_{\mathbf{k}_s}}\right] \\ &\quad + (2\pi)^3\sum_{j=1}^{n}\sum_{s=1}^{l}(2E_{\mathbf{k}_s})\,e^{-iE_{\mathbf{k}_s}t}\,\delta^3(\mathbf{p}_j-\mathbf{k}_s)\prod_{j'\neq j}\left[e^{-iE_{\mathbf{p}_{j'}}t}f(t,\mathbf{p}_{j'})\sqrt{2E_{\mathbf{p}_{j'}}}\right]\prod_{s'\neq s}\left[-f^*(t,\mathbf{k}_{s'})\sqrt{2E_{\mathbf{k}_{s'}}}\right] \\ &\quad + \quad \text{all combinations with two and more Dirac deltas}\Bigg\}. \end{aligned} \tag{2.3.11}$$

The final equality is gained using the commutation relation (2.3.9) and the actions on the vacuum (2.3.10), it gives one term without any Dirac delta, and nl terms (all the combinations between p's and $k's$) with a single Dirac delta. If both n and l are larger than 1, then there are $n(n-1)l(l-1)$ terms with two deltas (all the combinations for two contractions), and so on until either $n-n$ or $l-l$ is hit. The numerical factor is the same in all instances except that the functions for the indices that appear in the deltas are omitted. To finish the calculation, all that is left is to compute the overlap ${}_t\langle 0|0\rangle$. The absolute value can be follows from the normalization of the physical states, for instance of $|0\rangle$:

$$\begin{aligned}1 = \langle 0|0\rangle = \langle 0|\, U^\dagger(t,0)\, \mathbb{1}\, U(t,0)\, |0\rangle &= \sum_{n=0}^{\infty}\left[\prod_{j=1}^{n}\int \frac{d^3p_j}{(2\pi)^3 2E_{\mathbf{p}_j}}\right] |\langle \mathbf{p}_1, \cdots, \mathbf{p}_n|\, U(t,0)\, |0\rangle|^2 \\ &= \sum_{n=0}^{\infty}\frac{1}{n!}\left[\prod_{j=1}^{n}\int \frac{d^3p_j}{(2\pi)^3}\right] |{}_t\langle 0|\, a_{\mathbf{p}_1}(t)\cdots a_{\mathbf{p}_n}(t)|0\rangle|^2 \\ &= \sum_{n=1}^{\infty}\frac{|{}_t\langle 0|0\rangle|^2}{n!}\left(\int \frac{d^3p}{(2\pi)^3}\ |f(t,\mathbf{p})|^2\right)^n = |{}_t\langle 0|0\rangle|^2\, e^{N_0(t)}\ ,\end{aligned} \tag{2.3.12}$$

Where we recall $N_0(t)$ is the expectation value of the particle number operator given in (2.2.11), leading to

$$|{}_t\langle 0|0\rangle| = e^{-\frac{1}{2}N_0(t)}\ . \tag{2.3.13}$$

The terms in the series in (2.3.12) are also the probabilities for the particle vacuum to decay into n-particle states after a time t. The use of t states simplifies the calculation of these to a few lines, compared to a more standard procedure of projecting onto eigenstates of the Hamiltonian. These probabilities are given by a Poisson distribution with expectation value $N_0(t)$ (as expected), which fully contains the time dependence. The probabilities are normalized to one because of the normalization of the initial time vacuum state $|0\rangle$, i.e. (2.3.12). This just leaves the phase of the overlap ${}_t\langle 0|0\rangle$ as unknown. Because we are primarily interested in the modulus over the overlap to calculate probabilities with, we will just give the result for the phase. The derivation can be found in the appendix of [13]. Writing the overlap as ${}_t\langle 0|0\rangle = |{}_t\langle 0|0\rangle|\, e^{i\varphi(t)}$, the phase $\varphi(t)$ is given by:

$$\varphi(t) = \frac{i}{2}\int_0^t dx^0 \int \frac{d^3p}{(2\pi)^3}\left[\partial_{x^0} f^*(x^0,\mathbf{p})\, f(x^0,\mathbf{p}) - f^*(x^0,\mathbf{p})\,\partial_{x^0} f(x^0,\mathbf{p})\right]\ . \tag{2.3.14}$$

2.3.2 One particle scattering

As a concrete example of a nontrivial scattering amplitude, we will consider the scattering of a single initial state particle with the classical static source. Since there are no other interactions by which virtual particles can mediate the interaction, we would expect that the particle seems like a free particle as long as it misses the source. We will show explicitly that this expectation holds. We write down the single particle initial state as

$$|\psi_1\rangle = \int \frac{d^3k}{(2\pi)^3 2E_{\mathbf{k}}}\ \psi_1(\mathbf{k})\ |\mathbf{k}\rangle,\ . \tag{2.3.15}$$

Moreover, we define $\psi_0(t;\mathbf{p}_1,\cdots,\mathbf{p}_n)$ as the n-particle partial wave of the time evolved initial $t=0$ vacuum

$$\psi_0(t;\mathbf{p}_1,\cdots,\mathbf{p}_n) = \langle \mathbf{p}_1,\cdots,\mathbf{p}_n|\, U(t,0)\, |0\rangle = \frac{{}_t\langle 0|0\rangle}{\sqrt{n!}}\prod_{j=1}^{n}\left[e^{-iE_{\mathbf{p}_j}t} f(t,\mathbf{p}_j)\sqrt{2E_{\mathbf{p}_j}}\right], \tag{2.3.16}$$

which is computed from (2.3.11), and we know its modulus from (2.3.12). It will be convenient to recognize in the scattering amplitude formula. For $n=0$ it is the survival amplitude of the particle vacuum which is given by $\psi_0(t) = {}_t\langle 0|0\rangle$. For a single particle in the initial state, the only nonzero terms in (2.3.11) are

$$\begin{aligned}\langle \mathbf{p}_1 \cdots \mathbf{p}_n|\, U(t,0)\,|\psi_1\rangle = &-\psi_0(t;\mathbf{p}_1\cdots\mathbf{p}_n)\int \frac{d^3k}{(2\pi)^3\sqrt{2E_{\mathbf{k}}}}\, f^*(t,\mathbf{k})\,\psi_1(\mathbf{k}) \\ &+\frac{1}{\sqrt{n}}\sum_{j=1}^{n}\Big[\psi_1(\mathbf{p}_j)\,e^{-iE_{\mathbf{p}_j}t}\;\psi_0(t;\mathbf{p}_1,\cdots\mathbf{p}_{j-1},\mathbf{p}_{j+1},\cdots,\mathbf{p}_n)\Big]\,.\end{aligned} \tag{2.3.17}$$

The simplest cases to consider are for $n = 0$ or $n = 1$. In the $n = 0$ case the sum in the second term is empty, so the only term is the absorption of the incoming particle by the source, but nothing is emitted as a result. For $n = 1$ there is a contribution where the particle is absorbed and re-emitted, and a contribution where it does not interact with the source and propagates freely. Diagrammatically, for $n = 1$ the amplitude can be understood as

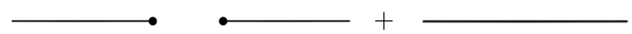
, (2.3.18)

corresponding to the amplitude given by

$$\langle \mathbf{p}|\, U(t,0)\,|\psi_1\rangle = -\psi_0(t;\mathbf{p})\int \frac{d^3k}{(2\pi)^3\sqrt{2E_{\mathbf{k}}}}\, f^*(t,\mathbf{k})\,\psi_1(\mathbf{k}) + \big[\psi_1(\mathbf{p})\,e^{-iE_{\mathbf{p}}t}\;\psi_0(t)\big]\;, \tag{2.3.19}$$

The first term on the RHS contains the amplitude $\psi_0(t;\mathbf{p})$ describing the emission of a particle with momentum $\mathbf{p}$ out of the initial particle vacuum after a time t has elapsed, multiplied by the amplitude for the annihilation of the original state $|\psi_1\rangle$. It includes all vacuum contributions with creation and annihilation of an arbitrary number of particles. The second term on the RHS contains the amplitude for the free propagation of $|\psi_1\rangle$ multiplied by the vacuum survival amplitude $\psi_0(t)$, which also includes the creation and subsequent annihilation of any number of particles.
The above pictures are strictly speaking not Feynman diagrams, since we are not doing a perturbative expansion and $\psi_0(t;\mathbf{p}_1,\cdots,\mathbf{p}_n)$ implicitly contains many contributions of creation and annihilation of intermediate particles. Yet they offer an intuitive picture for the process. The general structure for n outgoing particles is largely similar. In general the amplitude can be diagrammatically written as

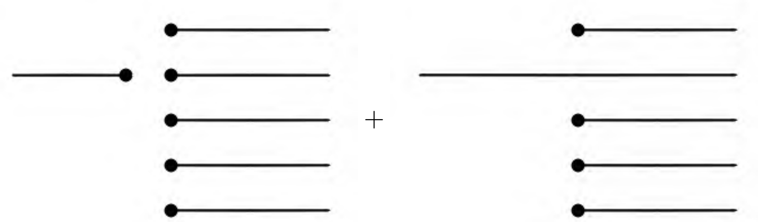
. (2.3.20)

The first term can be understood as the probability amplitude that the initial particle is absorbed by the source, times the n-particle wave-function of the vacuum. The second part is the free-particle wave-function $\psi_i(\mathbf{p})e^{-iE_{\mathbf{p}}t}$ times the $(n-1)$-particles vacuum contribution, where the $\mathbf{p}_j$ is excluded from the vacuum contribution. The summation ensures that this contribution is manifestly symmetric in the exchange of any identical particle, and the $1/\sqrt{n}$ gives the proper normalization to 1. The full dynamics can be understood as the interference between three components: the decay of the vacuum, the amplitude for absorption of the initial particle, and the free propagation of the original mode. The vacuum decay is a necessary component

of the scattering; if the vacuum did not decay, there would have been no scattering.
Is it instructive to examine the absorption amplitude in terms of integrals over space rather than momentum, calling $\psi_1(x)$

$$\psi_1(x) = \int \frac{d^3p}{(2\pi)^3 2E_{\mathbf{p}}}\, e^{-ip\cdot x}\psi_1(\mathbf{p}), \tag{2.3.21}$$

the wave function in space-time that the original state would have if it were a free system, making use of the definition of $f(t,\mathbf{k})$ in (2.2.8), we have

$$\begin{aligned}\mathcal{A}(t) &= -\int \frac{d^3k}{(2\pi)^3\sqrt{2E_{\mathbf{k}}}}\, f^*(t,\mathbf{k})\,\psi_1(\mathbf{k}) = -i\,g\int_0^t dy^0 \int d^3y \int \frac{d^3k}{(2\pi)^3 2E_{\mathbf{k}}}\,\rho(\mathbf{y})\,e^{-ip\cdot y}\psi_1(\mathbf{k}) \\ &= -i\int_0^t dy^0 \int d^3y\; g\,\rho(\mathbf{y})\;\psi_1(y).\end{aligned} \tag{2.3.22}$$

This absorption amplitude vanishes if the time integral of the overlap between the free-like wave-function $\psi_1(x)$ and the classical source is vanishing. This corresponds to the intuitive notion of “the wave-packet misses the classical source”, i.e.

$$\rho(\mathbf{x})\psi_1(x) = 0, \qquad \forall\, x^0 \in [0,t],\ \forall\, \mathbf{x} \in \mathbb{R}. \tag{2.3.23}$$

Because of the exact and general (2.3.17), if the amplitude $\mathcal{A}$ is vanishing the only remaining part of the dynamics is the eventual decay of the vacuum, in the form of the ψ_0's, in an appropriate symmetric combination with the free-like part. It is not possible to remove the vacuum decay, but we can look at the conditional probability that no extra particles come from the vacuum decay. That is, we normalize the probability amplitudes by dividing by $\int \frac{d^3\mathbf{p}}{(2\pi)^3 2E_{\mathbf{p}}}|\langle \mathbf{p}|U|\psi_1\rangle|^2$, so the probabilities are conditional on the observation of ‘one particle goes in, one particle comes out’, while keeping the original phase in the wave functions. This operation also corresponds to the ‘collapse’ of the wave function if the final state is measured to contain one particle only. By construction, the resulting wave functions are normalized to 1. When the absorption amplitude is zero, the resulting one particle wave function after scattering is

$$e^{i\varphi(t)}\; e^{-iE_{\mathbf{p}}t}\psi_1(\mathbf{p})\ . \tag{2.3.24}$$

This is almost the wavefunction of a free particle in the Schrödinger picture. The energy phase e^{-iEt} is a consequence of the time evolution of the states for free fields. The phase $e^{i\varphi}$ is not, but it can be removed from the theory without changing the equations of motion since it corresponds to a (time-dependent) phase-convention of the basis, rather than any physical observable. Since $\varphi(t)$ is given as a time integral (2.3.14), it is possible to add the function $-\partial_t\varphi(t)$ to the Lagrangian of the system to compensate for this phase in the final formulas.
In this sense, for a vanishing overlap $\mathcal{A}(t) = 0$, the elastic scattering with the classical source $g\rho$ is trivial and indistinguishable from a free particle. The nontrivial dynamics involve the creation of and interference with the extra particles from the vacuum decay. It goes without saying that the elastic scattering is not trivial for a non-vanishing $\mathcal{A}$. In that case the normalized partial wave is given by:

$$\Big[\mathcal{A}(t)\,\psi_0(t;\mathbf{p})\;+\;\psi_0(t)\,e^{-iE_{\mathbf{p}}t}\psi_i(\mathbf{p})\Big]\,\frac{\exp\big[\frac{1}{2}N_0(t)\big]}{\sqrt{|\mathcal{A}(t)|^2\,\big[N_0(t)-2\big]+1}}. \tag{2.3.25}$$

This will be zero if $\sqrt{2E_{\mathbf{p}}}f(t,\mathbf{p})$ happens to be exactly equal to the starting ψ_1, $f(t,\mathbf{p})\sqrt{2E_{\mathbf{p}}}=\psi_1(\mathbf{p})$. All of this can be extended to the case of multi-particle initial states. Instead of one absorption amplitude there are amplitudes for the absorption of one or more of the initial particles, the vacuum decays as in the one particle case, and the initial state that evolves freely.

2.4 Vacuum decay and Schwinger mechanism

In the previous subsection we have seen that the initial particle vacuum $|0\rangle$ is not an energy eigenstate and so it will decay and produce particles. Conceptually, We then have a situation quite similar to the Schwinger mechanism, in which particle-antiparticle pairs are created from an initial vacuum in the presence of a strong static electric field. There are however some interesting differences in the result. In (2.3.12) we can see the probability distribution for the particle vacuum to decay into n particle after a time t has elapsed. This gives a Poisson distribution with the expectation value found earlier in (2.2.11), that is

$$\begin{aligned} P_{0\to n}(t) &= \frac{e^{-N_0(t)}}{n!}\,\Big[N_0(t)\Big]^n\,, \\ N_0(t) &= \langle 0|\,N(t)\,|0\rangle = 2\int\frac{d^3p}{(2\pi)^3}\Big(1-\cos(E_{\mathbf{p}}t)\Big)\,|h(\mathbf{p})|^2\,. \end{aligned} \tag{2.4.1}$$

The function $h(\mathbf{p})$ is a weighted Fourier transform of the source $g\rho(\mathbf{x})$, given in (2.2.8). As expected, in the limit of $t\to 0$ the expectation value is 0 and so the vacuum is stable. The limit $t\to\infty$ depends on the form of the source. Later on we will look into some specific forms of ρ, but right now we can already argue that it is finite. The integral can be re-written as an integral over energy and angle (which is bounded), and is absolutely convergent. Therefore the Riemann-Lebesgue lemma applies which says that in the limit of $t\to\infty$ the oscillatory term goes to 0, meaning the expectation value goes to the finite nonzero positive value:

$$\lim_{t\to\infty}N_0(t) = 2\int\frac{d^3p}{(2\pi)^3}\,|h(\mathbf{p})|^2 < \infty\,. \tag{2.4.2}$$

This implies that the particle production rate goes to zero for large times, leaving us with a finite amount of particles (or particle density for large volumes), without any need to turn off the source. Since the derivation of subsection 2.3 was valid even for time dependent sources, the source can of course be chosen so that it turns off after some time. This is already in stark contrast with the Schwinger mechanism, where the particle production rate is constant, so the number of particles is linear in time.

As a short aside, one could think that there might be a different initial state which is with no particles stable. However we can see that there is no state that fulfills such a generalized definition of a vacuum that has zero particle number expectation value for all times. Of course the lowest energy eigenstate is stable, but we have seen earlier that this is not a particle number eigenstate. The argument that there is no such state then looks at time $t=0$, for which an arbitrary pure state $|\psi\rangle$ has particle number expectation value

$$\int\frac{d^3p}{(2\pi)^3}\,\langle\psi|\,a^\dagger_{\mathbf{p}}a_{\mathbf{p}}\,|\psi\rangle = \int\frac{d^3p}{(2\pi)^3}\,|a_{\mathbf{p}}\,|\psi\rangle|^2\,. \tag{2.4.3}$$

This is only zero when $a_{\mathbf{p}} |\psi\rangle = 0$ for all $\mathbf{p}$. Since there is no other degree of freedom other than the field ϕ, this is only true for the unique state $|0\rangle$. This argument generalizes to mixed states as well, because the density matrix eigenvalues are non-negative. Since $|0\rangle$ is the only state that fulfills zero particle number at $t = 0$, and for $t > 0$ it has a nonzero particle number expectation value as per (2.2.11), it must be that a state with zero particle number expectation value for all time does not exist.

2.4.1 Quantum Zeno effect

The (quantum) Zeno effect [50, 51, 52, 53, 54] is a phenomenon where repeated measurements shortly after one another can freeze the system into the initial state. It is a general consequence of QM and QFT provided the expectation value of the Hamiltonian is finite [51]. It can be identified by the condition $P'(0) = 0$, which also implies that the survival probability for short times is not given by an exponential. It is measured for example in cavity QED [55, 56] and is speculated to have an effect in Hawking radiation in large black holes [57]. We can show the occurrence of the Zeno effect explicitly for the decay law given by (2.4.1). Namely, the vacuum survival probability

$$P_{0\to 0}(t) = \exp\left\{-2\int \frac{d^3q}{(2\pi)^3}\Big(1-\cos(E_{\mathbf{q}}t)\Big)\left|h(\mathbf{q})\right|^2\right\} \tag{2.4.4}$$

can be expanded for short times:

$$\exp\left\{-\int \frac{d^3q}{(2\pi)^3}E_{\mathbf{q}}^2t^2\left|h(\mathbf{q})\right|^2\right\} = e^{-\frac{t^2}{\tau_Z^2}}\ , \tag{2.4.5}$$

where we define a 'Zeno time' τ_Z by

$$\frac{1}{\tau_Z^2} \equiv \int \frac{d^3q}{(2\pi)^3}E_{\mathbf{q}}^2\left|h(\mathbf{q})\right|^2. \tag{2.4.6}$$

We then look at the situation where we have repeated measurements of the vacuum and whether or not it survived. We let the system evolve over a (possibly large) time T with N measurements separated by equally spaced small time intervals $t = T/N$. For the vacuum to survive at time T, it needs to survive at each measurement, meaning

$$P_{0\to 0}(T) = (P_{0\to 0}(t))^N \approx \exp\left[-N\frac{t^2}{\tau_Z^2}\right] = \exp\left[-\frac{1}{N}\frac{T^2}{\tau_Z^2}\right]. \tag{2.4.7}$$

given N is chosen sufficiently large so that t is sufficiently small, the short time behavior of the survival probability now also determines the behavior for long times T. Furthermore, for a given time T, N can be chosen arbitrarily large, which makes the survival probability approach 1, preserving the initial state which would normally be prone to change over time. Moreover, upon inspection of (2.4.4), we can reason there is no regime where an exponential decay law is a good approximation. For small times the leading behavior is given by (2.4.5), after which the oscillatory behavior becomes relevant. At large time the oscillation dies out and the particle number expectation value becomes a non-vanishing constant (2.4.2).

2.4.2 Numerical examples

As a computational example, and to illustrate the time dependence, we will compute the probability distribution for two different forms of the external source, one which has a Gaussian distribution and one which is constant (flat) inside a finite box. We will take them of the forms:

$$g\rho_1(\mathbf{x}) = g\, m^3 \, \exp\left(-\pi\frac{\mathbf{x^2}}{L^2}\right), \tag{2.4.8}$$

$$g\rho_2(\mathbf{x}) = g\, m^3\, \theta\left(\frac{L}{2}-x\right)\theta\left(\frac{L}{2}+x\right)\theta\left(\frac{L}{2}-y\right)\theta\left(\frac{L}{2}+y\right)\theta\left(\frac{L}{2}-z\right)\theta\left(\frac{L}{2}+z\right)\ , \tag{2.4.9}$$

where g is the same dimensionless coupling constant we used before which determines the strength of the interaction, and L is a length parameter that determines the volume of the sources. The sources are normalized such that their total charges and strengths at the origin are equal: $\int d^3\mathbf{x} g\rho_1(\mathbf{x}) = \int d^3\mathbf{x} g\rho_2(\mathbf{x}) = g\, m^3 L^3$, and $\rho_1(0) = \rho_2(0) = g\, m^3$. For the expectation value we need the weighted Fourier transforms of the sources (2.2.8), which are given by

$$h_1(\mathbf{p}) = -\frac{g}{(\mathbf{p^2}+m^2)^{3/4}}\, m^3 L^3\, e^{-\frac{p^2L^2}{4\pi}}, \tag{2.4.10}$$

$$h_2(\mathbf{p}) = -\frac{g}{(\mathbf{p^2}+m^2)^{3/4}}\frac{8m^3\sin\left(\frac{Lp_x}{2}\right)\sin\left(\frac{Lp_y}{2}\right)\sin\left(\frac{Lp_z}{2}\right)}{p_xp_yp_z}, \tag{2.4.11}$$

where p_x, p_y, p_z are the components of the 3-momentum $\mathbf{p}$. This allows us to compute the integral (2.4.1) numerically. Since the mass is the only parameter with dimension of energy for this form of the sources, we will set the mass $m = 1$. Consequently the time t and length-scale L will be expressed in units of $1/m$. The dependence on g is simple: $N_0(t)$ scales with g^2, even though the result is non-perturbative, and the dependence on L has no simple form except in the large L limit, which we look at shortly. The particle number expectation value for both types of sources with g and L set to 1 is shown in figure 2.1, where we can see that saturation of the particle expectation value sets in quite quickly. The vacuum survival probability for the Gaussian source and its short time approximation are shown in figure 2.2.

Connecting back to the dilaton, the scalar glueball, which is thought to have a mass of around 1.7 Gev, the units of time are approximately $4 \cdot 10^{-25}$ seconds. Looking at figure 2.1, the particle number expectation value is close to saturation after about 5-10 units of $m\,t$, putting the typical timescale for the vacuum decay for dilatons in the order of 10^{-24} seconds, or $\sim 1\,\mathrm{fm}/c$, a typical timescale for QCD processes.

In figure 2.3 the vacuum survival probabilities are compared with an exponential approximation of the form $z_i + (1-z_i)\exp\{-\Gamma t\}$, where z_i is the saturation value found by taking the exponent of (2.4.2), the index $i = 1, 2$ denotes which shape of the source i.e. (2.4.10) or (2.4.11) it belongs to. We have also taken $\Gamma \sim m$ and $g = 1$, but scaling to $g \neq 1$ is done simply by taking the probability to the power of g^2. The choice $\Gamma = m$ is arbitrary and is chosen just for illustrative purposes in order to show that an exponential does not lead to a good description of the actual survival probability. The only regime where the exponential approximation is close is at large times when the fluctuations around the saturation value are too small. A better description of the theoretical curve could be obtained by a modified exponential fit where the saturation is implemented on the level of the probability amplitude $a_{i\to f}(t)$. If we instead take

$$a_{i\to f}(t) = z + (1-z)e^{i\alpha t + \frac{\Gamma}{2}t}, \tag{2.4.12}$$

and take the modulus squared, we find a probability with oscillations just like the full expression. In figure 2.4 the survival probability in the presence of a flat source is compared with a modified exponential fit. The frequency of the oscillations is not quite accurate but otherwise it provides a much better description than a

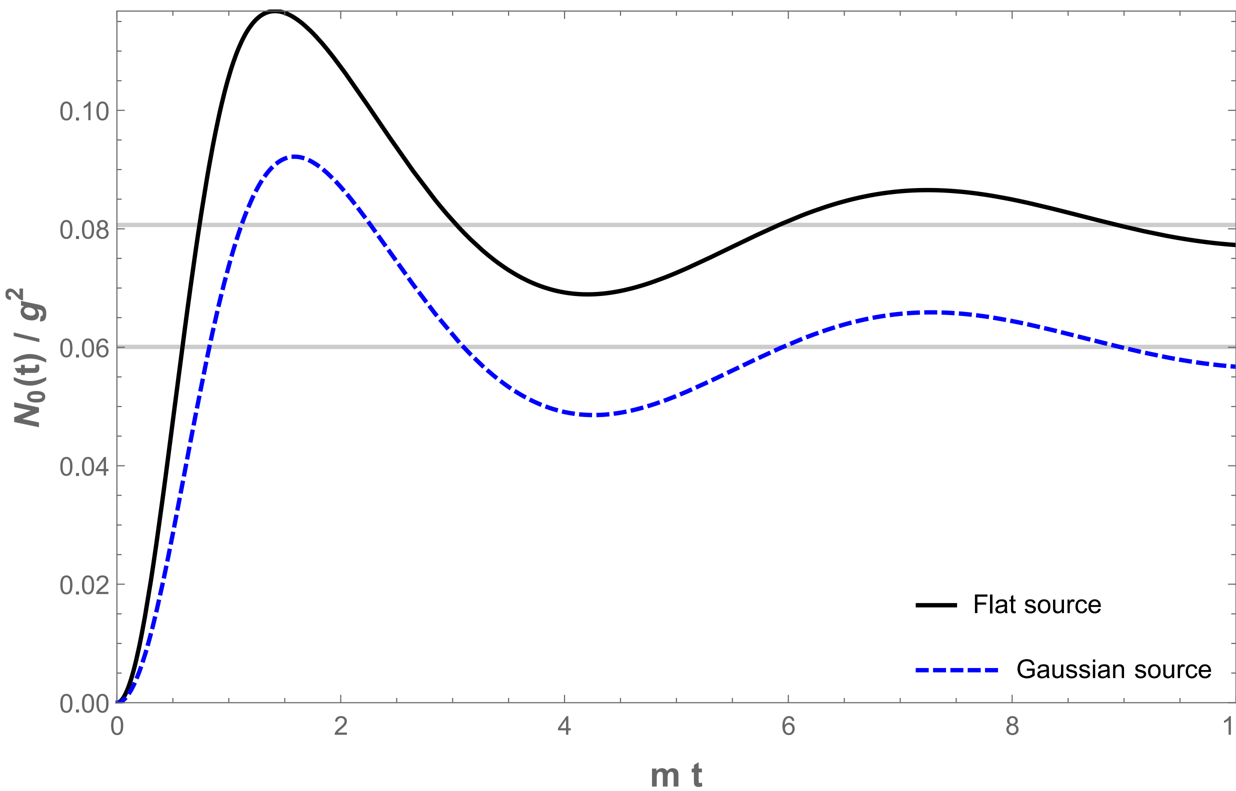

Figure 2.1: Expectation value for the number of particles produced for the different sources as a function of time. The parameters g and m are absorbed in the expectation value and time units respectively, and we use $L = 1$ (in $1/m$ units). The grey lines are the infinite time asymptotes found by setting the oscillatory term to 0.

simple exponential. Similar oscillations, but not decays also occur in cases of mixing of bosonic fields [61, 62], which in turn might be relevant for neutrino oscillations [63].

2.4.3 Large volume limit

The limit in which the size of the classical source is much larger than the scales probed by the system is of course a simplification which is however interesting for practical purposes, and becomes more accurate the larger the particle's mass m becomes. In our system, this large volume limit can be explicitly computed for both sources. Starting with the Gaussian shaped source, the particle number expectation value per volume element L^3 is found using (2.4.1):

$$\frac{1}{L^3} N_0(t) = 2 \int \frac{d^3\mathbf{p}}{(2\pi)^3} \left(1 - \cos(E_{\mathbf{p}} t)\right) \frac{g^2}{(\mathbf{p}^2 + m^2)^{3/2}} m^6 L^3 \, e^{-\frac{p^2 L^2}{2\pi}}. \tag{2.4.13}$$

Clearly particle density becomes a better observable than the particle number since it would just diverge together with the volume. For taking the large volume limit, that is $L \to \infty$, we will want to identify representations of the Dirac delta function. For the Gaussian source, the relevant representation of the Dirac delta is

$$\delta(x) = \lim_{\epsilon \to 0^+} \frac{e^{-x^2/4\epsilon}}{2\sqrt{\pi\epsilon}} \tag{2.4.14}$$

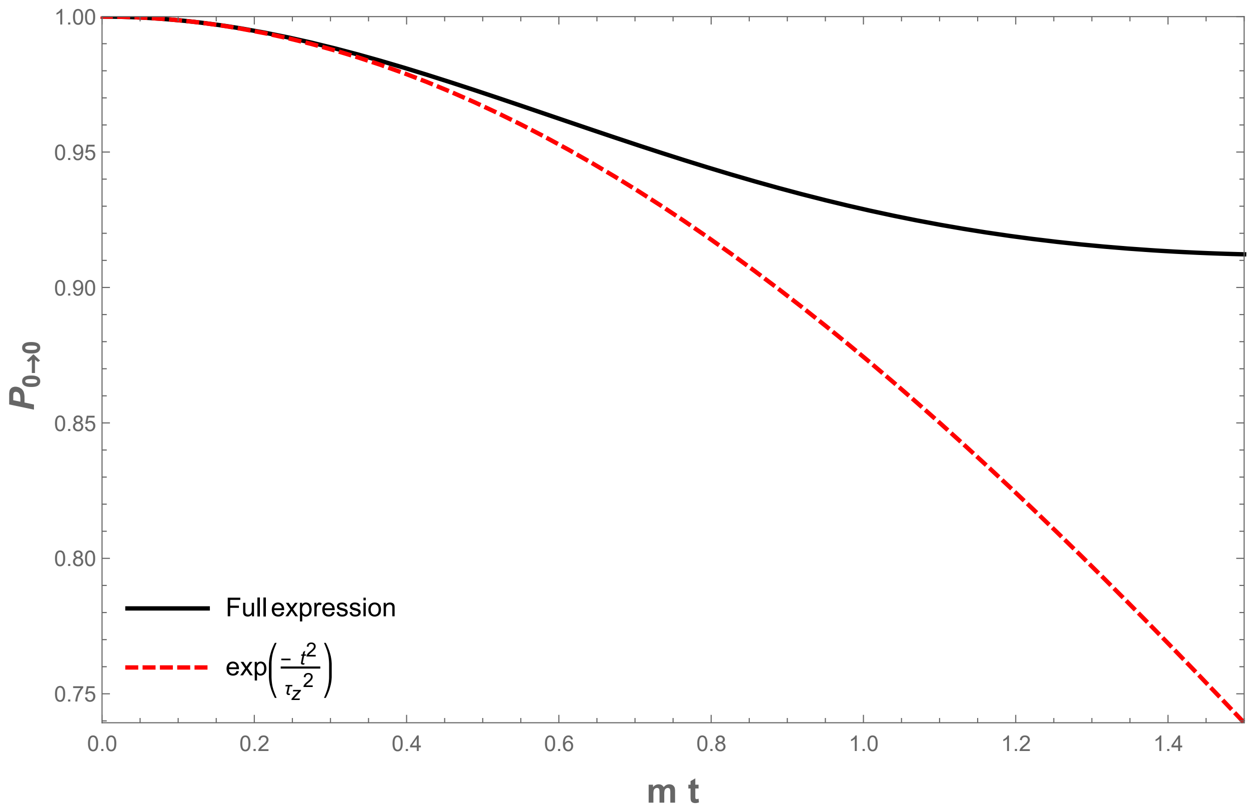

Figure 2.2: Vacuum survival probability with a Gaussian source, compared with the small time behaviour found in (2.4.5). The parameter m is absorbed in the time units, and $g = 1$ and $L = 1$ are used.

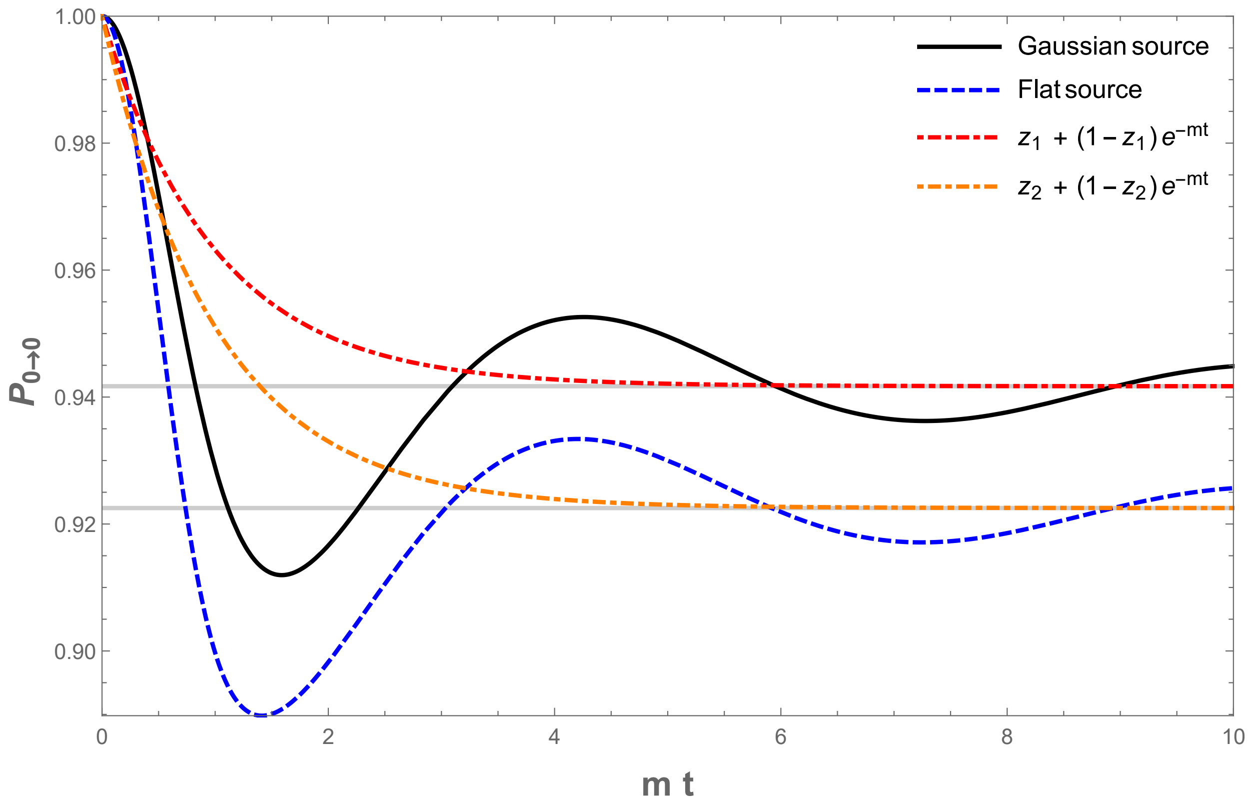

Figure 2.3: Vacuum survival probability with both sources with a longer timescale, compared with a exponential decay which saturates to a non-zero value at infinity. The parameter m is absorbed in the time units, and we set $L = 1$ in units of $1/m$, and $g = 1$. The grey lines indicate the asymptotic values for the survival probability for the two different sources.

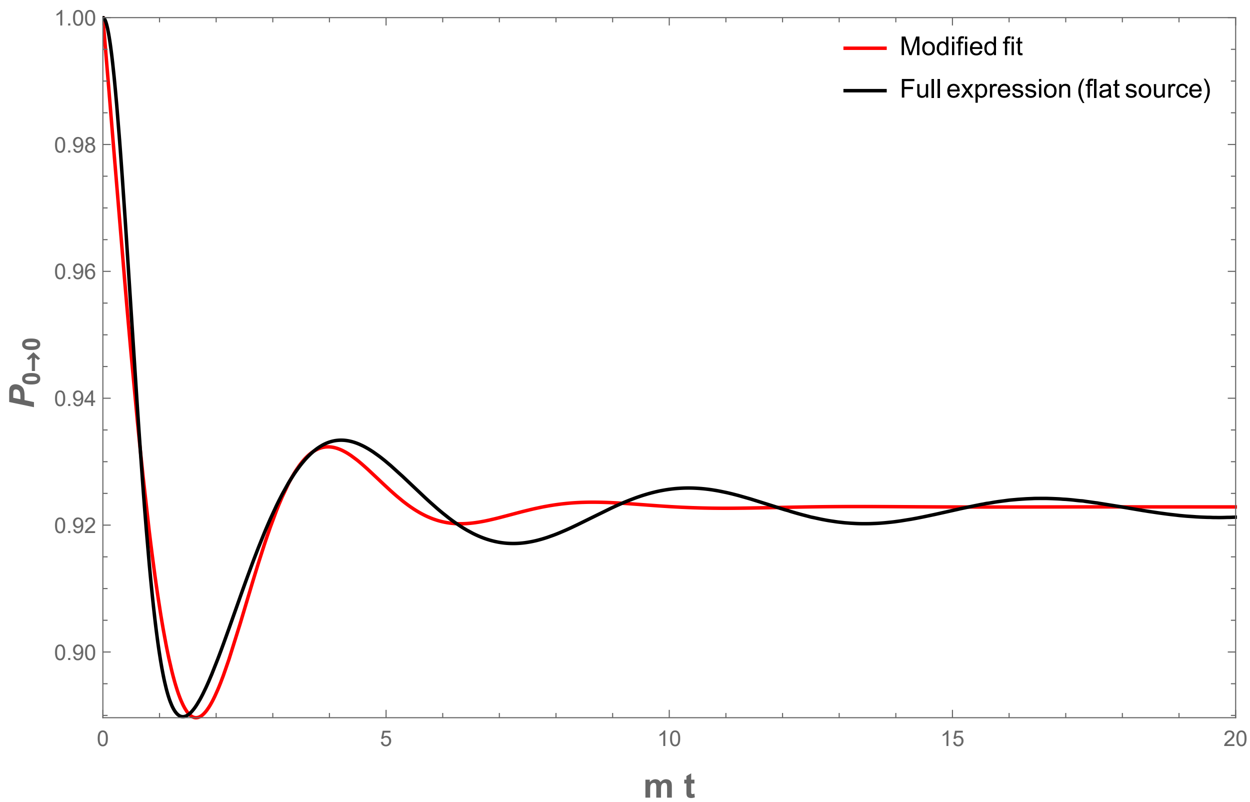

Figure 2.4: Vacuum survival probability with a constant source, compared with a fit using a modified exponential probability amplitude (2.4.12). The parameter m is absorbed in the time units, and $g = 1$ and $L = 1$ are used.

Renaming $\frac{L^2}{2\pi} = \frac{1}{4\epsilon}$ on the RHS of (2.4.13) this form of the Dirac deltas will be more easily identifiable:

$$\frac{1}{L^3} N_0(t) = 2 \int \frac{d^3\mathbf{p}}{(2\pi)^3} \left(1 - \cos(E_{\mathbf{p}} t)\right) \frac{g^2 m^6}{(\mathbf{p}^2 + m^2)^{3/2}} \pi^3 \sqrt{8} \left(\frac{e^{-p_x^2/4\epsilon}}{2\sqrt{\pi\epsilon}}\right) \left(\frac{e^{-p_y^2/4\epsilon}}{2\sqrt{\pi\epsilon}}\right) \left(\frac{e^{-p_z^2/4\epsilon}}{2\sqrt{\pi\epsilon}}\right). \tag{2.4.15}$$

When we take the large volume limit $L \to \infty$ which implies $\epsilon \to 0^+$ the last 3 factors approach delta functions of the components of $\mathbf{p}$. Evaluating the momentum integral with these delta functions gives

$$\frac{1}{L^3} N_0(t) = \frac{g^2}{\sqrt{2}} m^3 (1 - \cos(mt)). \tag{2.4.16}$$

Similarly, in the computation for the square source we will need the following representation of the Dirac delta:

$$\delta(x) = \lim_{L \to \infty} \frac{\sin^2(L\,x)}{\pi L\, x^2} \tag{2.4.17}$$

Using the weighted Fourier transform of the flat source (2.4.11) in the expectation value (2.4.1) gives

$$\frac{1}{L^3} N_0(t) = 2 \int \frac{d^3\mathbf{p}}{(2\pi)^3} \left(1 - \cos(E_{\mathbf{p}} t)\right) \frac{g^2}{(\mathbf{p}^2 + m^2)^{3/2}} \frac{64 m^6}{L^3} \left[\frac{\sin^2(L p_x/2)}{p_x^2}\right] \left[\frac{\sin^2(L p_y/2)}{p_y^2}\right] \left[\frac{\sin^2(L p_z/2)}{p_z^2}\right]. \tag{2.4.18}$$

Once again, we bring it into the form where Dirac deltas are easily identifiable:

$$\frac{1}{L^3} N_0(t) = 2 \int \frac{d^3\mathbf{p}}{(2\pi)^3} \left(1 - \cos(E_{\mathbf{p}} t)\right) \frac{g^2 m^6}{(\mathbf{p}^2 + m^2)^{3/2}} \pi^3 \left[\frac{\sin^2(L p_x/2)}{\pi L (p_x/2)^2}\right] \left[\frac{\sin^2(L p_y/2)}{\pi L (p_y/2)^2}\right] \left[\frac{\sin^2(L p_z/2)}{\pi L (p_z/2)^2}\right] \tag{2.4.19}$$

In the limit $L \to \infty$ the sinc squared functions become delta functions of the components of $\mathbf{p}/2$, which gives 8 times the delta function of $\mathbf{p}$ and we find

$$\frac{1}{L^3} N_0(t) = 2 g^2 m^3 (1 - \cos(mt)). \tag{2.4.20}$$

Taking this limit does not commute with taking the $t \to \infty$ limit, as here the oscillation does not die down anymore since the integral is already evaluated. Taking the infinite time limit before the volume limit, the oscillatory term vanishes while leaving the rest of the derivation entirely the same. Then the large volume and infinite time limit is

$$\begin{aligned} \lim_{L\to\infty} \lim_{t\to\infty} \frac{1}{L^3} N_0(t) &= 2 g^2 m^3 \qquad\qquad \text{(flat source)}, \\ \lim_{L\to\infty} \lim_{t\to\infty} \frac{1}{L^3} N_0(t) &= \frac{g^2}{\sqrt{2}} m^3 \qquad\quad \text{(Gaussian source)}. \end{aligned} \tag{2.4.21}$$

Most of this result could have been guessed only using dimensional analysis, since both sides have dimension mass^3, and m is the only dimensionful parameter left after taking the $L \to \infty$ and $t \to \infty$ limits. The dependence on g simply stays as g^2. Curiously though, the prefactor depends on the shape of the source and on how its volume is defined. In this sense the flat source gives the same result using the informal statement '$\delta^3(0) \to (2\pi)^3 V$', but for the Gaussian source it does not.

These results are qualitatively different from the Schwinger mechanism, where the particle production rate is constant, so the number of particles is linear in time and diverges for $t \to \infty$. This divergence is of course unphysical. In this simpler theory we can calculate the full result exactly up to all orders, which tells us that the particle production rate goes to zero, making it unnecessary to turn the source off. Since the derivation of subsection 2.3 was valid even for time dependent sources, the source can of course be turned off, even in a non-adiabatic way.

2.5 Comparison to literature

The quantum field theory of a real scalar field coupled to a classical external source is one of the simplest interacting QFTs one can write down. Unsurprisingly, It has been studied in the past and it has been mentioned or discussed in textbooks as an example of calculations in QFT, see e.g. [19, 20, 21, 22]. For a time dependent source $\rho(t, \mathbf{x})$ which is Fourier transformable in spacetime, it is commonly accepted that the dynamics can be nontrivial. The case of a time independent source is then treated as a limit of the time dependent case. Specifically, the time independent classical source is multiplied by an adiabatic function of time that switches off the interaction in the distant past and future. In the limit where the interaction persists for infinite amount of time, the scattering matrix is found to be essentially the identity matrix. This is usually assumed to imply an equivalence between the interacting system (without the adiabatic function) and a free quantum field theory and so there is no scattering. Since some of the intuitive statements commonly used are incomplete, and it is easy to miss some fundamental conceptual steps looking just at the scattering matrix, we will go into a more detailed discussion.

In this subsection we will take a closer look at the reasons why the results of this chapter, where we found nontrivial scattering amplitudes, contradict the results found in the literature. We will refer in particular to the analysis in the seminal lectures on QFT by Coleman [20], since the treatment is rather extensive and it inspired some of the other books on QFT, such as [22], especially on the triviality of scattering on a time independent source. The starting point is the exact solution for the case of a time dependent source, obtained by resumming all the terms of the Dyson series [20]. Written in the notation of this chapter, the scattering matrix reads

$$\begin{aligned} S = U_I(\infty, -\infty) =: \exp \Bigg\{ &-\frac{g^2}{2} \int d^4x \int d^4y \, \rho(x)\rho(y) \, \Delta_F(x-y) \\ &-ig \int d^4x \int \frac{d^3p}{(2\pi)^3\sqrt{2E_{\mathbf{p}}}} \left[\rho(x) e^{-ip\cdot x} \, a_{\mathbf{p}} + \rho(x) e^{ip\cdot x} \, a^\dagger_{\mathbf{p}} \right] \Bigg\} : . \end{aligned} \tag{2.5.1}$$

This formula makes sense for a fast decreasing (and hence Fourier transformable in spacetime) classical source $\rho(x)$. In particular the field is asymptotically free in the far past and far future $(\Box + m^2)\phi \to 0$ as $t \to \pm\infty$ by the assumption that the source decreases fast enough in both space and time. Making use of the momentum integrated form of the Feynman propagator

$$\Delta_F(x-y) = \int \frac{d^3p}{(2\pi)^3 2E_{\mathbf{p}}} \left[\theta(x^0 - y^0) e^{-ip\cdot(x-y)} + \theta(y^0 - x^0) e^{ip\cdot(x-y)} \right], \tag{2.5.2}$$

it can be shown that the first term in the right hand side of (2.5.1) is ${}_t\langle 0|0\rangle_{t_0}$ in the $t \to \infty$ and $t_0 \to -\infty$ limit. This uses a generalized form of the function $f(t, \mathbf{p})$ which reduces to (2.2.8) for $t_0 \to 0$ and a time independent source:

$$f(t,t_0,p) = i\,g\int_{t_0}^{t} dy^0 \int d^3y\,\frac{\rho(y)}{\sqrt{2E_{\mathbf{p}}}}\,e^{ip\cdot y}. \tag{2.5.3}$$

With this, the relations between the $|\cdots\rangle_t$ and $|\cdots\rangle$ bases can be generalized to the $|\cdots\rangle_t$ and $|\cdots\rangle_{t_0}$ bases using the same arguments, using propagators $U(t,t_0)$ instead of $U(t,0)$. The second term which involves the creation operator reads

$$\exp\left\{-\int \frac{d^3p}{(2\pi)^3}\,f(\infty,-\infty;\mathbf{p})\,a^\dagger_{\mathbf{p}}\right\}, \tag{2.5.4}$$

and the term with the annihilation operator is its Hermitian conjugate:

$$\exp\left\{-\int \frac{d^3p}{(2\pi)^3}\,f^*(\infty,-\infty;\mathbf{p})\,a_{\mathbf{p}}\right\}\ . \tag{2.5.5}$$

Because of the normal ordered product the two terms factorizes into the two exponentials separately, with the creation term on the left and the annihilation one on the right, since within normal ordered products the creation and annihilation operators commute. The matrix elements of the S matrix (2.5.1) can also be written down as the limit

$$\langle\mathbf{p}_1,\cdots,\mathbf{p}_n|S|\mathbf{q}_1,\cdots,\mathbf{q}_m\rangle = \lim_{t_-\to-\infty}\left[\lim_{t_+\to\infty}\left({}_{t_+}\langle\mathbf{p}_1,\cdots,\mathbf{p}_n|\mathbf{q}_1,\cdots,\mathbf{q}_m\rangle_{t_-}\right)\right]. \tag{2.5.6}$$

This is essentially (2.3.6) but generalized to a time dependent source and infinite time limits. In the usual approach it is then assumed that the scattering matrix for the time independent case follows from the time dependent one (2.5.1) in a certain limit. Since the expression in (2.5.1) requires a classical source which is also Fourier transformable in time, and not only in space, one considers the particular case of $\rho(t,\mathbf{x}) = s(t)\rho(\mathbf{x})$. The (smooth) adiabatic function $s(t)$ has the following properties:

$$0\le s(t)\le 1, \qquad s(t)=1\,\forall|t|<\frac{T}{2}, \qquad \lim_{t\to\pm\infty} s(t)t^n = 0 \quad \forall n\in\mathbb{Z}^+. \tag{2.5.7}$$

This adiabatic function effectively switches the interaction on in the distant past and off again in the far future, done in a Fourier transformable way while keeping the interaction in the bulk $t\in\{-T/2,T/2\}$ the same as the required time independent one. After this, over a time $\Delta\ge 0$, the function adiabatically goes to zero. The intuitive idea is that in the limit of $T\to\infty$ one recovers the full time-independent theory, and the limit $\Delta\to\infty$ makes the transition adiabatic. This procedure works well in other cases, but not for this theory, despite the fact that for a sudden (non-adiabatic) switch $s(t)=\theta(t+T/2)\theta(T/2-t)$ equation (2.5.6) is fulfilled in the $T\to\infty$ limit[5]. The conditions in (2.5.7) should be supplemented to fully describe the adiabatic function, as already mentioned in the lectures [20]. In order to recover the correct imaginary part of the function in (2.5.1) in the $T\to\infty$ limit, it is necessary to add the conditions

$$s(t) = 0 \quad \forall|t|\ge T/2+\Delta, \qquad \lim_{T\to\infty}\frac{\Delta}{T} = 0\ . \tag{2.5.8}$$

The last condition also fits in the intuitive picture: the transition time during which the source changes from $\rho(\mathbf{x})$ to 0 should be subleading compared to the time it is constant. With these conditions the Fourier

[5]Technically, both in the left hand side and in the right hand side there is an undefined phase that diverges. It can be treated by adding a constant counterterm in the Lagrangian (not the Lagrangian density) to offset the minimum of the Hamiltonian and have a well-defined phase. This same treatment has been done in [20] to cure the ill-defined the phase in "model II".

transform of the adiabatic function fulfills the following relations

$$\int dt\, e^{\pm iEt} s(t) \xrightarrow{T\to\infty} (2\pi)\,\delta(E), \quad \frac{1}{T}\left|\int dt\, e^{\pm iEt} s(t)\right|^2 \xrightarrow{T\to\infty} (2\pi)\,\delta(E). \tag{2.5.9}$$

The conditions (2.5.8) are not really necessary for the first limit, any adiabatic function would suffice. However from a direct calculation[6] it follows they are needed for the second limit.
At this point, the lectures [20] use an intuitive but ultimately misleading argument to dismiss the operator parts (2.5.4) and (2.5.5) of the S matrix. For a source ρ factorized into a time independent part and an adiabatic function, the function f (2.5.3) is given by

$$f(\infty, -\infty, \mathbf{p}) = \int dt\; e^{iE_{\mathbf{p}}t}\, s(t)\, \left[i\frac{g}{\sqrt{2E_{\mathbf{p}}}} \int d^3x\, \rho(\mathbf{x})\, e^{-i\mathbf{p}\cdot\mathbf{x}} \right], \tag{2.5.10}$$

the t integral of which approaches a Dirac delta $\delta(E_{\mathbf{p}})$ for $T \to \infty$ as per the first equation in (2.5.9). It is then assumed that the operators (2.5.4), (2.5.5) go to zero in this limit, since the Dirac Delta is zero except for when $E_{\mathbf{p}} = 0$, which is never the case for a massive field. This argument would be valid if $a^\dagger_{\mathbf{p}}$ were a test function rather than an operator. For operators, the convergence properties in the space of generalized functions or distributions are not guaranteed to apply. In the lectures [20] an incorrect argument is presented to argue that the integral of the adiabatic function is going to be vanishing for on-shell energies. It is based on the common misconception that, since some successions of functions converging to a Dirac delta are sharply peaked in 0 and point wise converging to 0 outside of the origin, for instance a succession of Gaussian functions with a decreasing width $\sigma \to 0$, this must happen for any succession. This is not the case for all delta families, take for example the family

$$\delta_\varepsilon(x) = \sqrt{\frac{2}{\pi}}\,\frac{1}{\varepsilon}\sin\left(\frac{x^2}{\varepsilon^2}\right) \xrightarrow{\varepsilon\to 0} \delta(x), \tag{2.5.11}$$

which is converging to a Dirac delta[7]. For every $\varepsilon > 0$, all the functions are vanishing in $x = 0$, the (for $\varepsilon \to 0$ infinite) peaks and valleys are just less dense around $x = 0$. For any $x \neq 0$ the $\varepsilon \to 0$ limit of $\delta_\varepsilon(x)$ does not converge as a function. We have essentially the same situation if we directly try to take the $t \to \infty$ limit of $f(t, \mathbf{p})$ as discussed in 2.2. Adjusting the times from 0 and t to $-T/2$ and $T/2$ in subsection 2.3, we get the same formulas as in the sudden limit $s(t) \sim \theta(t + T/2)\theta(t - T/2)$, namely f goes to

$$\frac{2\sin\left(\frac{E_{\mathbf{p}}T}{2}\right)}{E_{\mathbf{p}}} \xrightarrow{T\to\infty} (2\pi)\delta(E_{\mathbf{p}}). \tag{2.5.12}$$

It still converges, distribution-wise, to a Dirac delta, it has a peak $\propto T$ in 0. But like the example, the functions for an on-shell energy $E_{\mathbf{p}} > 0$ do not converge in the $T \to \infty$ limit. The functions keep bouncing periodically between the extremes $\pm 2/E_{\mathbf{p}}$. The oscillations become more and more rapid in the $T \to \infty$ limit,

[6] The function s must be suppressed strongly enough for $|t| > T/2$ to be able to use minorants of the modulus square outside of $t \in \{-T/2, T/2\}$ to show that they do not contribute. The rest of the proof consists just of the properties of the delta function representations $[\sin(x/\epsilon)]/(\pi x) \xrightarrow{\epsilon\to 0} \delta(x)$ and $\epsilon[\sin^2(x/\epsilon)]/(\pi x) \xrightarrow{\epsilon\to 0} \delta(x)$.

[7] Any function $g(x)$ normalized to $1 = \int dx\, g(x)$, that does not spoil the uniform convergence of the integral $\int dy\, g(y)\phi(y\varepsilon) \xrightarrow{\varepsilon\to 0} \int dy\, g(y)\phi(0) = \phi(0)$ with the test functions $\phi(y)$, produces a family of nascent delta functions $1/\varepsilon\, g(x/\varepsilon) \xrightarrow{\varepsilon\to 0} \delta(x)$. Namely, their action converges to the action of a Dirac delta: $\int dx/\varepsilon\, g(x/\varepsilon)\phi(x) = \int dy\, g(y)\phi(y\varepsilon) \xrightarrow{\varepsilon\to 0} \phi(0)$ for any test function $\phi(x)$.

and do not grant any convergence, certainly not to 0. The Riemann-Lebesgue lemma we have previously used for the limit of $N_0(t)$ does not help us here as it works for functions, not operators. The correct procedure is to apply the operators to a physical states, pick the partial waves amplitude (which might not be defined in the $T \to \infty$ limit), compute the expectation values of the observable operators and take the large time limit of these physical observables, if they are well defined in the large time limit. The fact that when using the scattering matrix in the sudden limit, one obtains the same amplitudes and (limits of) probabilities as in subsection 2.3 should not be interpreted as proof that the sudden switch is the "correct way to insert the interaction for a finite time". In fact, as we will argue at the end of this subsection, there is no correct way to switch off the interaction asymptotically to recover the full results of the theory, not even when restricting to the long time limit behavior. The analysis of the sudden switch is to point out that if the adiabatic function $s(t)$ fulfilling (2.5.7) and (2.5.8) converges to a sudden switch (the precise meaning will be apparent later) the result of a trivial scattering matrix as in [20] cannot be recovered. In order to recover the trivial scattering, one has to add additional conditions to the existing ones:

$$\Delta \xrightarrow{T\to\infty} \infty, \quad \sup|\partial_t s(t)| \leq \frac{M}{\Delta}, \qquad \forall\, T > \bar{T} > 0\ . \tag{2.5.13}$$

That is, the modulus of the derivative of the (smooth) adiabatic function $|\dot{s}|$ must be smaller than a maximum that decreases at least linearly with Δ in the limit $T \to \infty$. This bound is allowed to be violated at finite times as we require it only in the large T limit. By intergrating by parts we can rewrite the integral as

$$\int dt\, s(t)\, e^{iE_{\mathbf{p}}t} = \frac{i}{E_{\mathbf{p}}} \int dt\ \partial_t s(t)\, e^{iE_{\mathbf{p}}t}\ . \tag{2.5.14}$$

The derivation by parts can be done because of the smoothness of s and the positivity of the on-shell energy $E_{\mathbf{p}} \geq m > 0$. The time derivative of the adiabatic function is nonzero only during the "transition" period of length Δ, that is for the intervals $t \in (-T/2 - \Delta, -T/2)$ and $t \in (T/2, T/2 + \Delta)$. It is convenient then to define the functions $s_\pm$ in terms of a dimensionless variable λ

$$s_\pm(\lambda) = s\left(\pm\lambda\,\Delta \pm \tfrac{T+\Delta}{2}\right), \qquad \lambda \in (-\tfrac{1}{2}, \tfrac{1}{2}). \tag{2.5.15}$$

The integral (2.5.14) can then be rewritten in two parts containing $s_\pm$

$$\frac{i}{E_{\mathbf{p}}} \exp\left\{-iE_{\mathbf{p}}\left(\frac{T+\Delta}{2}\right)\right\} \int d\lambda\ s'_-(\lambda)\, e^{-i(E_{\mathbf{p}}\Delta)\lambda} - \frac{i}{E_{\mathbf{p}}} \exp\left\{iE_{\mathbf{p}}\left(\frac{T+\Delta}{2}\right)\right\} \int d\lambda\ s'_+(\lambda)\, e^{i(E_{\mathbf{p}}\Delta)\lambda}, \tag{2.5.16}$$

with $s'_\pm = \partial_\lambda s_\pm$. The condition (2.5.13) then implies $|s'_\pm| \leq M$ in the large T limit. From this it follows that both the s'_- and the s'_- integrals vanish in the large-T (hence large Δ) limit[8]. The simplest case would be if $s_-(\lambda) = s_+(-\lambda)$ independent of T in the first place, then the highly oscillatory integrals vanish as a consequence of the Riemann-Lebesgue lemma. It can be seen also that, removing the bound requirement on gradient $s'_\pm$, one could have a family of functions converging to a Dirac delta[9] $\delta(\lambda)$, substantially recovering the results of the sudden limit. Of course other outcomes are possible for adiabatic functions with unbounded

[8]This can be proven for instance by using the fact that any Fourier transform $\tilde{f}(\xi) = \int dx\, e^{ix\xi} f(x)$ can be written as $\tilde{f}(\xi) = \int dx\, e^{ix\xi}[f(x) - f(x + \pi/\xi)]/2$, and using the absolute convergence of the integral, the continuity and bound of $s'_\pm$ at any $T > \bar{T}$ to prove that a large enough T can always be found such that the integral is arbitrarily small, regardless of the specific function $s_\pm$. Hence, it vanishes in the large T limit.

[9]Any delta family $\delta_\varepsilon(\lambda)$ can be used as a start. To get the function s it should be multiplied by a smooth drop to the border, such as $e^{-4\lambda^2/(1-4\lambda^2)}$ and properly normalized to 1 for all ε. As long as $\varepsilon\Delta \xrightarrow{T\to\infty} 0$ the integrals in $s'_\pm$ converge to just 1.

derivatives in the $T \to \infty$ limit.

The smoothness of the adiabatic function can be relaxed to just continuity and smoothness except in a finite (constant) number of points, for instance $\{-\Delta - T/2, -T/2, T/2, \Delta + T/2\}$. One has just to be careful with the integration by parts and the derivatives of s. On the other hand all the conditions in (2.5.7), (2.5.8) and (2.5.13) are crucial.

It is then possible to force the system to have a trivial scattering matrix[10] even if the full interaction is on for a long time. However it is not the general case for any function with (pointwise) convergence $s(t) \to 1$. Requiring long permanence of the interaction does not lead to a unique limit. Instead, the behavior in the distant past and far future – the way in which the function s goes from 1 to 0, e.g. with a derivative bounded by (2.5.13), some other bound or no bound at all – drastically changes the final outcome. Consequently, we conclude that none of these limits in particular is supposed to reproduce all aspects of the full theory.

It is possible to rework the arguments presented in this subsection[11] to prove the analogue of the Adiabatic theorem

$$U(t, -\tfrac{T}{2} - \Delta)|\mathbf{p}_1, \cdots, \mathbf{p}_n\rangle \sim \exp\left\{-i\left[E_0 + \sum_{j=1}^{n} E_{\mathbf{p}_j}\right]\left(t + \frac{T}{2} + \Delta\right)\right\}|\mathbf{p}_1, \cdots, \mathbf{p}_n\rangle_\Omega \tag{2.5.17}$$

The states $|\mathbf{p}_1, \cdots, \mathbf{p}_n\rangle_\Omega$ build the basis of energy eigenstates, made from the lowest energy vacuum state $|\Omega\rangle$ acted on by operators $b^\dagger_{\mathbf{p}} = a^\dagger_{\mathbf{p}} + h^*(\mathbf{p})$. The $\sim$ instead of an equality represents two facts: the first one is that it is valid in the large T limit and only if all the requirements (2.5.7), (2.5.8) and (2.5.13) are fulfilled. The second is that there is an additional phase so that the effective time for the E_0 coefficient different than the one for the $E_{\mathbf{p}_j}$'s $\Delta t_{\text{eff}} \neq \Delta t = t + T/2 + \Delta$. However, in the large T limit, the phase is asymptotic to the correct phase $\Delta t_{\text{eff}}/(t + T/2 + \Delta) \to 1$.

On the other hand in the sudden case $s(t) = \theta(T/2 + \Delta + t)\theta(T/2 + \Delta - t)$ one has

$$\begin{aligned}&\langle \mathbf{q}_1, \cdots, \mathbf{q}_m|U_S(t, -\tfrac{T}{2} - \Delta)|\mathbf{p}_1, \cdots, \mathbf{p}_n\rangle \\ &\quad = \exp\left\{-i\left(\sum_{j=1}^{n} E_{\mathbf{p}_j}\right)\Delta t\right\}{}_{\Delta t}\langle \mathbf{q}_1, \cdots, \mathbf{q}_m|\mathbf{p}_1, \cdots, \mathbf{p}_n\rangle, \qquad t \in [-\tfrac{T}{2} - \Delta, \tfrac{T}{2} + \Delta],\end{aligned} \tag{2.5.18}$$

where we call the time evolution operator U_S in this case to distinguish it from the previous case. This result is rather obvious since the system is the exact one for $t \in (-\frac{T}{2} - \Delta, \frac{T}{2} + \Delta)$, hence we get the same results of subsection 2.3 as long as t remains in its bound. For initial conditions or final t outside of the bound, i.e. $t_0 < -T/2 - \Delta$ or $t > T/2 + \Delta$ the phases keep evolving but the Δt in the t dependent basis is constant and the results become different from the exact ones.

The difference between the adiabatic and sudden cases stems from the fact that

$${}_{\Delta t}\langle \mathbf{q}_1, \cdots, \mathbf{q}_m|\mathbf{p}_1, \cdots, \mathbf{p}_n\rangle \neq e^{-iE_0\Delta t}\langle \mathbf{q}_1, \cdots, \mathbf{q}_m|\mathbf{p}_1, \cdots, \mathbf{p}_n\rangle_\Omega \ . \tag{2.5.19}$$

[10] Besides a diverging phase that can be removed with a counterterm in the Lagrangian as discussed in [20].

[11] The calculations in the lectures [20] regarding "Model I" and "Model II" are essentially a way to resum the Dyson series. At no point is there a switch to momentum space, and all the calculations can be repeated without much effort when integrating time in a compact domain, rather than the full real axis. In this way one obtains the $U_I(t, -T/2 - \Delta)$. The formulas are the same as the ones presented at the beginning of this subsection, except that the time integral has an upper bound in t, instead of at the end of the support of the adiabatic function s.

This can be seen clearly by explicitly working out these bases by exactly solving, but when only looking at the Dyson series for the U_I this is more obscured. Namely, for free fields (and interaction picture fields) there is no difference between the particle number/momentum basis $|\mathbf{p}_1, \cdots, \mathbf{p}_n\rangle$ at different times and the basis of the energy excitations $|\mathbf{p}_1, \cdots, \mathbf{p}_n\rangle_\Omega$. They are all the same basis since energy is essentially given by the momentum. This is related to the fact that the regular basis of in and out states (usually assumed to exist, rather than proved) simply does not exist for a time independent classical source[12]. This is mostly due to the fact that the state corresponding to the minimum of the Hamiltonian $|\Omega\rangle$ is not a momentum eigenstate. This difference between these bases is crucial from the physical point of view. In the full theory, the initial and final states can be written in any basis, even different ones for the initial and final states. The matrix elements of U with respect to the regular $|\mathbf{p}_1, \cdots, \mathbf{p}_n\rangle$ basis are enough to write the matrix elements in all bases, using the ordinary rules for changing basis. If one artificially switches off the interaction in the far past and future it is not possible to distinguish, eg, if the initial or final conditions were given in the energy basis or in the particle momentum one, as they are the same. Which way we have to insert the interaction for a long time depends on in which basis the initial and final states are given. For instance, if the initial and final condition are given in the energy eigenstate basis one should use the proper adiabatic case. Because of (2.5.17) this approach smoothly connects the free states to the energy eigenstates, then back to the corresponding free states in the far future. Seen from this perspective it is obvious that the scattering is trivial. The initial and final conditions are in energy eigenbasis where the only time evolution is a phase. The nontrivial part of this evolution is that the spectrum of the full Hamiltonian is the same as the free Hamiltonian up to an offset, and has no additional degeneracy. This can only be proven with the full exact solutions, as done in this chapter, and cannot be obtained only from the Dyson series. On the other hand, if the initial states are given in terms of momentum (and particle number) eigenstates, the proper switch is a sudden one. The former sends free states to energy eigenstates (which have an undefined particle number), while the latter keeps the momentum and particle number eigenstates (which are not energy eigenstates). Other bases are of course possible, but these are the most physically relevant ones for us. It might also be possible that for some, more complicated, basis there is not any corresponding way to switch off the interaction at asymptotically large times. In any case, there is no universal "correct" way to keep the interaction for a finite, but arbitrarily large time.

2.6 Conclusion

In this chapter we have studied the theory of a scalar field interacting with an external classical source, motivated by the scalar fields that arise with space dependent nonzero expectation value due to a medium. We show that an external classical source causes the particle vacuum to be unstable, and its decay into n particles is given by a Poisson distribution, which is well-defined whenever the source has a Fourier transform. The vacuum decay plays an important role because the full dynamics can be reduced to an absorption probability amplitude of the initial particles and an interference pattern between the remaining particles and the ones produced by the vacuum. The time dependence of the vacuum survival probability has a complicated behavior; it oscillates and exhibits a quadratic time scaling at short times that gives rise to the quantum Zeno effect. The oscillation of the survival probability dies out at large times, and it tends to a constant greater than zero, at odds with standard particle decay. In the large volume limit the particle number density saturates, and the particle production never displays a constant rate, in contrast with the

[12] In general, it will also not exist for time- dependent sources that are not Fourier transformable in time.

Schwinger mechanism. In addition, the precise shape of the source and its tails, and not just its overall volume, is relevant for the particle production even in the large volume limit.

Aside from phenomenological applications, the exact calculations of this simple model also points to some implications for formal theory. First off, we see a concrete example how an interaction can make it so the Hamiltonian and momentum operator no longer share a basis of eigenstates, and how this is an obstacle in using the conventional formalism of in- and out states. The intuitive procedure of approaching a time independent interaction by a time dependent one which is constant for a very long time and adiabatically switched off at infinity leads to the wrong conclusions. Whichever way the interaction is turned off, the difference between the particle number and energy eigenstates (and vacua) is spoiled and the full dynamics of the theory cannot be recovered. The way to resolve this is to only take the infinite time limit after time dependent inner products and expectation values are taken. The techniques involving t states used in this chapter to calculate the scattering amplitudes can potentially be used in other theories as well, since they are based on finding solutions to the equations of motion which can be done perturbatively. Secondly, in the large volume limit of the source, we noticed the shape still influences the final result by a different numerical prefactor. This implies that in calculations where the shape is not properly defined or a shorthand argument such as "$\delta(0) = V$" (modulo factors 2π) is used, there might be some ambiguity in this prefactor of the result.

In high energy experiments, a possible use of this specific model would be to simulate (a part of) the dilaton production out of a medium approximated by a time independent classical source. The assumption would be that the dilaton condensate is well approximated as behaving classically. The effect due to the vacuum decay is fully nonperturbative and could give a relevant contribution to dilaton production, where perturbative production mechanisms are suppressed. The produced dilatons (i.e. predominantly scalar glueballs) then decay and produce mesons that are measured, a similar process as discussed in [64].

In low energy experiments, the Schwinger mechanism and Zeno effect are more easily accessible, e.g. [65] for the Schwinger mechanism and [55, 56] for the Zeno effect. Therefore this model or an extension of it could work as a description of those phenomena at low energies.

Generalizations of the main results of this paper to higher spin and/or charged particles could be interesting and potentially prove useful in modeling production of particles other than the dilaton, but it remains a question if the same techniques can be used.

Finally, as an exactly solvable theory it can be a useful tool as a test for certain methods, for example if any of the vacuum decay or Zeno effect can be seen on the lattice, or on the accuracy of large N approximations described in e.g. [66].

Chapter 3

The extended Linear Sigma Model

In this chapter we will introduce the extended Linear Sigma Model (eLSM) which will be the basis of the following chapters. The presentation is roughly based on the lecture notes in [67] and the review in [68], which also reviews modern applications of the eLSM. The eLSM is an effective model of QCD directly using the hadronic degrees of freedom rather than quarks and gluons. The first Linear Sigma Model was written down in [69]. A great number of effective field theories can be written down, so we need a procedure to make sure it describes the important features of QCD. The use of symmetries turns out to be a powerful tool. In chapter 1.1 we reviewed the (broken) symmetries of QCD, which the eLSM will have to mimic.

3.1 Dilatation invariance and the Dilaton Lagrangian

We will start with examining how to implement the breaking of dilatation invariance. Since the main reason for this breaking was quantum fluctuations by gluons, we should introduce an effective field for the collective gluons:

$$G^4 \sim G_a^{\mu\nu} G_{\mu\nu}^a. \tag{3.1.1}$$

A general Lagrangian without higher momentum terms for this field will be

$$\mathcal{L}_G = \frac{1}{2}(\partial_\mu G)^2 - V_{\text{dil}}(G), \tag{3.1.2}$$

with $V_{\text{dil}}(G)$ being the dilaton potential, which has to be responsible for breaking dilatation invariance. As in chapter 1.1, the divergence of the Noether current is the trace of the stress tensor:

$$\partial_\mu J^\mu_{\text{dil}} = T^\mu_\mu = 4V_{\text{dil}}(G) - (\partial_\mu G)^2 = 4V_{\text{dil}}(G) - G\frac{\partial V_{\text{dil}}}{\partial G}, \tag{3.1.3}$$

where for the last equality we have used the equations of motion, so it holds only on-shell. From this equation one can clearly see that a mass term leads to a nonconserved current and therefore a breaking of dilatation invariance, but a $\lambda_4 G^4$ interaction (which has a dimensionless coupling) preserves dilatation invariance. To mimic the breaking in the YM sector (1.1.11), the divergence should be proportional to G^4:

$$\partial_\mu J^\mu_{\text{dil}} = 4V_{\text{dil}}(G) - G\frac{\partial V_{\text{dil}}}{\partial G} = \frac{-\lambda_G}{4} G^4, \tag{3.1.4}$$

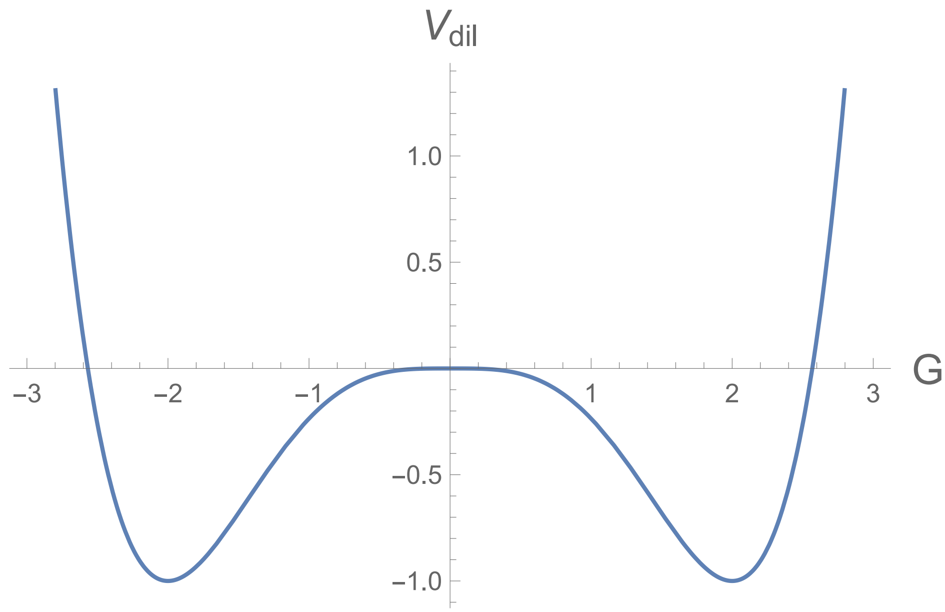

Figure 3.1: The shape of the dilaton potential with $\lambda_G = 1$ and $\Lambda_G = 2$ in arbitrary units

where $\lambda_G > 0$ is a free positive parameter, such that the entire expression is negative (because the beta-function in (1.1.11) is negative). The solution to this differential equation for V_{dil} is [5, 70, 71]

$$V_{\text{dil}}(G) = \frac{\lambda_G}{4}\left(G^4 \ln\left|\frac{G}{\Lambda_G}\right| + \lambda_4 G^4\right), \tag{3.1.5}$$

where Λ_G is an energy scale, and λ_4 is free since G^4 is a solution to the homogeneous part. Choosing $\lambda_4 = \frac{-1}{4}$ leads to the most natural normalization, with

$$V_{\text{dil}}(G) = \frac{\lambda_G}{4}\left(G^4 \ln\left|\frac{G}{\Lambda_G}\right| - \frac{G^4}{4}\right). \tag{3.1.6}$$

In Fig, 3.1 the shape of the dilaton potential is shown. It has a minimum at $G = \Lambda_G$, which will be the value of the G field condensate, and is supposed to mimic the gluon condensate. Expanding around this minimum shows that excitations around the minimum have a mass $m_G^2 = \lambda_G \Lambda_G^2$. This is the scalar glueball, also called the dilaton, the mass of which is predicted by lattice [72, 73, 74] to be in the range of 1.5-1.8 GeV. A study using functional methods put the mass at approximately 1.8 GeV [75]. QCD sum rules predict the mass to be 1.3-1.7 GeV [76], and a holographic model also finds a scalar glueball at 1.5 GeV, although a lighter, non-dilaton glueball was also found [77, 78]. The eLSM strongly favors the $f_0(1710)$ as the lightest scalar glueball [79], but the recent discovery of a potential isovector partner of the $f_0(1710)$ [80, 81, 82] might refute this in the future.

To get a numerical estimate on Λ_G, we can compare it to the YM result. Rewriting it as

$$\langle T^\mu_\mu \rangle_{\text{QCD}} = \frac{\beta(g)}{2g}\langle G^a_{\mu\nu} G^{\mu\nu}_a \rangle = -\frac{11N_c - 2N_f}{96\pi^2} g^2 \langle G^a_{\mu\nu} G^{\mu\nu}_a \rangle = -\frac{11N_c - 2N_f}{24}\langle \frac{\alpha_s}{\pi} G^a_{\mu\nu} G^{\mu\nu}_a \rangle \equiv -\frac{11N_c - 2N_f}{24} C^4, \tag{3.1.7}$$

where C is the gluon condensate, and $\alpha_s \equiv \frac{g^2}{4\pi}$ is a common way to write the coupling. Calculations for YM theory [83, 84, 85] find that C ranges from 0.3 to 0.6 GeV. Comparing this with the trace of the stress tensor in the dilaton model

$$\langle T^\mu_\mu \rangle_{\text{dil}} = -\frac{m_G^2}{4\Lambda_G^2} \langle G^4 \rangle = -\frac{m_G^2 \Lambda_G^2}{4}, \tag{3.1.8}$$

and setting them equal, we find

$$\Lambda_G = \sqrt{\frac{11 N_c C^4}{6 m_G^2}} \approx 0.1 - 0.5\,\text{GeV}. \tag{3.1.9}$$

This puts Λ_G at the same order as Λ_{QCD}, with a significant uncertainty. While quark masses also break dilatation invariance, the eLSM does not include these for the symmetry breaking. Anomalous terms related to instantons that break the axial anomaly also break dilatation invariance, and have been recently incorporated in the eLSM [86, 87]. Interactions of other fields with the dilaton will, after breaking of dilatation invariance (and chiral symmetry), give rise to mass terms.

3.2 Spontaneous chiral symmetry breaking

We will first look at the simplified $N_f = 1$ eLSM, where only 1 scalar and 1 pseudoscalar meson, the sigma and the "pion", exist. This "pion" is not cleanly related to the pions in the full $N_f = 3$ spectrum; it is a (pseudo)Goldstone boson like the pions, but it is an isospin scalar like the η, while the pions make up an isospin triplet. We will refer to this field as the pion, but one should keep this difference in mind. The sigma and pion are combined in a chiral multiplet as $\Phi = \sigma + i\pi$ which has a U(1) symmetry. The Lagrangian is

$$\mathcal{L} = \frac{1}{2}\partial_\mu \Phi^\dagger \partial^\mu \Phi - \frac{1}{2} m_0^2 \Phi^\dagger \Phi - \frac{\lambda}{4}(\Phi^\dagger \Phi)^2, \tag{3.2.1}$$

which expanded in the fields σ and π is

$$\mathcal{L} = \frac{1}{2}\partial_\mu \sigma \partial^\mu \sigma + \frac{1}{2}\partial_\mu \pi \partial^\mu \pi - \frac{1}{2} m_0^2(\sigma^2+\pi^2) - \frac{\lambda}{4}(\sigma^2+\pi^2)^2 \equiv \frac{1}{2}\partial_\mu \sigma \partial^\mu \sigma + \frac{1}{2}\partial_\mu \pi \partial^\mu \pi - V(\sigma,\pi), \tag{3.2.2}$$

with the potential

$$V(\sigma,\pi) = \frac{1}{2} m_0^2(\sigma^2+\pi^2) + \frac{\lambda}{4}(\sigma^2+\pi^2)^2. \tag{3.2.3}$$

Since it is a function of $\sigma^2+\pi^2$ it is manifestly invariant under chiral U(1) transformations acting on Φ. We necessarily have $\lambda > 0$ to have a lowest energy state. Just like in the Higgs mechanism, if $m_0^2 > 0$, the only minimum is at $\sigma = \pi = 0$ and is stable. Both particles have a mass of m_0, and thus chiral symmetry is unbroken. The more physically interesting scenario is a tachyonic mass $m_0^2 < 0$, which results in $V(0,0)$ becoming a local maximum, and new minima at

$$\sigma^2 + \pi^2 = -\frac{m_0^2}{\lambda} \equiv \phi_N, \tag{3.2.4}$$

with ϕ_N being the v.e.v. of the chiral condensate. This describes a circle of equivalent minima, see figure 3.2. The massless direction along this circle is interpreted as the Goldstone boson. after choosing the minimum

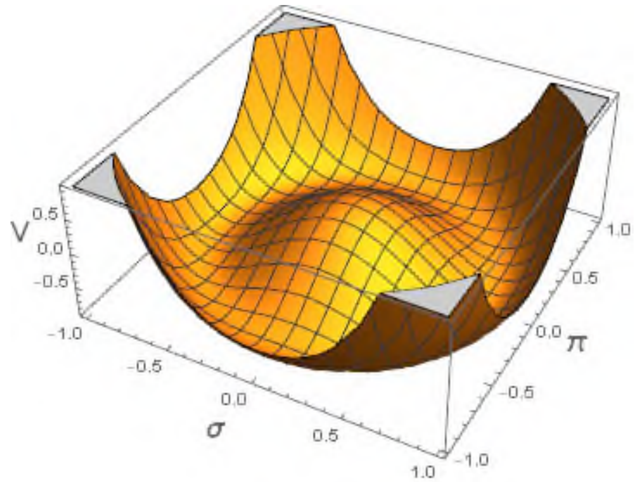

Figure 3.2: The shape of the potential given by (3.2.3), with $m_0^2 < 0$

for example as$(\sigma_m, \pi_m) = (\phi_N, 0)$ we can calculate the masses:

$$m_\pi^2 = \frac{\partial^2 V}{\partial^2 \pi}\Big|_{\min} = 0, \tag{3.2.5}$$

$$m_\sigma^2 = \frac{\partial^2 V}{\partial^2 \sigma}\Big|_{\min} = -2m_0^2 = 2\lambda\phi_N^2. \tag{3.2.6}$$

Experimentally, the pion has a mass of 135 MeV, while the sigma has a mass of at least 500 MeV, and potentially up to 1350 MeV[1]. While we can model the mass difference like this, we are still missing the fact that the pion is not completely massless. From the arguments in chapter 1, we know this is because of the explicit breaking of chiral symmetry by the quark masses. With this in mind, we add a term that explicitly breaks chiral symmetry:

$$V(\sigma, \pi) = \frac{1}{2}m_0^2(\sigma^2 + \pi^2) + \frac{\lambda}{4}(\sigma^2 + \pi^2)^2 - h\sigma. \tag{3.2.7}$$

This shifts ϕ_N to a different value, but more importantly the minimum $(\sigma_{\min}, \pi_{\min}) = (\phi_N, 0)$ is now unique, see figure 3.3. The masses are now

$$m_\pi^2 = \frac{\partial^2 V}{\partial^2 \pi}\Big|_{\min} = m_0^2 + \lambda\phi_N^2 = \frac{h}{\phi_N} \tag{3.2.8}$$

$$m_\sigma^2 = \frac{\partial^2 V}{\partial^2 \sigma}\Big|_{\min} = m_0^2 + 3\lambda\phi_N^2 = m_\pi^2 + 2\lambda\phi_N^2. \tag{3.2.9}$$

The mass difference stays the same so the σ mass is always larger than the pion mass. The chiral condensate affects the masses and decay rates. When we expand around $\sigma = \phi_N$, we get for example a term proportional to $\lambda\phi_N\pi^2\sigma$, which leads to a decay of the σ into 2 pions.

In (3.2.7), λ is dimensionless and h is related to nonzero quark masses, but we have not explained the origin of m_0^2. Aside from the quark masses, the only origin of a scale and hence dimensionful couplings is the trace anomaly. Therefore m_0^2 has to come from a coupling of the Φ and G fields. It can be implemented by the

[1]The identification of the σ meson is still not completely clear. It is commonly seen as either the $f_0(500)$ or $f_0(1370)$, see [88].

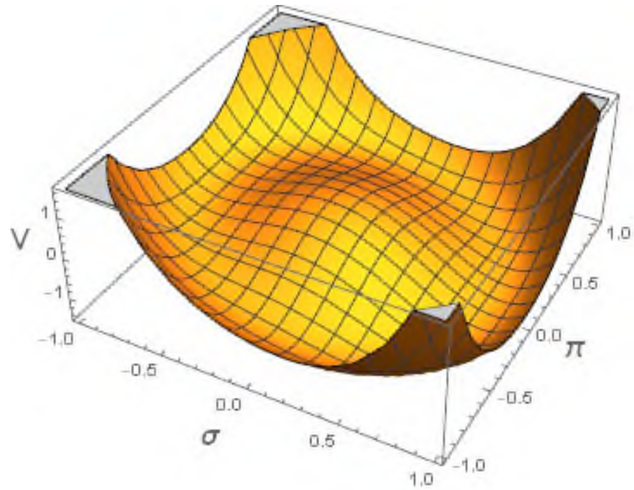

Figure 3.3: The shape of the potential (3.2.7) with explicit breaking term $h > 0$.

interaction term

$$-\frac{1}{2}aG^2\Phi^\dagger\Phi, \tag{3.2.10}$$

which, after condensation $G \to G_0 + G$ gives the mass term in (3.2.7) with $m_0^2 = aG_0^2$, and an interaction term by which the scalar glueball can decay into mesons, for example into 2 pions. The complete Lagrangian is then

$$\mathcal{L}_{G\Phi} = \frac{1}{2}\partial_\mu\Phi^\dagger\partial^\mu\Phi + \frac{1}{2}\partial_\mu G\partial^\mu G - \frac{1}{2}aG^2\Phi^\dagger\Phi - \frac{\lambda}{4}(\Phi^\dagger\Phi)^2 - V_{\text{dil}}(G). \tag{3.2.11}$$

Since renormalizability is not necessary condition for an effective field theory, one might think to add higher dimension interaction vertices. However, the reason why we cannot add higher dimension terms is because the only mass scale comes from the condensation of G. An operator of dimension 5 or higher then has to be compensated by powers of $1/G_0$, coming from powers of $1/G$, which are singular in the origin.

The same procedure could also be done for fields with higher spin, as we will do further on with spin 2 mesons in chapter 4. In the full $N_f = 3$ eLSM masses and interactions arise by going through the same mechanism, just with more fields.

3.3 The three-flavor Linear Sigma Model

3.3.1 Three-flavor meson nonets

Having seen the 1-flavor toy model above, we can now finish the construction by introducing the $N_f = 3$ eLSM. We will not repeat the chiral symmetry breaking mechanisms here, as they are analogous to the simple case, but is important to establish the objects we are working with. The field Φ now gets upgraded to a 3×3 matrix of the (anti)quarks $\bar{q}_i, q_i$, which follows transformations like the object

$$\Phi_{ij} \sim \sqrt{2}\bar{q}_{j,R}q_{i,L}, \tag{3.3.1}$$

where we use the notation $\sim$ because Φ is not just a quark-antiquark current, but it should include non-perturbative effects and dressing by gluons. It is useful to think of this current because it describes the constituent quarks of the matrix elements and it shows the chiral transformation rule, which for Φ is

$$\Phi \to U_L \Phi U_R^\dagger. \tag{3.3.2}$$

One can write Φ as:

$$\Phi_{ij} \sim \sqrt{2}\bar{q}_{j,R} q_{i,L} = \sqrt{2}\bar{q}_j P_L P_L q_i = \sqrt{2}\bar{q}_j P_L q_i = \frac{1}{\sqrt{2}}(\bar{q}_j q_i + i\bar{q}_j i\gamma^5 q_i), \tag{3.3.3}$$

where $P_L = \frac{1}{2}(1-\gamma^5)$ is the left-handed chiral projection operator. The two terms are the scalar and pseudoscalar matrices:

$$S_{ij} \sim \frac{1}{\sqrt{2}}\bar{q}_j q_i, \;\; P \sim \frac{1}{\sqrt{2}}\bar{q}_j i\gamma^5 q_i, \tag{3.3.4}$$

and so

$$\Phi = S + iP. \tag{3.3.5}$$

Completing the analogy to the 1 flavor case where we had $\Phi = \sigma + i\pi$. We will now go over the content of these matrices, in the strange-nonstrange basis. The pseudoscalar mesons P with $J^{PC} = 0^{-+}$ are the 3 pions, four kaons, the $\eta(547)$ and the $\eta'(958)$. The meson matrix (nonet) is given by

$$P = \frac{1}{\sqrt{2}}\begin{pmatrix} \frac{\eta_N+\pi^0}{\sqrt{2}} & \pi^+ & K^+ \\ \pi^- & \frac{\eta_N-\pi^0}{\sqrt{2}} & K^0 \\ K^- & \bar{K}^0 & \eta_S \end{pmatrix}, \tag{3.3.6}$$

where the η_N and η_S are made up of nonstrange and strange quarks respectively:

$$\eta_N \sim \frac{1}{\sqrt{2}}\left(\bar{u}i\gamma^5 u + \bar{d}i\gamma^5 d\right), \;\; \eta_S \sim \bar{s}i\gamma^5 s. \tag{3.3.7}$$

These are interaction-eigenstates, not physical (mass) eigenstates. These are isospin scalars (isoscalars). The physical fields are a mixture of these states:

$$\begin{pmatrix} \eta \\ \eta' \end{pmatrix} = \begin{pmatrix} \cos\beta_P & \sin\beta_P \\ -\sin\beta_P & \cos\beta_P \end{pmatrix} \begin{pmatrix} \eta_N \\ \eta_S \end{pmatrix}, \tag{3.3.8}$$

with a mixing angle $\beta_P = -43.4°$ [89]. The large mixing angle is a consequence of the $U_A(1)$ axial anomaly [90, 12].

The scalar mesons ($J^{PC} = 0^{++}$) are the chiral partners of the pseudoscalars. The identification of the scalar states is not yet clear, but the set $\{a_0(1450),\, K_0^*(1430),\, f_0(1370),\, f_0(1500)/f_0(1710)\}$ is a good contender. Since the masses of the scalars are close to the scalar glueball, there is a strong possibility that (a mixture of) these states is a glueball [91, 79, 92, 93, 94, 95]. This would have to be taken into account on top of the strange-nonstrange mixing. The scalar meson nonet is then written as

$$S = \frac{1}{\sqrt{2}}\begin{pmatrix} \frac{\sigma_N+a_0^0}{\sqrt{2}} & a_0^+ & K_0^{\star+} \\ a_0^- & \frac{\sigma_N-a_0^0}{\sqrt{2}} & K_0^{\star0} \\ K_0^{\star-} & \bar{K}_0^{\star0} & \sigma_S \end{pmatrix}. \tag{3.3.9}$$

Next are the vector mesons with $J^{PC} = 1^{--}$, their current involves Dirac matrices:

$$V^{\mu}_{ij} \sim \frac{1}{\sqrt{2}}(\bar{q}_j \gamma^{\mu} q_i). \tag{3.3.10}$$

These are the states $\{\rho(770),\, K^{*}(892),\, \omega(782),\, \phi(1020)\}$. The matrix V^{μ} has the form

$$V^{\mu} = \frac{1}{\sqrt{2}} \begin{pmatrix} \frac{\omega_N^{\mu}+\rho^{0\mu}}{\sqrt{2}} & \rho^{+\mu} & K^{*+\mu} \\ \rho^{-\mu} & \frac{\omega_N^{\mu}-\rho^{0\mu}}{\sqrt{2}} & K^{*0\mu} \\ K^{*-\mu} & \bar{K}^{*0\mu} & \omega_S^{\mu} \end{pmatrix}, \tag{3.3.11}$$

where the mixing of the non-strange and strange states ω_N and ω_S is similar to the pseudoscalar case:

$$\begin{pmatrix} \omega(782) \\ \phi(1020) \end{pmatrix} = \begin{pmatrix} \cos\beta_V & \sin\beta_V \\ -\sin\beta_V & \cos\beta_V \end{pmatrix} \begin{pmatrix} \omega_N \\ \omega_S \end{pmatrix}, \tag{3.3.12}$$

where the small vector mixing angle $\beta_V = -3.9^{\circ}$ is [2]. In contrast to the pseudoscalar sector, this mixing angle is small, so ω is predominantly nonstrange while ϕ is predominantly of strange quarks. The chiral partners of the vector mesons are the $J^{PC} = 1^{++}$ axial vector mesons, desscribed by the current

$$A^{\mu}_{1,ij} \sim \frac{1}{\sqrt{2}} \bar{q}_j \gamma^5 \gamma^{\mu} q_i \tag{3.3.13}$$

$$A_1^{\mu} = \frac{1}{\sqrt{2}} \begin{pmatrix} \frac{f_{1,N}^{\mu}+a_1^{0\mu}}{\sqrt{2}} & a_1^{+\mu} & K_{1A}^{+\mu} \\ a_1^{-\mu} & \frac{f_{1,N}^{\mu}-a_1^{0\mu}}{\sqrt{2}} & K_{1A}^{0\mu} \\ K_{1A}^{-\mu} & \bar{K}_{1A}^{0\mu} & f_{1,S}^{\mu} \end{pmatrix}. \tag{3.3.14}$$

The isoscalar sector again has a mixing:

$$\begin{pmatrix} f_1(1285) \\ f_1(1420) \end{pmatrix} = \begin{pmatrix} \cos\beta_{A_1} & \sin\beta_{A_1} \\ -\sin\beta_{A_1} & \cos\beta_{A_1} \end{pmatrix} \begin{pmatrix} f_{1,N}^{\mu} \\ f_{1,S}^{\mu} \end{pmatrix}, \tag{3.3.15}$$

where the unknown mixing angle β_{A_1} is expected to be small because of the homochiral nature of the multiplet [86], see also Ref. [96]. We will take this unknown angle to be zero in this thesis. The kaonic axial vector mesons are not eigenstates of C, the axial vector state $K_{1,A}$ with $J^{PC} = 1^{++}$ mixes with the $K_{1,B}$, which belongs to the $J^{PC} = 1^{+-}$ pseudovector nonet [97]:

$$\begin{pmatrix} K_1(1270) \\ K_1(1400) \end{pmatrix}^{\mu} = \begin{pmatrix} \cos\varphi_K & -i\sin\varphi_K \\ -i\sin\varphi_K & \cos\varphi_K \end{pmatrix} \begin{pmatrix} K_{1,A} \\ K_{1,B} \end{pmatrix}^{\mu}. \tag{3.3.16}$$

The numerical value $\varphi_K = (56.4 \pm 4.3)^{\circ}$ [96, 97] is large, but not quite near perfect mixing. So we can say $K_1(1270)$ is predominantly $K_{1,B}$ and $K_1(1400)$ is predominantly $K_{1,A}$. Being chiral partners, the vectors and axial vectors combine to make

$$R^{\mu} = V^{\mu} - A_1^{\mu}, \tag{3.3.17}$$

$$L^{\mu} = V^{\mu} + A_1^{\mu}, \tag{3.3.18}$$

which transform under chiral transformations as

$$R^\mu \to U_R R^\mu U_R^\dagger,\ L^\mu \to U_L L^\mu U_L^\dagger. \tag{3.3.19}$$

In this thesis we will not focus on the pseudovectors and their chiral partners, the excited vector mesons. One can make similar nonets for them [98, 99], but as they are not relevant for the following chapters. we will skip them.

The final two of interest are the two tensor ($J = 2$) meson nonets. The $J^{PC} = 2^{++}$ tensor states have the current

$$T_{ij}^{\mu\nu} \sim \frac{1}{\sqrt{2}} \bar{q}_j (i\gamma^\mu \partial^\mu + \cdots) q_i. \tag{3.3.20}$$

They consist of the$a_2(1320)$, $K_2^*(1430)$, $f_2(1270)$, $f_2'(1525)\}$, and in nonet form are

$$T^{\mu\nu} = \frac{1}{\sqrt{2}} \begin{pmatrix} \frac{f_{2,N}^{\mu\nu}+a_2^{0\mu\nu}}{\sqrt{2}} & a_2^{+\mu\nu} & K_2^{*+\mu\nu} \\ a_2^{-\mu\nu} & \frac{f_{2,N}^{\mu\nu}-a_2^{0\mu\nu}}{\sqrt{2}} & K_2^{*0\mu\nu} \\ K_2^{*-\mu\nu} & \bar{K}_2^{*0\mu\nu} & f_{2,S}^{\mu\nu} \end{pmatrix}. \tag{3.3.21}$$

The physical isoscalar-tensor states are mixed as

$$\begin{pmatrix} f_2(1270) \\ f_2'(1525) \end{pmatrix} = \begin{pmatrix} \cos\beta_T & \sin\beta_T \\ -\sin\beta_T & \cos\beta_T \end{pmatrix} \begin{pmatrix} f_{2,N} \\ f_{2,S} \end{pmatrix}, \tag{3.3.22}$$

where $\beta_T \simeq 5.7°$ is the mixing angle reported by the PDG [2]. In chapter 4 we will find the mixing angle β_T by fiting to data on decays. Even though these are a higher spin meson, they are fairly well known and well studied, see e.g. [100, 101, 102].

The axial tensor mesons are the chiral partners of the tensor mesons, they have $J^{PC} = 2^{--}$ and currents

$$A_2^{\mu\nu} \sim \frac{1}{\sqrt{2}} \bar{q}_j \left(\gamma^5 \gamma^\mu \partial^\nu + ...\right) q_i. \tag{3.3.23}$$

This nonet is quite poorly known. Only the kaonic states $K_2(1820)$ and $K_2(1770)$ have been measured. Mixing is also expected but still unknown, the $K_2(1820)$ would be considered as predominately axial tensor and the $K_2(1770)$ as primarily pseudotensor. The matrix for this nonet reads:

$$A_2^{\mu\nu} = \frac{1}{\sqrt{2}} \begin{pmatrix} \frac{\omega_{2,N}^{\mu\nu}+\rho_2^{0\mu\nu}}{\sqrt{2}} & \rho_2^{+\mu\nu} & K_2^{+\mu\nu} \\ \rho_2^{-\mu\nu} & \frac{\omega_{2,N}^{\mu\nu}-\rho_2^{0\mu\nu}}{\sqrt{2}} & K_2^{0\mu\nu} \\ K_2^{-\mu\nu} & \bar{K}_2^{0\mu\nu} & \omega_{2,S}^{\mu\nu} \end{pmatrix}. \tag{3.3.24}$$

The isoscalar mixing is expected to be small because of of the homochiral nature [86] of this nonet. This means for the isoscalars:

$$\omega_{2,N} \simeq \omega_2, \qquad \omega_{2,S} \simeq \phi_2. \tag{3.3.25}$$

Recent theoretical work devoted to the vacuum properties and thermal properties of these resonances, have been done in [103, 104] and [105, 106] respectively. The tensor and axial tensor mesons combine in a similar way to the vectors and axial vectors to make a chiral multiplet:

$$\mathbf{L}^{\mu\nu} = T^{\mu\nu} + A_2^{\mu\nu}, \tag{3.3.26}$$

$$\mathbf{R}^{\mu\nu} = T^{\mu\nu} - A_2^{\mu\nu}, \tag{3.3.27}$$

and they have a similar transformation rule under chiral transformations:

$$\mathbf{R}^{\mu\nu} \to U_R \mathbf{R}^{\mu\nu} U_R^\dagger, \ \mathbf{L}^{\mu\nu} \to U_L \mathbf{L}^{\mu\nu} U_L^\dagger. \tag{3.3.28}$$

These, along with glueball states and charm-anticharm states, which will be simply itself times the unit matrix in flavor space, effectively making them flavor blind, are all the relevant ingredients for making the chiral Lagrangians that are used in the Linear Sigma Model and its extensions. The transformation rules under parity, charge conjugation, and flavor transformations for all the relevant nonets for this thesis are summarized in Table 3.1, and the transformations for the chiral multiplets under C, P and chiral transformations in Table 3.2. The chiral multiplets are used at first to build chirally invariant Lagrangians, which are then expanded in the physical fields in order to relate to experiments. The next chapters will go over the construction and use of these Lagrangians in more detail.

Nonet	Parity (P)	Charge conjugation (C)	Flavour $(U_V(3))$
$J^{PC} = 0^{-+} = P$	$-P(t, -\vec{x})$	P^t	$UPU^\dagger$
$J^{PC} = 0^{++} = S$	$S(t, -\vec{x})$	S^t	$USU^\dagger$
$J^{PC} = 1^{--} = V^\mu$	$V_\mu(t, -\vec{x})$	$-(V^\mu)^t$	$UV^\mu U^\dagger$
$J^{PC} = 1^{++} = A_1^\mu$	$-A_{1\,\mu}(t, -\vec{x})$	$(A_1^\mu)^t$	$UA_1^\mu U^\dagger$
$J^{PC} = 2^{++} = T^{\mu\nu}$	$T_{\mu\nu}(t, -\vec{x})$	$(T^{\mu\nu})^t$	$UT^{\mu\nu}U^\dagger$
$J^{PC} = 2^{--} = A_2^{\mu\nu}$	$-A_{2\,\mu\nu}(t, -\vec{x})$	$-(A_2^{\mu\nu})^t$	$UA_2^{\mu\nu}U^\dagger$

Table 3.1: Mesonic nonet transformations under P, C and $U_V(3)$.

Nonet	Parity (P)	Charge conjugation (C)	$U_R(3) \times U_L(3)$
$\Phi(t, \vec{x})$	$\Phi^\dagger(t, -\vec{x})$	$\Phi^t(t, \vec{x})$	$U_L \Phi U_R^\dagger$
$R^\mu(t, \vec{x})$	$L_\mu(t, -\vec{x})$	$-(L^\mu(t, \vec{x}))^t$	$U_R R^\mu U_R^\dagger$
$L^\mu(t, \vec{x})$	$R_\mu(t, -\vec{x})$	$-(R^\mu(t, \vec{x}))^t$	$U_L L^\mu U_L^\dagger$
$\mathbf{R}^{\mu\nu}(t, \vec{x})$	$\mathbf{L}_{\mu\nu}(t, -\vec{x})$	$(\mathbf{L}^{\mu\nu}(t, \vec{x}))^t$	$U_R \mathbf{R}^{\mu\nu} U_R^\dagger$
$\mathbf{L}^{\mu\nu}(t, \vec{x})$	$\mathbf{R}_{\mu\nu}(t, -\vec{x})$	$(\mathbf{R}^{\mu\nu}(t, \vec{x}))^t$	$U_L \mathbf{L}^{\mu\nu} U_L^\dagger$

Table 3.2: Transformations of the chiral multiplets under P, C, and $U_R(3) \times U_L(3)$.

3.3.2 The three-flavor Linear Sigma Model Lagrangian

With all the ingredients we have discussed previously we can construct the full Linear Sigma Model Lagrangian. In summary, it is based on

- Invariance under dilatation symmetry, with the only exceptions being the dilaton potential, terms due to nonzero quark masses, and the $\mathrm{U}(1)_\mathrm{A}$ anomaly. The dilaton potential mimics the trace anomaly and leads to a gluon condensate and a dimensionful quantity $\Lambda_G \sim \Lambda_{QCD}$,

- Global chiral symmetry and its spontaneous breaking, which leads to Goldstone bosons. While the trace anomaly gives a dimensionful quantity on which all masses depend, the mass hierarchy is determined by spontaneous chiral symmetry breaking.
- Chiral symmetry is also broken by the axial anomaly and explicitly by nonzero quark masses. These are the only exceptions to Chiral invariance in the LSM Lagrangian.
- C, P, and T all being individually conserved
- Before taking the appropriate shifts caused by symmetry breaking, all interaction terms are of dimension 4. The exceptions are those terms which explicitly break dilatation invariance, i.e. those from quark masses and the $\mathrm{U}(1)_A$ axial anomaly.

From these considerations, the number of terms that can be written down is finite. The Linear Sigma Model Lagrangian with (pseudo)scalar and (axial)vector mesons is given by [107]

$$\begin{aligned}
\mathcal{L} = \mathcal{L}_{dil} &+ \mathrm{Tr}[(D_\mu\Phi)^\dagger(D_\mu\Phi)] - m_0^2\left(\frac{G}{G_0}\right)^2 \mathrm{Tr}(\Phi^\dagger\Phi) - \lambda_1[\mathrm{Tr}(\Phi^\dagger\Phi)]^2 - \lambda_2\,\mathrm{Tr}(\Phi^\dagger\Phi)^2 \\
&- \frac{1}{4}\mathrm{Tr}(L_{\mu\nu}^2 + R_{\mu\nu}^2) + \mathrm{Tr}\left[\left(\left(\frac{G}{G_0}\right)^2\frac{m_1^2}{2} + \Delta\right)(L_\mu^2 + R_\mu^2)\right] + \mathrm{Tr}[H(\Phi+\Phi^\dagger)] \\
&+ c_1(\det\Phi - \det\Phi^\dagger)^2 + i\frac{g_2}{2}(\mathrm{Tr}\{L_{\mu\nu}[L^\mu, L^\nu]\} + \mathrm{Tr}\{R_{\mu\nu}[R^\mu, R^\nu]\}) \\
&+ \frac{h_1}{2}\mathrm{Tr}(\Phi^\dagger\Phi)\,\mathrm{Tr}(L_\mu^2 + R_\mu^2) + h_2\,\mathrm{Tr}[|L_\mu\Phi|^2 + |\Phi R_\mu|^2] + 2h_3\,\mathrm{Tr}(L_\mu\Phi R^\mu\Phi^\dagger) \\
&+ g_3[\mathrm{Tr}(L_\mu L_\nu L^\mu L^\nu) + \mathrm{Tr}(R_\mu R_\nu R^\mu R^\nu)] + g_4[\mathrm{Tr}\,(L_\mu L^\mu L_\nu L^\nu) + \mathrm{Tr}\,(R_\mu R^\mu R_\nu R^\nu)] \\
&+ g_5\,\mathrm{Tr}\,(L_\mu L^\mu)\;\mathrm{Tr}\,(R_\nu R^\nu) + g_6[\mathrm{Tr}(L_\mu L^\mu)\;\mathrm{Tr}(L_\nu L^\nu) + \mathrm{Tr}(R_\mu R^\mu)\;\mathrm{Tr}(R_\nu R^\nu)]\,, \qquad (3.3.29)
\end{aligned}$$

where $\mathcal{L}_{dil}$ is the dilaton Lagrangian, kinetic terms plus (3.1.6), the g_i, c_i, h_i are dimensionless couplings, the m_i are masses (before spontaneous chiral symmetry breaking, normalized with factors G_0 to make dimensionless combinations), and

$$\begin{aligned}
D^\mu\Phi &\equiv \partial^\mu\Phi - ig_1(L^\mu\Phi - \Phi R^\mu)\,, \\
L^{\mu\nu} &\equiv \partial^\mu L^\nu - \partial^\nu L^\mu\,, \\
R^{\mu\nu} &\equiv \partial^\mu R^\nu - \partial^\nu R^\mu\,.
\end{aligned}$$

The terms with Δ and H are proportional to quark masses and as such break both dilatation and chiral invariance. These matrices are given by

$$H = \begin{pmatrix} \frac{h_{0N}}{2} & 0 & 0 \\ 0 & \frac{h_{0N}}{2} & 0 \\ 0 & 0 & \frac{h_{0S}}{\sqrt{2}} \end{pmatrix}\,, \qquad (3.3.30)$$

$$\Delta = \begin{pmatrix} \delta_N & 0 & 0 \\ 0 & \delta_N & 0 \\ 0 & 0 & \delta_S \end{pmatrix}\,. \qquad (3.3.31)$$

These terms describe the effect of nonzero quark masses on the (pseudo)scalars and the (axial)vectors sectors. They are related to quark masses by $h_N \sim m_u$, $h_S \sim m_s$, $\delta_N \sim m_u^2$, $\delta_S \sim m_s^2$. The u and d quark masses are taken to be equal, but the s quark mass is different (larger). Thus flavor symmetry is broken to isopsin, which we will assume to be conserved in all strong interactions. Electromagnetic interactions which violate isospin conservation can be implemented as well, as will be done later. The terms involving a determinant are due to the axial anomaly, and break dilatation invariance as well.

We then go through the symmetry breaking mechanisms in the same way as described before, this has the following consequences:
(i) The scalar-isoscalar fields of the model acquire nonzero v.e.v. The dilaton field G condenses to G_0. Similarly, $q\bar{q}$ scalar-isoscalar fields develop a v.e.v. as a consequence of spontaneous chiral symmetry breaking, which in simple terms is due to the Mexican hat form of the effective potential when $m_0^2 < 0$. This gives the following shifts:

$$G \to G + G_0 \ , \ S \to S + \Phi_0 \qquad \text{with} \qquad \Phi_0 := \frac{1}{\sqrt{2}} \begin{pmatrix} \frac{\phi_N}{\sqrt{2}} & 0 & 0 \\ 0 & \frac{\phi_N}{\sqrt{2}} & 0 \\ 0 & 0 & \phi_S \end{pmatrix} . \tag{3.3.32}$$

where the numerical values are reported in Table 3.3.
(ii) The axial vector matrix must be shifted because chiral symmetry breaking induces a mixing of scalar and axial vector fields, which is proportional to the parameter $g_1 = \frac{m_{a_1}}{Z_\pi f_\pi}\sqrt{1-\frac{1}{Z_\pi^2}} \simeq 5.8$ [107, 108]. This operation amounts to:

$$A_{1\,\mu} \to A_{1\,\mu} + \partial_\mu \mathcal{P}, \ \mathcal{P} := \frac{1}{\sqrt{2}} \begin{pmatrix} \frac{Z_\pi w_\pi(\eta_N+\pi^0)}{\sqrt{2}} & Z_\pi w_\pi \pi^+ & Z_K w_K K^+ \\ Z_\pi w_\pi \pi^- & \frac{Z_\pi w_\pi(\eta_N-\pi^0)}{\sqrt{2}} & Z_K w_K K^0 \\ Z_K w_K K^- & Z_K w_K \bar{K}^0 & Z_{\eta_S} w_{\eta_S} \eta_S \end{pmatrix} . \tag{3.3.33}$$

The constants are also given in Table 3.3. The matrix $\mathcal{P}$ contains the pseudoscalar fields, just as the matrix P, but proper renormalization factors have been included. The shifts in Eqs. (3.3.32) and (3.3.33) will also have to be applied to the higher spin Lagrangians studied the next in chapter.

Parameters	Expressions	Numerical values [107]
$Z_\pi = Z_{\eta_N}$	$\frac{m_{a_1}}{\sqrt{m_{a_1}^2 - g_1^2\phi_S^2}}$	1.709
$w_\pi = w_{\eta_N}$	$\frac{g_1\phi_N}{m_{a_1}^2}$	0.683 GeV^{-1}
Z_K	$\frac{2m_{K_{1A}}}{\sqrt{4m_{K_{1A}}^2 - g_1^2(\phi_N+\sqrt{2}\phi_S)^2}}$	1.604
w_K	$\frac{g_1(\phi_N+\sqrt{2}\phi_S)}{2m_{K_{1,A}}^2}$	0.611 GeV^{-1}
Z_{η_S}	$\frac{m_{f_{1,S}}}{\sqrt{m_{f_{1,S}}^2 - 2g_1^2\phi_S^2}}$	1.539
w_{η_S}	$\frac{\sqrt{2}g_1\phi_S}{m_{f_{1,S}}^2}$	0.554 GeV^{-1}
ϕ_N	$Z_\pi f_\pi$	0.158 GeV
ϕ_S	$\frac{2Z_K f_K - \phi_N}{\sqrt{2}}$	0.138 GeV
g_1	$\frac{m_{a_1}}{Z_\pi f_\pi}\sqrt{1-\frac{1}{Z_\pi^2}}$	5.8

Table 3.3: Numerical values of scalar and axial vector shift-related quantities.

Chapter 4

Spin 2 tensor mesons and axial tensor mesons

4.1 Introduction

In table 1.1, the ground state ($n = 1$) mesons for different quantum numbers are listed in the non-relativistic spectroscopic notation $n^{2S+1}L_J$ and also the relativistic notation J^{PC}. Some of these meson nonets are very well established [2], such as the $J^{PC} = 0^{-+}$ pseudoscalar mesons, the $J^{PC} = 1^{--}$ vector mesons and the $J^{PC} = 1^{++}$ axial vector mesons. They are supported by other approaches such as a quark model [100] and using the Bethe-Salpeter equation [109]. The scalar meson nonet is not completely established since there are more discovered resonances than possible ground state quark-antiquark states, see [88, 110, 111, 112, 113, 114, 115, 81]. Unconventional mesons such as the scalar glueball will have to be identified to completely fix this nonet. These four nonets have also all been studied in the eLSM [107, 79]. The pseudovectors and their chiral partners, the orbitally excited vector mesons, are also reasonably well understood, with the exception of a missing orbitally excited vector state $\phi(?)$, with an expected mass at about 1.9 GeV [116]. These nonets have also been studied in the eLSM as decay products of the vector glueball [98]. Furthermore, in the eLSM hybrid meson states have also been analyzed [99].
Next are the spin 2 mesons, the tensor ($J^{PC} = 2^{++}$), the axial tensor mesons ($J^{PC} = 2^{--}$), and the pseudotensor mesons ($J^{PC} = 2^{-+}$). There are still some open questions on the pseudotensor mesons, in particular on their mixing behaviors, see e.g. [117, 118, 119], but we will focus on the other two spin 2 mesons, which are the chiral partners of one another. The tensor mesons are very well known, see e.g. [102, 101, 111]. Meanwhile the axial tensor mesons, as can be seen from table 1.1, are very poorly known. Only the kaonic $K_2(1820)$, with unknown mixing with $K_2(1770)$, is listed. The isovector member ρ_2 and the isotensor members ω_2 and ϕ_2 have not yet been discovered. Given that the eLSM has been used to describe the other nonets, it is then a natural next step to extend the eLSM to the spin 2 sector, and the eLSM is especially equipped to tackle this problem. Specifically, because the eLSM is based heavily on chiral symmetry, the tensor and axial tensor mesons are treated equally. That is, with the same couplings and interaction terms when written in the chiral multiplets discussed in the previous chapter. This lets us use the phenomenological data on the tensor mesons to predict the behavior of the axial tensor mesons. We fit to and postdict data on decays of tensor mesons, along with predicting radiative decay rates for the tensors, and predict the masses and decay rates of the axial tensor mesons. We find that the tensor meson

data is described well, meaning that the ground states states fit well in the conventional quark-antiquark assignment. For the axial tensor mesons we find that their decay rates are quite large, and dominated by the vector-pseudoscalar channel. The result that the axial tensor states are very broad could tie into the fact they have not been observed yet. The results of this chapter can be tested at a number of experiments, such as BESIII [120, 121], CLAS12 [122, 123], COMPASS [124], GlueX [125, 126, 127], as well as the planned PANDA experiment [128].

4.2 The spin-2 extension of the eLSM

In chapter 3.3.1 we introduced the building blocks for Lagangians of the eLSM. The eLSM Lagrangian – not yet involving spin 2 fields – built from these was of the form

$$\mathcal{L}_{\text{eLSM}} = \mathcal{L}_{\text{dil}} + \text{Tr}\Big[\Big(D_\mu\Phi\Big)^\dagger\Big(D_\mu\Phi\Big)\Big] - m_0^2\Big(\frac{G}{G_0}\Big)^2\text{Tr}\Big[\Phi^\dagger\Phi\Big] - \frac{1}{4}\text{Tr}\Big[\Big(L_{\mu\nu}^2 + R_{\mu\nu}^2\Big)\Big] + \text{Tr}\Big[\Big(\frac{m_{\text{vec}}^2 G^2}{2G_0^2} + \Delta\Big)\Big(L_\mu^2 + R_\mu^2\Big)\Big] + \cdots \; . \tag{4.2.1}$$

Using the same procedure as in Chapter 3, we will construct chiral Lagrangians involving the spin 2 fields. We will consider exact isospin symmetry, but isospin symmetry breaking – an unexpected level of which has been recently confirmed by experiments [129, 130] – can be included in the eLSM, see [68] for an implementation. The full interaction Lagrangian can be split up into four Lagrangian terms, leading to the mass terms of the (axial) tensor mesons as well as the interactions and decays. The first one has the form

$$\mathcal{L}_{\text{mass}} = \text{Tr}\Big[\Big(\frac{m_{\text{ten}}^2 G^2}{2\,G_0^2} + \Delta^{\text{ten}}\Big)\Big(\mathbf{L}_{\mu\nu}^2 + \mathbf{R}_{\mu\nu}^2\Big)\Big] + \frac{h_1^{\text{ten}}}{2}\text{Tr}\Big[\Phi^\dagger\Phi\Big]\text{Tr}\Big[\mathbf{L}^{\mu\nu}\mathbf{L}_{\mu\nu} + \mathbf{R}^{\mu\nu}\mathbf{R}_{\mu\nu}\Big] + h_2^{\text{ten}}\text{Tr}\Big[\Phi^\dagger\mathbf{L}^{\mu\nu}\mathbf{L}_{\mu\nu}\Phi + \Phi\mathbf{R}^{\mu\nu}\mathbf{R}_{\mu\nu}\Phi^\dagger\Big] + 2h_3^{\text{ten}}\text{Tr}\Big[\Phi\mathbf{R}^{\mu\nu}\Phi^\dagger\mathbf{L}_{\mu\nu}\Big]. \tag{4.2.2}$$

Here, $\Delta^{\text{ten}} = \text{diag}\{\delta_N^{\text{ten}}, \delta_N^{\text{ten}}, \delta_S^{\text{ten}}\}$ is a contribution from the bare/current quark masses just like the one in (3.3.31), and the fields are those described in section 3.3.1. We can absorb the small light-quark contribution into the term proportional to m_{ten}, essentially setting $\delta_N^{\text{ten}} = 0$. The value of δ_S^{ten} is then obtained from the mass relation $\delta_S^{\text{ten}} = m_{K_2}^2 - m_{\mathbf{a}_2}^2 \simeq 0.3\,\text{GeV}^2$ using PDG [2] values for the masses of the tensor mesons. The term proportional to Δ^{ten} is the only one breaking dilatation invariance in this Lagrangian, as all other terms have dimensionless coupling constants.

In the large N_c limit [131, 132, 133], where N_c is the number of colors of the SU(N$_\text{c}$) gauge group, the coupling constants scale as

$$m_{\text{ten}} \sim N_c^0 \tag{4.2.3}$$
$$h_1^{\text{ten}} \sim N_c^{-3} \tag{4.2.4}$$
$$h_2^{\text{ten}} \sim N_c^{-1} \tag{4.2.5}$$
$$h_3^{\text{ten}} \sim N_c^{-1} \tag{4.2.6}$$
$$G_0 \sim N_c. \tag{4.2.7}$$

Consequently, the interaction with the coupling h_1^{ten} is suppressed in the large N_c limit, and the dimensionless coupling m_{ten}^2/G_0^2 scales as N_c^{-2}. While we are in the physical $N_c = 3$ case, the large N_c limit is still a useful way to distinguish leading and subleading terms.

The next interaction terms each generate some of the decays of (axial)tensor mesons. The first of these is of the form

$$\mathcal{L}_{g_2^{\text{ten}}} = \frac{g_2^{\text{ten}}}{2}\Big(\mathrm{Tr}\Big[\mathbf{L}_{\mu\nu}\{L^\mu, L^\nu\}\Big] + \mathrm{Tr}\Big[\mathbf{R}_{\mu\nu}\{R^\mu, R^\nu\}\Big]\Big) + \frac{g_2'^{\,\text{ten}}}{6}\mathrm{Tr}\Big[\mathbf{L}_{\mu\nu} + \mathbf{R}_{\mu\nu}\Big]\mathrm{Tr}\Big[\{L^\mu, L^\nu\} + \{R^\mu, R^\nu\}\Big]\,. \tag{4.2.8}$$

The coupling constants scale as $g_2^{\text{ten}} \propto N_c^{-1/2}$ and $g_2'^{\text{ten}} \propto N_c^{-3/2}$. Hence g_2^{ten} is dominant and $g_2'^{\text{ten}}$ is suppressed. Terms that are even more suppressed in large N_c do exist, but we will not treat them in this work. This Lagrangian is written down after condensation of G, which makes it so that the coupling constants have the dimension of energy. Only the terms proportional to G_0 are kept, and the interactions with the dilaton G are omitted as this will not be relevant to the phenomenology. This Lagrangian leads to the two following types of decays

1. $2^{++} \longrightarrow 0^{-+} + 0^{-+}$, i.e. $T \to PP$;
2. $2^{--} \longrightarrow 1^{--} + 0^{-+}$, i.e. $A_2 \to VP$.

Later on we will see that these two decay channels turn out to be the dominant ones for the tensor and axial tensor mesons respectively. Since they appear in together in the chiral multiplets $\mathbf{L}_{\mu\nu}, \mathbf{R}_{\mu\nu}, L_\mu, R_\mu$, these are proportional to the same combination of the coupling constants g_2^{ten} and $g_2'^{\text{ten}}$. Using the experimental data on the tensor decays we will estimate the axial tensor decay modes.
The next interaction terms relevant for us all involve derivatives, which ties in the fact that the decays from (4.2.8) turn out to be dominant. The first of these can be written down as

$$\mathcal{L}_{A^{\text{ten}}} = \frac{a^{\text{ten}}}{2}\mathrm{Tr}\Big[\mathbf{L}_{\mu\nu}\{L^\mu_\beta, L^{\nu\beta}\} + \mathbf{R}_{\mu\nu}\{R^\mu_\beta, R^{\nu\beta}\}\Big] + \frac{a'^{\,\text{ten}}}{6}\mathrm{Tr}\Big[\mathbf{L}_{\mu\nu} + \mathbf{R}_{\mu\nu}\Big]\mathrm{Tr}\Big[\{L^\mu_\beta, L^{\nu\beta}\} + \{R^\mu_\beta, R^{\nu\beta}\}\Big]\,. \tag{4.2.9}$$

In the large N_c limit the couplings scale as $a^{\text{ten}} \propto N_c^{-1/2}$ and $a'^{\text{ten}} \propto N_c^{-3/2}$, hence the first term is seen as the leading one. The difference in structure between the leading and subleading terms is similar as in (4.2.8), with two traces being subleading compared to one trace. The coupling constants have dimension [Energy^{-1}], which means that, as mentioned before, these terms cannot be made dilatation invariant without introducing a singularity in $G = 0$. These terms breaking dilatation invariance is another reason to believe why decays via this Lagrangian are not the most prominent. However, they are still important for us, since by using a vector meson dominance (VMD) model, we can include the photon field A_μ. In doing this, this Lagrangian gives us in total the decay of a tensor meson to two photons, one photon and one vector meson, and into two vector mesons when the photon is not included. When discussing radiative decays we will go into more detail on the implementation of VMD.
The final chiral interaction terms have the form

$$\begin{aligned}\mathcal{L}_{c^{\text{ten}}} = {}& c_1^{\text{ten}}\,\mathrm{Tr}\Big[\partial^\mu\mathbf{L}^{\nu\alpha}\tilde{L}_{\mu\nu}\,\partial_\alpha\Phi\,\Phi^\dagger - \partial^\mu\mathbf{R}^{\nu\alpha}\Phi^\dagger\,\partial_\alpha\Phi\tilde{R}_{\mu\nu} - \partial^\mu\mathbf{R}^{\nu\alpha}\tilde{R}_{\mu\nu}\partial_\alpha\Phi^\dagger\Phi + \partial^\mu\mathbf{L}^{\nu\alpha}\Phi\partial_\alpha\Phi^\dagger\tilde{L}_{\mu\nu}\Big]\\ &+c_2^{\text{ten}}\,\mathrm{Tr}\Big[\partial^\mu\mathbf{L}^{\nu\alpha}\partial_\alpha\Phi\tilde{R}_{\mu\nu}\,\Phi^\dagger - \partial^\mu\mathbf{R}^{\nu\alpha}\Phi^\dagger\,\tilde{L}_{\mu\nu}\partial_\alpha\Phi - \partial^\mu\mathbf{R}^{\nu\alpha}\partial_\alpha\Phi^\dagger\tilde{L}_{\mu\nu}\Phi + \partial^\mu\mathbf{L}^{\nu\alpha}\Phi\tilde{R}_{\mu\nu}\partial_\alpha\Phi^\dagger\Big]\,,\end{aligned} \tag{4.2.10}$$

where $\tilde{L}_{\mu\nu}$ and $\tilde{R}_{\mu\nu}$ are the Hodge duals for $L_{\mu\nu}$ and $R_{\mu\nu}$, i.e. $\tilde{L}_{\mu\nu} = \frac{1}{2}\epsilon_{\mu\nu\rho\sigma}L^{\rho\sigma}$, and the similar expression

Decay Mode	$\frac{1}{5} \times \lvert\mathcal{M}\rvert^2$
$2^{++} \longrightarrow 0^{-+} + 0^{-+}$	$g_2^{\text{ten}\,2} \times \frac{2\lvert\vec{k}_{p(1),p(2)}\rvert^4}{15}$
$2^{--} \longrightarrow 0^{-+} + 1^{--}$	$g_2^{\text{ten}\,2} \times \frac{\lvert\vec{k}_{v,p}\rvert^2}{15}\left(5 + \frac{2\lvert\vec{k}_{v,p}\rvert^2}{m_v^2}\right)$
$2^{--} \longrightarrow 0^{-+} + 2^{++}$	$\frac{4h_3^{\text{ten}\,2}}{45}\left(45 + \frac{4\lvert\vec{k}_{t,p}\rvert^4}{m_t^4} + \frac{30\lvert\vec{k}_{t,p}\rvert^2}{m_t^2}\right)$
$2^{++} \longrightarrow 0^{-+} + 1^{--}$	$\frac{(c_1^{\text{ten}}+c_2^{\text{ten}})^2\, m_t^2 \lvert\vec{k}_{v,p}\rvert^4}{5}$
$2^{--} \longrightarrow 0^{-+} + 1^{++}$	$\frac{(c_1^{\text{ten}}-c_2^{\text{ten}})^2\, m_{a_2}^2 \lvert\vec{k}_{a_1,p}\rvert^4}{5}$

Table 4.1: Decay amplitudes for different decay modes.

for $\tilde{R}_{\mu\nu}$. This Lagrangian breaks also dilatation invariance because it involves the Levi-Civita tensor $\epsilon_{\mu\nu\rho\sigma}$. Both constants c_1^{ten} and c_2^{ten} scale as $N_c^{-1/2}$, and will appear as their sum in decay formulas. For the decay channels of these terms we will not look at large N_c suppressed terms, as they are not needed to describe the current data. The pseudoscalars appear here as a decay product because of the shift of (3.3.33). The decay channels that follow from this Lagrangian are:

1. $2^{++} \longrightarrow 1^{--} + 0^{-+}$, i.e. $T \to VP$;
2. $2^{--} \longrightarrow 1^{++} + 0^{-+}$, i.e. $A_2 \to AP$.

The tree-level decay rate of a generic spin-2 state has the form:

$$\Gamma^{tl}_{T \to A+B} = \frac{|\vec{k}_{a,b}|}{8\,\pi\, m_t^2} \times \frac{1}{5}|\mathcal{M}|^2 \times \kappa_i \times \Theta(m_t - m_a - m_b)\,, \tag{4.2.11}$$

where m_t is the mass of the decaying spin 2 particle, and m_a and m_b are the masses of the decay products. The Heaviside step function $\Theta(x)$ ensures that only kinematically allowed decays take place. The vector $\vec{k}_{a,b}$ is the outgoing 3-momentum of one of the decay products, its modulus is given by:

$$|\vec{k}_{a,b}| = \frac{1}{2\, m_t}\sqrt{(m_t^2 - m_a^2 - m_b^2)^2 - 4m_a^2 m_b^2}\ \ . \tag{4.2.12}$$

The κ_i are channel dependent coefficients for the decay channel i, they depend on the coupling constants and on the parameters in Table 3.3 with some numerical prefactor, and can have a dimension depending on the decay channel. Finally, $\mathcal{M}$ is the matrix element for the Feynman diagram of the decay. They are listed in Table 4.1.

4.3 Results

Now we will move onto the results for the decays of spin 2 tensor mesons. First, we compute their masses that arise due to the spontaneous breaking of chiral symmetry. The well established tensor meson masses will allow us to get the value of the masses of their poorly known chiral partners, the axial tensor mesons. Afterwards we turn to the decays, first to those of the tensor mesons (that are well measured and serve as a test of the approach and for parameter determination), and then to the decays of the ground-state axial tensor mesons (that are mostly experimentally unknown). In Table 4.2, all the parameters of the eLSM related to the (axial)tensor decays and masses that will be obtained in the following subsections are shown.

Parameters	Numerical Values	Fitting Data
h_3^{ten}	-41	Table 4.3
δ_S^{ten}	$0.3\,\text{GeV}^2$	Table 4.3
g_2^{ten}	$(1.392 \pm 0.024) \cdot 10^4(\text{MeV})$	Table 4.5
$g_2^{\prime\,\text{ten}}$	$(0.024 \pm 0.041) \cdot 10^4(\text{MeV})$	Table 4.5
$g_{2\,\text{lat}}^{\text{ten}}$	$(0.7 \pm 0.4) \cdot 10^4(\text{MeV})$	Table 4.12
c^{ten}	$(4.8 \pm 0.9) \cdot 10^{-7}(\text{MeV})^{-3}$	Table 4.6
a^{ten}	$(-2.09 \pm 0.06) \cdot 10^{-2}(\text{MeV})^{-1}$	Table 4.8
$a^{\prime\,\text{ten}}$	$(3.5 \pm 0.4) \cdot 10^{-3}(\text{MeV})^{-1}$	Table 4.8
β_T	$(3.16 \pm 0.81)^\circ$	Table 4.5

Table 4.2: Parameters of the eLSM connected to the (axial) tensor mesons as determined by fits to known experimental data.

4.3.1 Masses of (axial)tensor mesons

To find the masses of the tensor mesons, we expand (4.2.2), with the condensation of G and shifts of (3.3.32) and (3.3.33). The resulting expressions for the masses of the tensor mesons are

$$m_{\mathbf{a}_2}^2 = \left(m_{\text{ten}}^2 + 2\delta_N^{\text{ten}}\right) + \frac{h_3^{\text{ten}}\phi_N^2}{2} + \frac{h_2^{\text{ten}}\phi_N^2}{2} + \frac{h_1^{\text{ten}}}{2}(\phi_N^2 + \phi_S^2)\,, \tag{4.3.1}$$

$$m_{K_2}^2 = \left(m_{\text{ten}}^2 + \delta_N^{\text{ten}} + \delta_S^{\text{ten}}\right) + \frac{h_1^{\text{ten}}}{2}(\phi_N^2 + \phi_S^2) + \frac{1}{\sqrt{2}}h_3^{\text{ten}}\phi_N\phi_S + \frac{h_2^{\text{ten}}}{4}(\phi_N^2 + 2\phi_S^2)\,, \tag{4.3.2}$$

$$m_{f_{2,N}}^2 = \left(m_{\text{ten}}^2 + 2\delta_N^{\text{ten}}\right) + \frac{h_3^{\text{ten}}\phi_N^2}{2} + \frac{h_1^{\text{ten}}}{2}(\phi_N^2 + \phi_S^2) + \frac{h_2^{\text{ten}}\phi_N^2}{2}\,, \tag{4.3.3}$$

$$m_{f_{2,S}}^2 = \left(m_{\text{ten}}^2 + 2\delta_S^{\text{ten}}\right) + \frac{h_1^{\text{ten}}}{2}(\phi_N^2 + \phi_S^2) + h_3^{\text{ten}}\phi_S^2 + h_2^{\text{ten}}\phi_S^2\,. \tag{4.3.4}$$

In the same way we find the masses for the axial tensor mesons, the expressions for their masses read:

$$m_{\rho_2}^2 = \left(m_{\text{ten}}^2 + 2\delta_N^{\text{ten}}\right) - \frac{h_3^{\text{ten}}\phi_N^2}{2} + \frac{h_2^{\text{ten}}\phi_N^2}{2} + \frac{h_1^{\text{ten}}}{2}(\phi_N^2 + \phi_S^2)\,, \tag{4.3.5}$$

$$m_{K_{2A}}^2 = \left(m_{\text{ten}}^2 + \delta_N^{\text{ten}} + \delta_S^{\text{ten}}\right) + \frac{h_1^{\text{ten}}}{2}(\phi_N^2 + \phi_S^2) - \frac{1}{\sqrt{2}}h_3^{\text{ten}}\phi_N\phi_S + \frac{h_2^{\text{ten}}}{4}(\phi_N^2 + 2\phi_S^2)\,, \tag{4.3.6}$$

$$m_{\omega_{2,N}}^2 = \left(m_{\text{ten}}^2 + 2\delta_N^{\text{ten}}\right) - \frac{h_3^{\text{ten}}\phi_N^2}{2} + \frac{h_2^{\text{ten}}\phi_N^2}{2} + \frac{h_1^{\text{ten}}}{2}(\phi_N^2 + \phi_S^2)\,, \tag{4.3.7}$$

$$m_{\omega_{2,S}}^2 = \left(m_{\text{ten}}^2 + 2\delta_S^{\text{ten}}\right) - h_3^{\text{ten}}\phi_S^2 + h_2^{\text{ten}}\phi_S^2 + \frac{h_1^{\text{ten}}}{2}(\phi_N^2 + \phi_S^2)\,. \tag{4.3.8}$$

Fot both the tensor and axial tensor mesons, the masses of the isovector and the nonstrange isoscalar members are equal:

$$m_{\rho_2}^2 = m_{\omega_{2,N}}^2 \text{ and } m_{\mathbf{a}_2}^2 = m_{f_{2,N}}^2 \ . \tag{4.3.9}$$

However, these are not the physical states yet. The actual physical states will differ in mass because there is a small isoscalar mixing angle.

Relating the expressions for the masses of the tensor and axial tensor mesons, we find the following three equations relating the masses of chiral partners:

$$m_{\rho_2}^2 = m_{\mathbf{a}_2}^2 - h_3^{\text{ten}}\phi_N^2, \tag{4.3.10}$$
$$m_{K_{2A}}^2 = m_{K_2}^2 - \sqrt{2}h_3^{\text{ten}}\phi_N\phi_S, \tag{4.3.11}$$
$$m_{\omega_{2,S}}^2 = m_{f_{2,S}}^2 - 2h_3^{\text{ten}}\phi_S^2 \ , \tag{4.3.12}$$

where the first equation also describes the masses $\omega_{2,N}$ and $f_{2,N}$ because of (4.3.9). Putting in the masses of the $K_2(1820)$ and $K_2^*(1430)$, we can find a numerical estimate for h_3^{ten}:

$$h_3^{\text{ten}} = \frac{m_{K_{2A}}^2 - m_{K_2}^2}{\sqrt{2}\phi_N\phi_S} \simeq -41 \ . \tag{4.3.13}$$

Next, we can find the value of δ_S^{ten} by using the PDG masses of the two tensor mesons K_2 and a_2 and taking $\delta_N^{\text{ten}} = 0$ and $\phi_N^2 \simeq 2\phi_S^2$:

$$\delta_S^{\text{ten}} = m_{K_2}^2 - m_{\mathbf{a}_2}^2 \simeq 0.3\,\text{GeV}^2 \ . \tag{4.3.14}$$

With these parameters and masses of the known tensor mesons, we can find the masses of the axial tensor mesons:

1. The mass of the purely strange resonance $\omega_{2,S} \simeq \phi_2$ is:

$$m_{\phi_2}^2 \simeq m_{\omega_{2,S}}^2 = m_{\mathbf{a}_2}^2 + 2\delta_S^{\text{ten}} - \frac{3}{2}h_3^{\text{ten}}\phi_N^2 \,, \tag{4.3.15}$$

   which implies the value for the mass of the missing strange-antistrange resonance $\phi_2(?) \simeq \omega_{2,S}$ of Table 1 is:

$$m_{\phi_2} \approx 1971\,\text{MeV} \ . \tag{4.3.16}$$

2. The mass of the ρ_2 is related to its chiral partner a_2 by

$$m_{\rho_2}^2 = m_{\mathbf{a}_2}^2 - h_3^{\text{ten}}\phi_N^2 \ ,$$

   so we predict a mass for the not-yet discovered resonance ρ_2 as:

$$m_{\rho_2} = 1663\,\text{MeV} \ . \tag{4.3.17}$$

   Since we neglect the isoscalar mixing in the axial tensor sector, we also have

$$m_{\omega 2,N} \simeq 1663 \text{ MeV}. \tag{4.3.18}$$

3. We also calculate the mass of the known purely strange isoscalar tensor meson and compare it to

experimental data:

$$m^2_{f_{2,S}} = m^2_{\omega_{2,S}} + 2h_3^{\text{ten}}\phi_S^2 \simeq 1520 \text{ MeV} . \tag{4.3.19}$$

This result is slightly below the physical value of the resonance $f_2'(1525)$ that amounts to 1538 MeV. From the relation $m^2_{\mathbf{a}_2} = m^2_{f_{2,N}}$, it also follows that $m_{f_{2,N}} = 1317$ MeV. This is slightly above the measured mass of the $f_2(1270)$ which is 1297 MeV.

These small differences between the theoretical and experimental results can be resolved by introducing a small isoscalar mixing angle. In our case, we shall determine this mixing angle with the two-pseudoscalar decay channel in subsection 4.3.2. Upon including the isoscalar mixing in the tensor sector (but still neglecting it in the axial tensor sector), Table 4.3 shows the results for the (axial) tensor masses.

Resonances	Masses (in MeV)	Resonances	Masses (in MeV)
$a_2(1320)$	**1317**	$\rho_2(?)$	1663
$K_2^*(1430)$	**1427**	$K_2(1820)$	**1819**
$f_2(1270)$	1297	$\omega_{2,N}$	1663
$f_2'(1525)$	1538	$\omega_{2,S}$	1971

Table 4.3: Masses of the spin 2 mesons predicted by the eLSM. Bold entries are the PDG values used as inputs. The mixing for the tensor-isoscalar mesons has been taken into account.

4.3.2 Decays of tensor mesons

In this subsection, we compare the predictions for the strong and radiative decay of tensor mesons with available PDG data.

$T \longrightarrow P + P$ decay mode

The Lagrangian describing the decay of spin-2 tensor mesons to two pseudoscalar mesons follows from the chiral Lagrangian of Eq. (4.2.8) by applying the shift (3.3.33) to the axial vector states. Its form is

$$\mathcal{L}_{Tpp} = g_2^{\text{ten}} \,\text{Tr}\Big[T^{\mu\nu}\big\{(\partial_\mu \mathcal{P}), (\partial_\nu \mathcal{P})\big\}\Big] + \frac{g_2'^{\text{ten}}}{3}\text{Tr}\Big[T^{\mu\nu}\Big]\text{Tr}\Big[\big\{(\partial_\mu \mathcal{P}), (\partial_\nu \mathcal{P})\big\}\Big] \ . \tag{4.3.20}$$

The coupling $g_2'^{\text{ten}}$ is scaled by a factor 1/3 so that that for the singlet state the same normalization occurs. We can decompose the tensor meson nonet as

$$\sqrt{2}T_{2,\mu\nu} = \sum_{a=0}^{8} T^a_{\mu\nu}\frac{\lambda^a}{\sqrt{2}}, \tag{4.3.21}$$

with $\lambda^0 = \sqrt{\frac{2}{3}}\mathbf{1}$. We then have that

$$T_{\mu\nu} = \frac{1}{\sqrt{6}}T^0_{\mu\nu}\mathbf{1} + ... \tag{4.3.22}$$

For the singlet state the Lagrangian then reduces to

$$\mathcal{L}_{Tpp} = (g_2^{\text{ten}} + g_2'^{\text{ten}})T^{0\,\mu\nu}\,\text{Tr}\Big[\big\{(\partial_\mu \mathcal{P}), (\partial_\nu \mathcal{P})\big\}\Big] + ..., \tag{4.3.23}$$

wherein the couplings g_2^{ten} and $g_2^{'\text{ten}}$ appear with the same prefactor. Since this is just a rescaling of $g_2^{'\text{ten}}$, this convention does not affect physical predictions. the same convention is used in other terms as well.
The tree-level decay rate for the decay into two pseudoscalars is given by

$$\Gamma^{tl}_{T\longrightarrow P^{(1)}+P^{(2)}}(m_t, m_{p^{(1)}}, m_{p^{(2)}}) = \kappa_{tpp\,,i}\,\frac{|\vec{k}_{p^{(1)},p^{(2)}}|^5}{60\,\pi\, m_t^2}\Theta(m_t - m_{p^{(1)}} - m_{p^{(2)}}) \ , \tag{4.3.24}$$

where the coefficients $\kappa_{tpp\,,i}$ (with dimension [Energy^{-2}]) are listed in Table 4.4. We then perform a χ^2 fit

Decay process	$\kappa_{tpp\,,i}$
$a_2(1320) \longrightarrow \bar{K}\,K$	$2\left(\frac{g_2^{\text{ten}} Z_k^2 w_k^2}{2}\right)^2$
$a_2(1320) \longrightarrow \pi\,\eta$	$\left(g_2^{\text{ten}} Z_\pi Z_{\eta_N} w_\pi w_{\eta_N} \cos\beta_P\right)^2$
$a_2(1320) \longrightarrow \pi\,\eta'$	$\left(-\,g_2^{\text{ten}} Z_\pi Z_{\eta_N} w_\pi w_{\eta_N} \sin\beta_P\right)^2$
$K_2^*(1430) \longrightarrow \pi\,\bar{K}$	$3\left(\frac{g_2^{\text{ten}} Z_k w_k Z_\pi w_\pi}{2}\right)^2$
$f_2(1270) \longrightarrow \bar{K}\,K$	$2\left(\frac{Z_k^2 w_k^2\left((4g_2'^{\,\text{ten}}+3g_2^{\text{ten}})\cos\beta_T+\sqrt{2}(2g_2'^{\,\text{ten}}+3g_2^{\text{ten}})\sin\beta_T\right)}{6}\right)^2$
$f_2(1270) \longrightarrow \pi\,\pi$	$6\left(\frac{Z_\pi^2 w_\pi^2\left((2g_2'^{\,\text{ten}}+3g_2^{\text{ten}})\cos\beta_T+\sqrt{2}g_2'^{\,\text{ten}}\sin\beta_T\right)}{6}\right)^2$
$f_2(1270) \longrightarrow \eta\,\eta$	$2\left(\frac{Z_{\eta_N}^2 w_{\eta_N}^2 \cos\beta_P^2\left((2g_2'^{\,\text{ten}}+3g_2^{\text{ten}})\cos\beta_T+\sqrt{2}g_2'^{\,\text{ten}}\sin\beta_T\right)+Z_{\eta_S}^2 w_{\eta_S}^2 \sin\beta_P^2\left(\sqrt{2}(g_2'^{\,\text{ten}}+3g_2^{\text{ten}})\sin\beta_T+2g_2'^{\,\text{ten}}\cos\beta_T\right)}{6}\right)^2$
$f_2'(1525) \longrightarrow \bar{K}\,K$	$2\left(\frac{Z_k^2 w_k^2\left(-(4g_2'^{\,\text{ten}}+3g_2^{\text{ten}})\sin\beta_T+\sqrt{2}(2g_2'^{\,\text{ten}}+3g_2^{\text{ten}})\cos\beta_T\right)}{6}\right)^2$
$f_2'(1525) \longrightarrow \pi\,\pi$	$6\left(\frac{Z_\pi^2 w_\pi^2\left(-(2g_2'^{\,\text{ten}}+3g_2^{\text{ten}})\sin\beta_T+\sqrt{2}g_2'^{\,\text{ten}}\cos\beta_T\right)}{6}\right)^2$
$f_2'(1525) \longrightarrow \eta\,\eta$	$2\left(\frac{Z_{\eta_N}^2 w_{\eta_N}^2 \cos\beta_P^2\left(-(2g_2'^{\,\text{ten}}+3g_2^{\text{ten}})\sin\beta_T+\sqrt{2}g_2'^{\,\text{ten}}\cos\beta_T\right)+Z_{\eta_S}^2 w_{\eta_S}^2 \sin\beta_P^2\left(\sqrt{2}(g_2'^{\,\text{ten}}+3g_2^{\text{ten}})\cos\beta_T-2g_2'^{\,\text{ten}}\sin\beta_T\right)}{6}\right)^2$

Table 4.4: Coefficients $\kappa_{tpp\,,i}$ for the decay channel $T \longrightarrow P^{(1)} + P^{(2)}$.

to the PDG data referenced in Table 4.5. The fit contains three free parameters: the two coupling constants g_2^{ten} and $g_2'^{\,\text{ten}}$, as well as the isoscalar mixing angle β_T. The fit result for the free parameters is:

$$\begin{aligned} g_2^{\text{ten}} &= (1.392 \pm 0.024)\cdot 10^4(\text{MeV})\,,\\ g_2'^{\,\text{ten}} &= (0.024 \pm 0.041)\cdot 10^4(\text{MeV})\,,\\ \beta_T &= (3.16 \pm 0.81)^\circ\ . \end{aligned} \tag{4.3.25}$$

In agreement with large N_c arguments, the fit shows us that the coupling constant $g_2'^{\,\text{ten}}$ is much smaller than g_2^{ten}. Because of its large error, it is also compatible with zero. It turns out that in this case considering suppressed large N_c terms was not necessary, but this is not true in general. In some other cases, such as the decays of the J/ψ [134], these higher order terms, even if small, do not vanish. Furthermore, the following prediction was not included in the fit due to the large experimental uncertainty

$$\Gamma\Big[K_2^*(1430) \longrightarrow \eta\,\bar{K}\Big] = (1.13 \pm 0.03)\cdot 10^{-3}\ \text{MeV},\ \ \text{PDG}:\ \ 0.15^{+0.34}_{-0.10}\ \text{MeV}. \tag{4.3.26}$$

While the theoretical result does not quite match the experimental value, they agree qualitatively in that they are both small. The isospin mixing angle $\beta_T = 3.16^\circ$ is also a decent approximation to the value

Decay process (in model)	eLSM (MeV)	PDG (MeV)
$a_2(1320) \longrightarrow \bar{K}\,K$	4.06 ± 0.14	$7.0^{+2.0}_{-1.5} \leftrightarrow (4.9 \pm 0.8)\%$
$a_2(1320) \longrightarrow \pi\,\eta$	25.37 ± 0.87	$18.5 \pm 3.0 \leftrightarrow (14.5 \pm 1.2)\%$
$a_2(1320) \longrightarrow \pi\,\eta'(958)$	1.01 ± 0.03	$0.58 \pm 0.10 \leftrightarrow (0.55 \pm 0.09)\%$
$K_2^*(1430) \longrightarrow \pi\,\bar{K}$	44.82 ± 1.54	$49.9 \pm 1.9 \leftrightarrow (49.9 \pm 0.6)\%$
$f_2(1270) \longrightarrow \bar{K}\,K$	3.54 ± 0.29	$8.5 \pm 0.8 \leftrightarrow (4.6^{+0.5}_{-0.4})\%$
$f_2(1270) \longrightarrow \pi\,\pi$	168.82 ± 3.89	$157.2^{+4.0}_{-1.1} \leftrightarrow (84.2^{+2.9}_{-0.9})\%$
$f_2(1270) \longrightarrow \eta\,\eta$	0.67 ± 0.03	$0.75 \pm 0.14 \leftrightarrow (0.4 \pm 0.08)\%$
$f_2'(1525) \longrightarrow \bar{K}\,K$	23.72 ± 0.60	$75 \pm 4 \leftrightarrow (87.6 \pm 2.2)\%$
$f_2'(1525) \longrightarrow \pi\,\pi$	0.67 ± 0.14	$0.71 \pm 0.14 \leftrightarrow (0.83 \pm 0.16)\%$
$f_2'(1525) \longrightarrow \eta\,\eta$	1.81 ± 0.05	$9.9 \pm 1.9 \leftrightarrow (11.6 \pm 2.2)\%$

Table 4.5: Decay rates for $T \longrightarrow P^{(1)} + P^{(2)}$.

$\beta_T = 5.7°$ in the PDG quark model review, calculated from the mass relation

$$\beta_T = 35.3° - \arctan\left(\sqrt{\frac{4m_{K_2}^2 - m_{a_2}^2 - 3m_{f_2'}^2}{-4m_{K_2}^2 + m_{a_2}^2 + 3m_{f_2}^2}}\right) . \tag{4.3.27}$$

Overall, the results shown in Table 4.5 show a good qualitative agreement, even if the exact values do not always quite match the experimental ones. The experimental data are quite precise and only three parameters were used in the fit, and some channels, such as $f_2'(1525) \longrightarrow \bar{K}\,K$, are primarily responsible for not fully matching the data. Further improvements could be made by including higher order large N_c suppressed terms as well as flavor-symmetry (or even isospin) breaking contributions.

$T \longrightarrow V + P$ decay mode

The next decay channel with good experimental data the is one of a tensor meson decaying into a vector-pseudoscalar pair. Upon taking the shift of (3.3.32), the chiral Lagrangian of (4.2.10) contains the following vertex:

$$\mathcal{L}_{Tvp} = (c_1^{\text{ten}} + c_2^{\text{ten}})\,\varepsilon_{\mu\nu\rho\sigma}\,\text{Tr}\Big[\partial^\mu T^{\nu\alpha}\left(\partial^\rho V^\sigma(\partial_\alpha P)\Phi_0 - \Phi_0(\partial_\alpha P\partial^\rho V^\sigma)\right)\Big] . \tag{4.3.28}$$

The tree-level decay rate is given by

$$\Gamma^{tl}_{T\longrightarrow V+P}(m_t, m_v, m_p) = \frac{(c^{\text{ten}})^2\,|\vec{k}_{v,p}|^5}{40\,\pi}\,\kappa_{tvp\,,i}\,\Theta(m_t - m_v - m_p)\,, \tag{4.3.29}$$

where $c^{\text{ten}} = c_1^{\text{ten}} + c_2^{\text{ten}}$, and the coefficients $\kappa_{tvp\,,i}$ have mass dimension 2 and are listed in Table 4.6. The value for the coupling c^{ten} is obtained by performing a χ^2-fit to the PDG data referenced in Table 4.6. The resulting value from the fit is

$$c^{\text{ten}} = (4.8 \pm 0.9) \cdot 10^{-7}(\text{MeV})^{-3}\ , \tag{4.3.30}$$

and in table 4.6 the theoretical results are also shown. The model results agree with the experimental data within one standard deviation. The final row has a prediction for the decay channel $f_2'(1525) \to \bar{K}^*(892)\,K + \text{c.c.}$ which has not yet been measured.

Decay process (in model)	eLSM (MeV)	PDG-2020 (MeV)	$\kappa_{tvp\,,i}$
$a_2(1320) \longrightarrow \rho(770)\,\pi$	71.0 ± 2.6	$73.61 \pm 3.35 \leftrightarrow (70.1 \pm 2.7)\%$	$2\left(\frac{\phi_N}{4}\right)^2$
$K_2^*(1430) \longrightarrow \bar{K}^*(892)\,\pi$	27.9 ± 1.0	$26.92 \pm 2.14 \leftrightarrow (24.7 \pm 1.6)\%$	$3\left(\frac{\phi_N}{8}\right)^2$
$K_2^*(1430) \longrightarrow \rho(770)\,K$	10.3 ± 0.4	$9.48 \pm 0.97 \leftrightarrow (8.7 \pm 0.8)\%$	$3\left(\frac{\sqrt{2}\phi_S}{8}\right)^2$
$K_2^*(1430) \longrightarrow \omega(782)\,\bar{K}$	3.5 ± 0.1	$3.16 \pm 0.88 \leftrightarrow (2.9 \pm 0.8)\%$	$\left(\frac{-\phi_S \cos\beta_V + \phi_N \sin\beta_V}{4\sqrt{2}})\right)^2$
$f_2'(1525) \longrightarrow \bar{K}^*(892)\,K + \text{c.c.}$	19.89 ± 0.73		$4\left(\frac{2\phi_S \cos\beta_T + \phi_N \sin\beta_T}{8})\right)^2$

Table 4.6: Decay rates and coefficients for the decay channel $T \longrightarrow P + V$.

$T \longrightarrow \gamma + P$ decay mode

As mentioned before, the photon can be included via a vector meson dominance procedure [135] by applying the additional shift

$$V_{\mu\nu} \to V_{\mu\nu} + \frac{e}{g_\rho} F_{\mu\nu} Q \;, \tag{4.3.31}$$

where $V_{\mu\nu} \equiv \partial_\mu V_\nu - \partial_\nu V_\mu$ is as usual the field strength for the corresponding vector field V_μ, $Q = \text{diag}\{2/3, -1/3, -1/3\}$ is the quark charge matrix, $F_{\mu\nu} = \partial_\mu A_\nu - \partial_\nu A_\mu$ is the electromagnetic field strength, $e = \sqrt{4\pi\alpha}$ is the electromagnetic charge, and $g_\rho \simeq 5.5 \pm 0.5$ [135] is a coupling which parametrizes the photon-vector-meson transition. first off, we consider $T \longrightarrow \gamma P$. Applying the VMD shift of (4.3.31) into (4.3.28) leads to the Lagrangian

$$\mathcal{L}_{T\gamma p} = \frac{e}{g_\rho} c^{\text{ten}}\, \text{Tr}\Big[\partial^\mu T^{\nu\alpha}\Big(F_{\mu\nu} Q (\partial_\alpha P)\Phi_0 - \Phi_0(\partial_\alpha P F_{\mu\nu} Q)\Big)\Big] \;, \tag{4.3.32}$$

with the corresponding decay rate

$$\Gamma^{tl}_{T\longrightarrow\gamma+P}(m_t, m_p) = \frac{c^{\text{ten}\,2}\, |\vec{k}_{\gamma,p}|^5}{40\,\pi}\, \kappa_{t\gamma p\,,i}\, \Theta(m_t - m_p)\,. \tag{4.3.33}$$

Decay process (in model)	eLSM	PDG-2020	$\kappa_{t\gamma p\,,i}$
$K_2^\pm(1430) \longrightarrow \gamma\, K^\pm$	1.12 ± 0.47 MeV	0.24 ± 0.05 MeV	$\frac{e^2}{g_\rho^2}\left(\frac{\phi_N + 2\sqrt{2}\phi_S}{12}\right)^2$
$K_2^0(1430) \longrightarrow \gamma\, K^0$	5.1 ± 2.2 keV	< 5.4 keV	$\frac{e^2}{g_\rho^2}\left(\frac{\phi_N - \sqrt{2}\phi_S}{12}\right)^2$
$a_2^\pm(1320) \longrightarrow \gamma\, \pi^\pm$	1.01 ± 0.43 MeV	0.31 ± 0.03 MeV	$\frac{e^2}{g_\rho^2}\left(\frac{\phi_N}{4}\right)^2$

Table 4.7: Decay rates and coefficients for the decay channel $T \longrightarrow \gamma + P$.

The coupling constant c^{ten} has been fitted before giving the result (4.3.30), and $g_\rho = 5.5 \pm 0.5$ is taken from [135]. The results for the photon-vector decays with theoretical errors based on the errors of the parameters are reported in Table 4.7. The decay rates qualitatively similar to the PDG values; they are in the same order of magnitude but overall a bit larger. The errors are also fairly large, so that at the level of about 2 standard deviations the two results agree.

$T \longrightarrow \gamma\gamma$ decay mode

Next, we describe decay into two photons. The chiral Lagrangian of (4.2.9) contains the following interaction term between a tensor meson and two vectors:

$$\mathcal{L}_{Tvv} = a^{\text{ten}}\text{Tr}\Big[T_{\mu\nu}\{V^{\mu}_{\beta}, V^{\nu\beta}\}\Big] + \frac{a'^{\,\text{ten}}}{3}\text{Tr}\Big[T_{\mu\nu}\Big]\text{Tr}\big[\{V^{\mu}_{\beta}, V^{\nu\beta}\}\big]\,. \tag{4.3.34}$$

Then, through the VMD shift (4.3.31) for both vector fields, we get the Lagrangian with vertices between the tensor and two photons:

$$\mathcal{L}_{T\gamma\gamma} = a^{\text{ten}}\frac{e^2}{g_\rho^2}\text{Tr}\Big[T_{\mu\nu}\{QF^{\mu}_{\beta}, QF^{\nu\beta}\}\Big] + \frac{a'^{\,\text{ten}}}{3}\frac{e^2}{g_\rho^2}\text{Tr}\Big[T_{\mu\nu}\Big]\text{Tr}\Big[\{QF^{\mu}_{\beta}, QF^{\nu\beta}\}\Big]\,, \tag{4.3.35}$$

which gives the decay rate

$$\Gamma^{tl}_{T\to\gamma\gamma} = \frac{e^4}{g_\rho^4}\frac{2\,|\vec{k}|^5}{5\,\pi\,m_t^2}\kappa_{t\gamma\gamma\,,i} = \frac{e^4}{g_\rho^4}\frac{m_t^3}{80\pi}\kappa_{t\gamma\gamma\,,i}\,, \tag{4.3.36}$$

where $m_t = 2|\vec{k}|$ (since the photons are massless) was used .In Table 4.8 the experimental values, as well as the theoretical results and coefficients $\kappa_{t\gamma\gamma,i}$, are shown. They are again derived from a χ^2 approach, now with the two free parameters a^{ten} and $a'^{\,\text{ten}}$. The mixing angle $\beta_T = 3.16°$ found earlier is kept fixed and there are three experimental data-points. The resulting values for the couplings are

$$a^{\text{ten}} = (-2.09 \pm 0.06)\cdot 10^{-2}(\text{MeV})^{-1}\,, \qquad a'^{\,\text{ten}} = (3.5 \pm 0.4)\cdot 10^{-3}(\text{MeV})^{-1}. \tag{4.3.37}$$

The observation that all 3 data points are described well indicates that the value of the mixing angle found by the earlier fit to two pseudoscalars $\beta_T = 3.16°$ is consistent with the data. Like before the fit result confirms the expectations from large N_c arguments, which is that $a'^{\,\text{ten}}$ is small compared to a^{ten}.

Decay process (in model)	eLSM (keV)	PDG-2020 (keV)	$\kappa_{t\gamma\gamma\,,i}$
$a_2(1320) \longrightarrow \gamma\gamma$	1.01 ± 0.06	1.00 ± 0.06	$\frac{a^{\text{ten}\,2}}{36}$
$f_2(1270) \longrightarrow \gamma\gamma$	1.95 ± 0.10	2.6 ± 0.5	$\left(\frac{(5a^{\text{ten}}+4a'^{\,\text{ten}})\cos\beta_T+\sqrt{2}(a^{\text{ten}}+2a'^{\,\text{ten}})\sin\beta_T}{18}\right)^2$
$f_2'(1525) \longrightarrow \gamma\gamma$	0.083 ± 0.009	0.082 ± 0.009	$\left(\frac{-(5a^{\text{ten}}+4a'^{\,\text{ten}})\sin\beta_T+\sqrt{2}(a^{\text{ten}}+2a'^{\,\text{ten}})\cos\beta_T}{18}\right)^2$

Table 4.8: Decay rates and coefficients for the decay channel $T \longrightarrow \gamma\gamma$.

$T \longrightarrow \gamma + V$ decay mode

Using the values of the couplings found in the previous fit, we can make predictions for the decay of a tensor into a photon and vector meson. Performing only one shift on the vector fields of the Lagrangian (4.3.34) we find

$$\mathcal{L}_{T\gamma V} = 2a^{\text{ten}}\frac{e}{g_\rho}\text{Tr}\Big[T_{\mu\nu}\{QF^{\mu}_{\beta}, V^{\nu\beta}\}\Big] + \frac{2a'^{\,\text{ten}}}{3}\frac{e}{g_\rho}\text{Tr}\Big[T_{\mu\nu}\Big]\text{Tr}\Big[\{QF^{\mu}_{\beta}, V^{\nu\beta}\}\Big]\,. \tag{4.3.38}$$

The vector-photon decay rates that follows from this Lagrangian has the form

$$\Gamma^{tl}_{T\longrightarrow\gamma+V}(m_t,m_v)=\frac{\kappa_{t\gamma v\,,i}\,e^2}{15\,\pi\,m_t^2 m_v^2 g_\rho^2}\Big(3|\vec{k}_{v,\gamma}|^7+5|\vec{k}_{v,\gamma}|^3 m_v^2+5|\vec{k}_{v,\gamma}|^4 m_v^2\sqrt{|\vec{k}_{v,\gamma}|^2+m_v^2}$$
$$+|\vec{k}_{v,\gamma}|^5\big(10m_v^2-3(|\vec{k}_{v,\gamma}|^2+m_v^2)\big)\Big)\ . \tag{4.3.39}$$

The coefficients $\kappa_{t\gamma v\,,i}$ are listed in Table 4.9 and the numerical predictions for the undiscovered decay rates are shown in Table 4.10. The corresponding errors follow from the ones of $a^{\rm ten}$ and $a'^{\,\rm ten}$ in (4.3.37), together with $g_\rho=5.5\pm0.5$ [135]. Additional sources of uncertainty, such as the uncertainties of the masses, were neglected for simplicity. This can increase the errors but they will be of similar order as the ones reported in Table 4.10.

Decay process (in model)	$\kappa_{t\gamma v\,,i}$
$a_2(1320)\longrightarrow\rho(770)\,\gamma$	$\left(\frac{a^{\rm ten}}{6}\right)^2$
$a_2^0(1320)\longrightarrow\omega(782)\,\gamma$	$\left(\frac{a^{\rm ten}\cos\beta_V}{2}\right)^2$
$a_2(1320)\longrightarrow\phi(1020)\,\gamma$	$\left(\frac{a^{\rm ten}\sin\beta_V}{2}\right)^2$
$K_2^{*\pm}(1430)\longrightarrow\bar{K}^{*\pm}(892)\,\gamma$	$\left(\frac{a^{\rm ten}}{6}\right)^2$
$K_2^{*\,0}(1430)\longrightarrow\bar{K}^{*\,0}(892)\,\gamma$	$\left(\frac{a^{\rm ten}}{3}\right)^2$
$f_2(1270)\longrightarrow\rho(770)\,\gamma$	$\left(\frac{(a^{\rm ten}+2a'^{\,\rm ten})\cos\beta_T+\sqrt{2}a'^{\,\rm ten}\sin\beta_T}{2}\right)^2$
$f_2(1270)\longrightarrow\omega(782)\,\gamma$	$\left(\frac{\cos\beta_V\left((a^{\rm ten}+2a'^{\,\rm ten})\cos\beta_T+\sqrt{2}a'^{\,\rm ten}\sin\beta_T\right)-2\sin\beta_V\left((a^{\rm ten}+a'^{\,\rm ten})\sin\beta_T+\sqrt{2}a'^{\,\rm ten}\cos\beta_T\right)}{6}\right)^2$
$f_2(1270)\longrightarrow\phi(1020)\,\gamma$	$\left(\frac{\sin\beta_V\left((a^{\rm ten}+2a'^{\,\rm ten})\cos\beta_T+\sqrt{2}a'^{\,\rm ten}\sin\beta_T\right)+2\cos\beta_V\left((a^{\rm ten}+a'^{\,\rm ten})\sin\beta_T+\sqrt{2}a'^{\,\rm ten}\cos\beta_T\right)}{6}\right)^2$
$f_2'(1525)\longrightarrow\rho(770)\,\gamma$	$\left(\frac{-(a^{\rm ten}+2a'^{\,\rm ten})\sin\beta_T+\sqrt{2}a'^{\,\rm ten}\cos\beta_T}{2}\right)^2$
$f_2'(1525)\longrightarrow\omega(782)\,\gamma$	$\left(\frac{\sin\beta_T\left(-(a^{\rm ten}+2a'^{\,\rm ten})\cos\beta_V+2\sqrt{2}a'^{\,\rm ten}\sin\beta_V\right)+\cos\beta_T\left(\sqrt{2}a'^{\,\rm ten}\cos\beta_V-2(a^{\rm ten}+a'^{\,\rm ten})\sin\beta_V\right)}{6}\right)^2$
$f_2'(1525)\longrightarrow\phi(1020)\,\gamma$	$\left(\frac{\cos\beta_T\left(-2(a^{\rm ten}+a'^{\,\rm ten})\cos\beta_V-\sqrt{2}a'^{\,\rm ten}\sin\beta_V\right)+\sin\beta_T\left(2\sqrt{2}a'^{\,\rm ten}\cos\beta_V+(a^{\rm ten}+2a'^{\,\rm ten})\sin\beta_V\right)}{6}\right)^2$

Table 4.9: Coefficients for the decay channel $T\longrightarrow\gamma+V$ decays.

Vector-vector decay mode of tensor mesons

Finally, we study the decay for the tensor mesons into two vector mesons, to describe the following data from the PDG:

$$\text{PDG}:\ \Gamma[f_2(1270)\longrightarrow\pi^+\pi^-2\pi^0]\approx19.5\,\text{MeV};$$
$$\text{PDG}:\ \Gamma[a_2(1320)\longrightarrow\omega(782)\pi\pi]\approx11.3\,\text{MeV};$$
$$\text{PDG}:\ \Gamma[K_2^\star(1430)\longrightarrow K^\star(892)\pi\pi]=13.5\pm2.3\,\text{MeV}.$$

Since the ρ decays primarily into two pions (all other decay modes have decay ratios of order 10^{-3} or lower), is natural to interpret these decays as the two vector decay channels ($\rho(770)\rho(770)$, $\omega(782)\rho(770)$, and $K^*(892)\rho(770)$), in which the $\rho(770)$ meson further decays into two pions. In order to describe this two-

Decay process (in model)	Decay Width (MeV)
$a_2(1320) \longrightarrow \rho(770)\,\gamma$	0.22 ± 0.04
$a_2^0(1320) \longrightarrow \omega(782)\,\gamma$	1.94 ± 0.04
$a_2(1320) \longrightarrow \phi(1020)\,\gamma$	0.0024 ± 0.0005
$K_2^{*\pm}(1430) \longrightarrow \bar{K}^{*\pm}(892)\,\gamma$	0.23 ± 0.04
$K_2^{*\,0}(1430) \longrightarrow \bar{K}^{*\,0}(892)\,\gamma$	0.94 ± 0.18
$f_2(1270) \longrightarrow \rho(770)\,\gamma$	0.70 ± 0.17
$f_2(1270) \longrightarrow \omega(782)\,\gamma$	0.068 ± 0.017
$f_2(1270) \longrightarrow \phi(1020)\,\gamma$	0.007 ± 0.002
$f_2'(1525) \longrightarrow \rho(770)\,\gamma$	0.32 ± 0.08
$f_2'(1525) \longrightarrow \omega(782)\,\gamma$	0.012 ± 0.005
$f_2'(1525) \longrightarrow \phi(1020)\,\gamma$	0.61 ± 0.12

Table 4.10: Predictions for $T \longrightarrow \gamma + V$.

stage decay chain, we use a properly normalized "Sill" spectral function introduced in [136] for the ρ-meson as

$$d_\rho(y) = \frac{2y}{\pi}\frac{\sqrt{y^2-4m_\pi^2}\,\tilde{\Gamma}_\rho}{(y^2-m_\rho^2)^2+(\sqrt{y^2-4m_\pi^2}\,\tilde{\Gamma}_\rho)^2}\,\Theta(x-2m_\pi), \qquad \int_0^\infty dy\, d_\rho(y) = 1\ , \tag{4.3.40}$$

where $\tilde{\Gamma}_\rho$ is defined as

$$\tilde{\Gamma}_\rho \equiv \frac{\Gamma_{\rho\to 2\pi}\, m_\rho}{\sqrt{m_\rho^2-4m_\pi^2}}\quad , \tag{4.3.41}$$

with $\Gamma_{\rho\to 2\pi} = 149.1$ MeV and $m_\rho = 775.11$ MeV are taken from the PDG.
We use the Sill spectral function rather than a usual Breit-Wigner for the following reasons. The normalization is guaranteed also for broad states, the contribution of virtual particles has a vanishing real part, and the threshold is properly taken into account.
The two chiral Lagrangians (4.2.8) and (4.2.9) contribute to the coupling of tensor mesons to two vector mesons. When the interference between these two channels is constructive, the decay rates are too large. Hence, we assume there is destructive interference between the corresponding amplitudes. We find the following estimates for the decay rates of these chains:

$$\Gamma_{f_2\to\rho\rho\to 4\pi} \simeq \int_0^\infty dy_1\, d_\rho(y_1)\int_0^\infty dy_2\, d_\rho(y_2)\,\Gamma_{f_2\to\rho\rho}(m_{f_2},y_1,y_2) \approx 29.9\,\text{MeV}\ ; \tag{4.3.42}$$

$$\Gamma_{a_2\to\omega\rho\to\omega 2\pi} \simeq \int_0^\infty dy_1\, d_\rho(y_1)\,\Gamma_{a_2\to\rho\omega}(m_{\mathbf{a}_2},m_{\omega_1},y_1) \approx 11.1\,\text{MeV}\ ; \tag{4.3.43}$$

$$\Gamma_{K_2\to K^\star\rho\to K2\pi} \simeq \int_0^\infty dy_1\, d_\rho(y_1)\,\Gamma_{K_2\to\rho\omega}(m_{K_2},m_{K_1},y_1) \approx 6.6\,\text{MeV}\ . \tag{4.3.44}$$

The results are in qualitative agreement with the experimental ones. This is quite interesting since only the previously fitted parameters are used. Furthermore, this is a nontrivial process that involves numerous different parts: two distinct interaction Lagrangians with destructive interference, and the integral over the spectral function of the ρ-meson, which is chosen as the Sill distrubition, where other choices were also possible. Finally, the direct decay into a pair of pions and a vector meson is not included, but still the decays are described well.

4.3.3 Decays of axial tensor mesons

We now move to the decays of the ground-state axial tensor mesons with $J^{PC} = 2^{--}$. As most of these have not yet been found and thus their decay rates are unknown, we will predict these decay rates. Where available, we will also compare our results with those found using lattice QCD (LQCD) and other theoretical results.

$A_2 \longrightarrow V + P$ decay mode

The decay of axial tensor states into a vector and pseudoscalar pair is found by expanding the chiral Lagrangian (4.2.8) into the physical nonets which gives the interaction term

$$\mathcal{L}_{A_2vp} = g_2^{\text{ten}}\, \text{Tr}\Big[A_2^{\mu\nu}\big\{(\partial_\mu \mathcal{P})\,, V_\nu\big\}\Big]\ . \tag{4.3.45}$$

The tree-level decay rate is given by

$$\Gamma^{tl}_{A_2\longrightarrow V+P}(m_{a_2}, m_v, m_p) = \frac{g_2^{\text{ten}\,2}\,|\vec{k}_{v,p}|^3}{120\,\pi\, m_{a_2}^2}\Big(5 + \frac{2\,|\vec{k}_{v,p}|^2}{m_v^2}\Big)\,\kappa_{a_2vp\,,i}\,\Theta(m_{a_2} - m_v - m_p)\,, \tag{4.3.46}$$

where the coefficient $\kappa_{a_2vp\,,i}$ can be found in Table 4.11, along with the predicted decay widths. The resulting decay rates for this decay mode are very large. We should take note that our results can be considered approximate for the following reasons:

1. The strength of the interactions is determined solely by the the data on tensor mesons, and extrapolated by means of chiral symmetry to the axial tensors. While this is correct if chiral symmetry is exact, chiral symmetry is broken in Nature and no corrections to it have been taken into account in this model. Chiral symmetry breaking effects are expected to be relevant between 1-2 GeV, and could be significant for these decays;

2. The κ_i depends on quantities of the type $(Zw)^2 \propto g_1^4$ (see Tables 4.11 and 3.3). Even a small uncertainty in the parameters of the original eLSM generates a much larger uncertainty in the results of the decays of axial tensor states. For example, a 20% uncertainty in g_1 propagates to a difference of a factor 2 in the decay rates;

3. The parameters g_1, g_2^{ten} and others are assumed to be constant over a large range of energies. However it is not unreasonable to assume that it has a (soft) energy dependence. It could become smaller when the mass of the decaying particle increases, necessitating the inclusion of form factors. Even a small change would significantly change the widths shown in table 4.11.

In summary, the parameters used (in particular g_1) imply a quite large and difficult to determine source of uncertainty in the decays of the axial tensor states. In order to be on the safe side, we estimate an error of about 50% for the reported numbers in Table 4.11.

For the ρ_2, $\omega_{2,N} \simeq \omega_2$, and $\omega_{2,S} \simeq \phi_2$, there is no experimental data. For the kaons, the resonances $K_2(1820)$ and $K_2(1770)$ are expected to emerge from the bare axial tensor and pseudotensor states which can mix the same way the axial vector and pseudovector mesons mix as in (3.3.16). Assuming that K_{2A} is closer to $K_2(1820)$, which we have done in Table 1.1 although this is not completely settled yet, The decay width for the K_{2A} state predicted by the eLSM is approximately twice of the experimentally measured decay of $K_2(1820)$. This suggests that we should probably assume the uncertainties mean the decay rates should be lower than the central values reported in Table 4.11.

This notion can be extended to the other decay channels as well. By comparing with the lattice QCD results reported in Table 4.12, we see that the eLSM theoretical results for the decays are of the same order of magnitude but about 2-3 times greater than the LQCD ones. This is another indication that we should interpret these results to be on the lower end in the given range of uncertainty.

For completeness we also determine the coupling directly from the LQCD results, which leads to

$$g^{\text{ten}}_{2\,\text{lat}} \simeq (0.7 \pm 0.4) \cdot 10^4 (\text{MeV}), \tag{4.3.47}$$

where we assume a 50% error in the lattice results of [3][1]. This value is within two standard deviation of the previous eLSM fit which gave (4.3.25). In Table 4.12, the decay rates for $A_2 \to V + P$ with the coupling $g^{\text{ten}}_{2\,\text{lat}}$ fitted to Lattice data from [3] are shown. Comparing the two tables 4.11 and 4.12, the various ratios of decay widths are consistent with each other, with the eLSM reproducing the lattice results well after the coupling is rescaled to (4.3.47).

In summary, the conclusion of the theoretical study is quite clear. The axial tensor states are expected to be broad even when taking the low side of our results, even given the large uncertainties. This could explain the fact that the states ρ_2, ω_2, and ϕ_2 have not been observed up to now.

$A_2 \longrightarrow A_1 + P$ decay mode

The chiral Lagrangian (4.2.10) generates the decay of an axial tensor into an axial vector and pseudoscalar pair:

$$\mathcal{L}_{A_2 a_1 p} = c'^{\,\text{ten}}\, \varepsilon_{\mu\nu\rho\sigma}\, \text{Tr}\Big[\partial^\mu A_2^{\nu\alpha} \Big((\partial^\rho A_1^\sigma)(\partial_\alpha P)\Phi_0 - \Phi_0(\partial_\alpha P)(\partial^\rho A_1^\sigma)\Big)\Big]\,, \tag{4.3.48}$$

where $c'^{\,\text{ten}} := c_1^{\text{ten}} - c_2^{\text{ten}}$. The corresponding decay rate is given by:

$$\Gamma^{tl}_{A_2\longrightarrow A_1+P}(m_{a_2}, m_{a_1}, m_p) = \frac{(c'^{\,\text{ten}})^2\, |\vec{k}_{a_1,p}|^5}{40\,\pi}\, \kappa_{a_2 ap\,,i} \Theta(m_{a_2} - m_{a_1} - m_p)\ . \tag{4.3.49}$$

The theoretical predictions and the coefficients $\kappa_{a_2 ap\,,i}$ for each channel are given in Table 4.13. For simplicity we assumethat $K_{1A} \approx K_1(1400)$. The predictions are all proportional to the combination $(\frac{c'^{\,\text{ten}}}{c^{\text{ten}}})^2$. This means that in this case the decay of the tensor mesons does not fix the strength for the axial tensor mesons. Two terms are present in the original Lagrangian (4.2.10), and the decay of tensor mesons depends on the sum $c_1^{\text{ten}} + c_2^{\text{ten}}$ while the axial tensor decays depend on the difference $c_1^{\text{ten}} - c_2^{\text{ten}}$. We could fix the sum with the tensor meson data but cannot fix the difference. Nevertheless, we can reasonably expect that $c'^{\,\text{ten}}$ is of

[1] This high error is chosen in part because the pions in lattice QCD calculations, based on SU(3) flavor symmetry, have a mass of about 700 MeV, compared to the physical mass of 130-140 MeV.

Decay process (in model)	eLSM (MeV)	$\kappa_{a_2 vp\,,i}$
$\rho_2(?) \longrightarrow \rho(770)\,\eta$	$\approx 99 \pm 50$	$\Big(-w_{\eta_N} Z_{\eta_N} \cos\beta_P\Big)^2$
$\rho_2(?) \longrightarrow \bar{K}^*(892)\,K + \text{c.c.}$	$\approx 85 \pm 43$	$4\Big(\frac{Z_K w_K}{2}\Big)^2$
$\rho_2(?) \longrightarrow \omega(782)\,\pi$	$\approx 419 \pm 210$	$\Big(-w_\pi Z_\pi \cos\beta_V\Big)^2$
$\rho_2(?) \longrightarrow \phi(1020)\,\pi$	≈ 0.8	$\Big(w_\pi Z_\pi \sin\beta_V\Big)^2$
$K_{2,A} \longrightarrow \rho(770)\,K$	$\approx 195 \pm 98$	$3\Big(\frac{Z_K w_K}{2}\Big)^2$
$K_{2,A} \longrightarrow \bar{K}^*(892)\,\pi$	$\approx 316 \pm 158$	$3\Big(\frac{Z_\pi w_\pi}{2}\Big)^2$
$K_{2,A} \longrightarrow \bar{K}^*(892)\,\eta$	≈ 0.01	$\Big(-\frac{1}{2}(\sqrt{2}Z_{\eta_S} w_{\eta_S} \sin\beta_P + Z_{\eta_N} w_{\eta_N} \cos\beta_P)\Big)^2$
$K_{2,A} \longrightarrow \omega(782)\,\bar{K}$	$\approx 51 \pm 26$	$\Big(-\frac{w_K Z_K}{2}(\sqrt{2}\sin\beta_V + \cos\beta_V)\Big)^2$
$K_{2,A} \longrightarrow \phi(1020)\,\bar{K}$	$\approx 50 \pm 25$	$\Big(\frac{w_K Z_K}{2}(-\sqrt{2}\cos\beta_V + \sin\beta_V)\Big)^2$
$\omega_{2,N} \longrightarrow \rho(770)\,\pi$	$\approx 1314 \pm 657$	$3\Big(-Z_\pi w_\pi\Big)^2$
$\omega_{2,N} \longrightarrow \bar{K}^*(892)\,K + \text{c.c.}$	$\approx 85 \pm 43$	$4\Big(-\frac{Z_K w_K}{2}\Big)^2$
$\omega_{2,N} \longrightarrow \omega(782)\,\eta$	$\approx 93 \pm 47$	$\Big(Z_{\eta_N} w_{\eta_N} \cos\beta_P \cos\beta_V\Big)^2$
$\omega_{2,N} \longrightarrow \phi(1020)\,\eta$	≈ 0.06	$\Big(Z_{\eta_N} w_{\eta_N} \cos\beta_P \sin\beta_V\Big)^2$
$\omega_{2,S} \longrightarrow \bar{K}^*(892)\,K + \text{c.c.}$	$\approx 510 \pm 255$	$4\Big(-\frac{Z_K w_K}{\sqrt{2}}\Big)^2$
$\omega_{2,S} \longrightarrow \omega(782)\,\eta$	$\approx 1.0 \pm 0.5$	$\Big(-\sqrt{2}Z_{\eta_S} w_{\eta_S} \sin\beta_P \sin\beta_V\Big)^2$
$\omega_{2,S} \longrightarrow \omega(782)\,\eta'(958)$	≈ 0.3	$\Big(-\sqrt{2}Z_{\eta_S} w_{\eta_S} \cos\beta_P \sin\beta_V\Big)^2$
$\omega_{2,S} \longrightarrow \phi(1020)\,\eta$	$\approx 101 \pm 51$	$\Big(-\sqrt{2}Z_{\eta_S} w_{\eta_S} \cos\beta_V \sin\beta_P\Big)^2$

Table 4.11: Predictions and coefficients for the decay channel $A_2 \longrightarrow V + P$.

the same order as c^{ten}. Based on this, we would expect small decay widths. Within this in mind, assuming that $\frac{c'^{\,\text{ten}}}{c^{\text{ten}}} \simeq 1$, our prediction for the $\rho_2 \to a_1(1260)\pi$ channel is similar to the one found in [103].

$A_2 \longrightarrow T + P$ decay mode

The last term of the mass Lagrangian (4.2.2) also has an interaction term which enables us to make predictions for the decay of an axial tensor mesons into a tensor and pseudoscalar pair. The interaction has the following form

$$\mathcal{L}_{A_2tp} = 2ih_3^{\text{ten}}\text{Tr}\Big[A_2^{\mu\nu}(PT_{\mu\nu}\Phi_0 - \Phi_0 T_{\mu\nu}P)\Big]\,, \tag{4.3.50}$$

which leads to the decay rate given by

$$\Gamma^{tl}_{A_2\longrightarrow T+P}(m_{a_2}, m_t, m_p) = \frac{(h_3^{\text{ten}})^2|\vec{k}_{t,p}|}{2\,m_{a_2}^2\pi}\Big(1 + \frac{4|\vec{k}_{t,p}|^4}{45m_t^4} + \frac{2|\vec{k}_{t,p}|^2}{3m_t^2}\Big)\,\kappa_{a_2tp\,,i}\,\Theta(m_{a_2} - m_t - m_p)\,. \tag{4.3.51}$$

The resulting decay widths and corresponding coefficients κ_i are reported in Table 4.14. In some channels the decays are again quite large, which are then promising avenues for future discovery of the axial tensor

Decay process (in model)	eLSM (MeV)	LQCD (MeV) [3]
$\rho_2(?) \longrightarrow \rho(770)\,\eta$	≈ 30	
$\rho_2(?) \longrightarrow \bar{K}^*(892)\,K + \text{c.c.}$	≈ 27	36
$\rho_2(?) \longrightarrow \omega(782)\,\pi$	≈ 122	125
$\rho_2(?) \longrightarrow \phi(1020)\,\pi$	≈ 0.3	
$K_{2,A} \longrightarrow \rho(770)\,K$	≈ 53	
$K_{2,A} \longrightarrow \bar{K}^*(892)\,\pi$	≈ 87	
$K_{2,A} \longrightarrow \bar{K}^*(892)\,\eta$	≈ 0.004	
$K_{2,A} \longrightarrow \omega(782)\,\bar{K}$	≈ 13.8	
$K_{2,A} \longrightarrow \phi(1020)\,\bar{K}$	≈ 13.7	
$\omega_{2,N} \longrightarrow \rho(770)\,\pi$	≈ 363	365
$\omega_{2,N} \longrightarrow \bar{K}^*(892)\,K + \text{c.c.}$	≈ 25	36
$\omega_{2,N} \longrightarrow \omega(782)\,\eta$	≈ 27	17
$\omega_{2,N} \longrightarrow \phi(1020)\,\eta$	≈ 0.02	
$\omega_{2,S} \longrightarrow \bar{K}^*(892)\,K + \text{c.c.}$	≈ 100	148
$\omega_{2,S} \longrightarrow \omega(782)\,\eta$	≈ 0.2	
$\omega_{2,S} \longrightarrow \omega(782)\,\eta'(958)$	≈ 0.02	
$\omega_{2,S} \longrightarrow \phi(1020)\,\eta$	≈ 17	44

Table 4.12: Predictions for the $A_2 \longrightarrow V + P$ based on LQCD results [3].

Decay process (in model)	eLSM (MeV)	$\kappa_{a_2 ap,i}$
$\rho_2(?) \longrightarrow a_1(1260)\,\pi$	$\simeq 13\left(\frac{c'^{\,\text{ten}}}{c^{\text{ten}}}\right)^2$	$2\left(\frac{\phi_N}{4}\right)^2$
$K_{2,A} \longrightarrow a_1(1260)\,K$	$\simeq 0.1\left(\frac{c'^{\,\text{ten}}}{c^{\text{ten}}}\right)^2$	$3\left(\frac{\sqrt{2}\phi_S}{8}\right)^2$
$K_{2,A} \longrightarrow \bar{K}_{1,A}\,\pi$	$\simeq 11\left(\frac{c'^{\,\text{ten}}}{c^{\text{ten}}}\right)^2$	$3\left(\frac{\phi_N}{8}\right)^2$
$K_{2,A} \longrightarrow f_1(1285)\,\bar{K}$	$\simeq 0.2\left(\frac{c'^{\,\text{ten}}}{c^{\text{ten}}}\right)^2$	$\left(\frac{\sqrt{2}}{8}(\phi_N \sin\beta_{A_1} - \phi_S\cos\beta_{A_1})\right)^2$
$\omega_{2,S} \longrightarrow \bar{K}_{1,A}\,K + \text{c.c.}$	$\simeq 6\left(\frac{c'^{\,\text{ten}}}{c^{\text{ten}}}\right)^2$	$4\left(\frac{\phi_S}{4}\right)^2$

Table 4.13: Predictions and coefficients for the decay channel $A_2 \longrightarrow A_1 + P$.

states. The decay rate of $\rho_2(?) \longrightarrow a_2(1320)\,\pi$ is calculated to be about 200 MeV in [103], twice as large as the one calculated here.

It should be emphasized that the total sum of the various decay rates for the axial tensor mesons gives quite large decay widths for these states, even when we take only the lower end of the given ranges of uncertainty. This makes finding these states very challenging, but the discovery of these missing axial tensor states is still possible, especially by looking into the dominant decay channels described in this chapter.

4.4 Conclusions

In this chapter we have analyzed the lightest tensor mesons and the lightest axial tensor mesons, who are the chiral partners of the tensor mesons. The tensor mesons are quite well known and there is a good amount of data describing them, this is used to fix a number of parameters and make predictions for the axial tensor mesons using chiral symmetry, as well as for some unknown decays of the tensor mesons. The analysis is

Decay process (in model)	eLSM (MeV)	$\kappa_{a_2tp,i}$
$\rho_2(?) \longrightarrow a_2(1320)\,\pi$	≈ 88	$2\left(\frac{\phi_N}{4}\right)^2$
$K_{2,A} \longrightarrow K_2^\star(1430)\,\pi$	≈ 49	$3\left(\frac{\sqrt{2}\phi_S}{8}\right)^2$
$K_{2,A} \longrightarrow a_2(1320)\,K$	≈ 84	$3\left(\frac{\sqrt{2}\phi_N}{8}\right)^2$
$K_{2,A} \longrightarrow f_2(1270)\,K$	≈ 4	$\left(\frac{\phi_N\cos\beta_T - 2\phi_S\sin\beta_T}{8}\right)^2$
$\omega_{2,S} \longrightarrow K_2^\star(1430)\,K + \text{c.c.}$	≈ 15	$4\left(\frac{\phi_S}{8}\right)^2$

Table 4.14: Predictions and coefficients for the decay channel $A_2 \to T + P$.

done in the framework of a chiral model for low-energy QCD, the eLSM, which we have introduced in chapter 3.

The resulting masses as well as the strong and radiative decays of the ground-state tensors we get from this model fit well with the data. As this treatment is based on the assumption that the states are conventional quark-antiquark states, it is a confirmation of the assignment given by the quark model review of the PDG. For the axial tensors, the masses are a bit above those of the tensor mesons owing to the chiral condensate. The decay widths of the axial tensors are large, even in their large range of uncertainty. the dominant decay channel is the one into a vector-pseudoscalar pair, followed by a tensor-pseudoscalar pair with the axial vector-pseudoscalar channel being the smallest decay channel. Comparing with lattice QCD, the decay into into vector-pseudoscalar pairs are similar to the ones we found, up to a rescaling of the coupling constant.

Even with large uncertainties that stem from a strong dependence on certain eLSM parameters, it is clear that the axial tensor mesons are broad states. This makes it challenging to detect them, but it also means that there are specific channels that are promising to look into for their discovery. The states ρ_2, ω_2, and ϕ_2 could be discovered in ongoing and future experiments, see e.g. [120, 121, 122, 124, 125, 126, 127, 128, 123, 137, 138, 139] and refs. therein.

Finally, the tensor glueball, with a mass predicted by lattice of around 2.2 GeV [73], is an interesting inclusion to the study of this chapter. Like the axial tensors this is a bound state of QCD expected to exist but not yet found experimentally. Various tensor mesons in the energy region at about 2 GeV exist which could be a glueball, but input from both experiment and theory is needed to determine which, if any, is a glueball. Glueballs can be directly implemented in the eLSM, so this is a promising avenue to study the tensor glueball. The following chapter will be dedicated to this study.

Chapter 5

The tensor glueball

5.1 Introduction

In chapters 2 and 3 we have discussed the scalar glueball, which is the lightest purely gluonic state. In fact, there should exist a large spectrum of glueballs of various spin quantum numbers. This spectrum is one of the earliest predictions of QCD and is intrinsically linked to its non-abelian gauge symmetry and confinement [140]. Since then, various theoretical approaches have corroborated the existence of glueballs, see e.g. [141, 142, 91, 143]. Among those approaches, Lattice QCD stands out, being able to compute, from first principle, a large spectrum of glueball states [73, 72, 74, 144, 145, 146, 147] in a quenched approximation, meaning that the quarks are non-dynamical. In [148] an unquenched calculation can be found. The glueball spectrum gained from lattice QCD, in particular the one of [74], is also supported by a glueball resonance gas model, similar to a hadron resonance gas model but with glueballs replacing the conventional hadrons, which showed that the thermodynamic properties fit with what is known of pure Yang-Mills theory [149]. Recently, functional methods have also been successful at reproducing the glueball spectrum given by lattice QCD, and could be a promising approach for calculating interactions and decays of glueballs [75, 150, 151], which are difficult to calculate in lattice QCD.

While the different theoretical methods do not always give the same numerical outcomes, they generally agree on several qualitative features. Namely, the lightest glueball state is a scalar ($J^{PC} = 0^{++}$), the second-lightest is a tensor with $J^{PC} = 2^{++}$ (the tensor/scalar mass ratio can be an interesting quantity, see e.g. [152]), and the third-lightest is a pseudoscalar ($J^{PC} = 0^{-+}$). For all the glueballs, their experimental status is still inconclusive. However, for the lightest three states there do exist some notable candidates [91]. Still, because glueballs will mix with regular mesons of the same quantum numbers and similar masses and because of their poorly known decays, conclusive identification of glueballs in experiments is very difficult.

In this chapter, we concentrate on the tensor glueball. The tensor glueball is of interest to us for a number of reasons. The first one, as we have mentioned before, is that it is the second lightest glueball state. The second reason is the experimental observation of several isoscalar-tensor resonances which lie in the 2 GeV region such as the $f_2(1430)$, $f_2(1565)$, $f_2(1640)$, $f_2(1810)$, $f_2(1910)$, $f_2(1950)$, $f_2(2010)$, $f_2(2150)$, and the $f_J(2220)$. One of these could be the tensor glueball, especially ones close to the lattice QCD predictions of about 2 GeV. Attempts to find the tensor glueball in one of those f_2 states has a long history, see e.g

[140, 153, 154, 155]. In particular, the $f_J(2220)$ was historically considered as a good candidate for the tensor glueball [156]. However in this chapter, our results will point towards the $f_J(2220)$ not being a good tensor glueball candidate anymore.

There have been various different lattice QCD simulations that have computed the physical mass of the tensor glueball. Some of these predictions are: 2150(30)(100) MeV [144], 2324(42)(32) MeV [145], 2376(32) MeV [74], 2390(30)(120) MeV [73], and 2400(25)(120) MeV [72]. Furthermore, using QCD sum rules, the tensor glueball mass has been found to be in the range of 2000-2300 MeV [76, 157]. The aforementioned functional method gave a tensor glueball mass of around 2610 MeV [75]. Holographic QCD methods, based on the AdS/CFT correspondence, have also been used to study glueballs for instance in [158, 78, 77, 159, 160, 161, 162, 163, 164]. The tensor glueball mass in these holographic calculations can be found anywhere from 1900 to 4300 MeV, depending on the model and the values of the parameters [161, 163]. In general, while the numerical result for the mass differs, different theoretical methods converge on the existence of a tensor glueball in the region near 2000 MeV.

Some results are also known for the decays of the tensor glueball. For instance, in [77, 159], the decays of the tensor glueball have been calculated in the Witten-Sakai-Sugimoto Model. It was found that if the tensor glueball mass is above the threshold where it is able to decay into $\rho\rho$, the tensor glueball state is quite broad. In other hadronic approaches such as [101, 165], decay ratios for the tensor glueball were also found. However, these did not yet include an explicit realization of chiral symmetry, which we will do in this chapter. The tensor glueball is also thought to be related to the occurrence of OZI suppressed process such as $\pi^- p \to \phi\phi n$ [166].

On the experimental side, a data analysis on decays of the J/ψ could be promising for the identification of the scalar and tensor glueballs [140, 113, 167, 168]. The tensor glueball mass from this analysis would be around 2210 MeV. Future experiments with measurable production of tensor glueballs are discussed in [169, 170].

With all these in mind, it is then quite natural to ask what a chiral hadronic approach like the eLSM can tell about us the tensor glueball state, especially in connection to its decays. This chapter deals exactly with this question: we study the tensor glueball via a suitable extension of the eLSM used in the previous chapter. In the past, other glueballs such as the scalar [171, 79], pseudoscalar [172, 173], and vector [98] glueballs have been studied in the eLSM, which makes this a natural next step.

Within the eLSM framework, we will evaluate various decay rates. The most important will turn out to be the $\rho\rho/\pi\pi$ decay ratio. We then compare the outcomes to the isoscalar-tensor states in the range close to 2000 MeV and find out that the resonance $f_2(1950)$ is, according to present data combined with the eLSM predictions, our best candidate. We will also comment on the partial decay widths of the glueball and the overall assignment of excited tensor states.

5.2 Chiral model

From the Lagrangians (4.2.2) and (4.2.8), we can include the tensor glueball by the following substitution

$$T_{\mu\nu} \longrightarrow \frac{1}{\sqrt{6}} G_{2,\mu\nu} \cdot \mathbf{1}_3 \ . \tag{5.2.1}$$

In other words, the glueball is blind to flavor. The first Lagrangian we will use couples the glueball to vector and axial vector fields:

$$\mathcal{L}_\lambda = \frac{\lambda}{\sqrt{6}} G_{2,\mu\nu} \Big(\mathrm{Tr}\Big[\{L^\mu, L^\nu\} \Big] + \mathrm{Tr}\Big[\{R^\mu, R^\nu\} \Big] \Big) \, . \tag{5.2.2}$$

Here, we follow the same convention that implies the normalization with respect to the flavor singlet state. The Lagrangian (5.2.2) leads to three kinematically allowed decay channels:

- Decays of the tensor glueball into two vector mesons, with the following decay rate

$$\Gamma_{G_2 \to V^{(1)} V^{(2)}}(m_{G_2}, m_{v^{(1)}}, m_{v^{(2)}}) = \frac{\kappa_{gvv\,,i} \lambda^2 |\vec{k}_{v^{(1)},v^{(2)}}|}{120\,\pi\, m_{G_2}^2} \Big(15 + \frac{5|\vec{k}_{v^{(1)},v^{(2)}}|^2}{m_{v^{(1)}}^2} + \frac{5|\vec{k}_{v^{(1)},v^{(2)}}|^2}{m_{v^{(2)}}^2} + \frac{2|\vec{k}_{v^{(1)},v^{(2)}}|^4}{m_{v^{(1)}}^2 m_{v^{(2)}}^2} \Big) \Theta(m_{G_2} - m_{v^{(1)}} - m_{v^{(2)}}) \, ; \tag{5.2.3}$$

- Two pseudoscalar mesons, by applying the shift of 3.3.33 twice, with decay rate

$$\Gamma^{tl}_{G_2 \longrightarrow P^{(1)} P^{(2)}}(m_{G_2}, m_{p^{(1)}}, m_{p^{(2)}}) = \frac{\kappa_{gpp\,,i}\, \lambda^2\, |\vec{k}_{p^{(1)},p^{(2)}}|^5}{60\,\pi\, m_{G_2}^2} \Theta(m_{G_2} - m_{p^{(1)}} - m_{p^{(2)}}) \, ; \tag{5.2.4}$$

- and into the axial vector and pseudoscalar mesons by applying the shift 3.3.33 once, with decay rate

$$\Gamma^{tl}_{G_2 \longrightarrow A_1 P}(m_{G_2}, m_{a_1}, m_p) = \frac{\kappa_{gap\,,i}\, \lambda^2\, |\vec{k}_{a_1,p}|^3}{120\,\pi\, m_{G_2}^2} \left(5 + \frac{2\,|\vec{k}_{a_1,p}|^2}{m_{a_1}^2} \right) \Theta(m_{G_2} - m_{a_1} - m_p) \, . \tag{5.2.5}$$

The coupling constant λ is not known, and we cannot fit it to data as the glueball has not been found. We are therefore limited to computing branching ratios rather than decay rates. Later on we will make a rough estimate of the decay rates based on large N_c scaling.
The second chirally invariant term we will use for tensor glueball decays based on the one of (4.2.9) is of the form

$$\mathcal{L}_\alpha = \frac{\alpha}{\sqrt{6}} G_{2,\mu\nu} \Big(\mathrm{Tr}\Big[\Phi \mathbf{R}^{\mu\nu} \Phi^\dagger \Big] + \mathrm{Tr}\Big[\Phi^\dagger \mathbf{L}^{\mu\nu} \Phi \Big] \Big) \, . \tag{5.2.6}$$

This Lagrangian will lead to the decay of a tensor glueball into a tensor meson and pseudoscalar meson. The decay rate for this process is given by

$$\Gamma^{tl}_{G_2 \longrightarrow TP}(m_{G_2}, m_t, m_p) = \frac{\alpha^2 |\vec{k}_{t,p}|}{2\, m_{G_2}^2 \pi} \Big(1 + \frac{4|\vec{k}_{t,p}|^4}{45 m_t^4} + \frac{2|\vec{k}_{t,p}|^2}{3 m_t^2} \Big) \kappa_{g_2 tp\,,i}\, \Theta(m_{G_2} - m_t - m_p) \, . \tag{5.2.7}$$

The coupling α is not fixed, so branching ratios are only calculated for decays in this channel.

The third chiral Lagrangian, derived from (4.2.10), describes the decay of a tensor glueball into a vector and pseudoscalar meson:

$$\mathcal{L}_{c^{\text{ten}}} = \frac{c_1}{\sqrt{6}}\,\partial^\mu G_2^{\nu\alpha}\mathrm{Tr}\Big[\tilde{L}_{\mu\nu}\,\partial_\alpha\Phi\,\Phi^\dagger - \Phi^\dagger\,\partial_\alpha\Phi\tilde{R}_{\mu\nu} - \tilde{R}_{\mu\nu}\partial_\alpha\Phi^\dagger\Phi + \Phi\partial_\alpha\Phi^\dagger\tilde{L}_{\mu\nu}\Big]$$
$$+\frac{c_2}{\sqrt{6}}\,\partial^\mu G_2^{\nu\alpha}\mathrm{Tr}\Big[\partial_\alpha\Phi\tilde{R}_{\mu\nu}\;\Phi^\dagger - \Phi^\dagger\,\tilde{L}_{\mu\nu}\partial_\alpha\Phi - \partial_\alpha\Phi^\dagger\tilde{L}_{\mu\nu}\Phi + \Phi\tilde{R}_{\mu\nu}\partial_\alpha\Phi^\dagger\Big]\,. \tag{5.2.8}$$

We again define the sum $c := c_1 + c_2$, and the tree-level decay rate formula then reads

$$\Gamma^{tl}_{G\longrightarrow VP}(m_{G_2}, m_v, m_p) = \frac{c^2\,|\vec{k}_{v,p}|^5}{40\,\pi}\,\kappa_{gvp\,,i}\,\Theta(m_{G_2} - m_v - m_p)\,, \tag{5.2.9}$$

This decay channel is heavily suppressed; the only nonzero κ is for KK^* decay products, and is proportional to a factor of $(\phi_N - \sqrt{2}\phi_S)$, which vanishes in the chiral limit. This is expected to be a very small contribution

The final Lagrangian couples the tensor glueball to nucleons with the following interaction term [174, 175]

$$\mathcal{L}_{GNN} = \frac{g_{NN}}{m_N} G_{2,\mu\nu}\bar{N}(\gamma^\mu\overleftrightarrow{\partial^\nu} + \gamma^\nu\overleftrightarrow{\partial^\mu})N, \tag{5.2.10}$$

where $\bar{N}, N$ is the (anti-)nucleon field containing the proton and neutron, i.e. $N^T = (p, n)$, m_N is the nucleon mass, and $\overleftrightarrow{\partial^\mu} = \overrightarrow{\partial^\mu} - \overleftarrow{\partial^\mu}$. The decay width for a boson decaying into two nucleons is given by [176]

$$\Gamma_{GN\bar{N}} = 2\frac{\sqrt{\frac{M^2}{4} - m_N^2}}{8\pi M^2}|\bar{\mathcal{M}}|^2 = \frac{1}{30}\left(\frac{2g_{NN}}{m_N}\right)^2\frac{\sqrt{\frac{M^2}{4} - m_N^2}}{\pi M^2}\left(3M^4 - 4m_N^2M^2 - 32m_N^4\right), \tag{5.2.11}$$

where the factor 2 counts the $p\bar{p}$ and $n\bar{n}$ modes. Note that $3M^4 - 4m_N^2M^2 - 32m_N^4 = 4(\frac{M^2}{4} - m_N^2)(3M^2 + 8m_N^2)$, and $\frac{M^2}{4} - m^2 = |\vec{k_1}|^2$, so the decay width is proportional to $|\vec{k_1}|^3$. As expected for a P-wave decay like this one, the decay width is proportional to $|\vec{k_1}|^{2l+1}$ with $l = 1$.

5.3 Results for the decay ratios

The coefficients $\kappa_{g\circ\circ,i}$, whose dimension depends on the channel, are shown in table 5.1. For the 2-pseudoscalar channel, κ has mass dimension of -4, in the vector-vector channel it is dimensionless, in the axial vector plus pseudoscalar channel it has mass dimension -2, for the tensor and pseudoscalar channel it has mass dimension 2.

Using the $\kappa_{g\circ\circ\,,i}$ shown in Table 5.1 and equations (5.2.3), (5.2.4), (5.2.5), we compute the tensor glueball decay ratios. They are shown in Table 5.2. In the BESIII data an enhancement in the mass distribution at around 2210 MeV was found in decay channels with high gluon production, where the tensor glueball can be relevant [113]. Therefore, we have chosen this mass value when illustrating the decay ratios in Table 5.2 The decays are primarily to 2 vector mesons, with $\rho\rho$ and K^*K^* being the two dominant decay products. The two ρ mesons would further decay into four pions before reaching the detector in an experiment. Likewise the K^*K^* pair decays to 2 $K\pi$ pairs.
As in the previous chapter, we expect a quite large uncertainty of our results, in particular in connection to the $\rho\rho$-$\pi\pi$ ratio. By the same argument, the decay rate has a scaling of Z_π^4. Assuming a 20 percent uncertainty in Z_π we have an uncertainty in the decay rate of about 50 percent. However, the main qualitative point stands,

Decay process	$\kappa_{g\circ\circ,i}$
$G_2 \longrightarrow \rho(770)\,\rho(770)$	1
$G_2 \longrightarrow \overline{K}^\star(892)\,K^\star(892)$	$\frac{4}{3}$
$G_2 \longrightarrow \omega(782)\,\omega(782)$	$\frac{1}{3}$
$G_2 \longrightarrow \omega(782)\,\phi(1020)$	0
$G_2 \longrightarrow \phi(1020)\,\phi(1020)$	$\frac{1}{3}$
$G_2 \longrightarrow \pi\,\pi$	$(Z_\pi^2 w_\pi^2)^2$
$G_2 \longrightarrow \bar{K}\,K$	$\frac{4}{3} \times (Z_k^2 w_k^2)^2$
$G_2 \longrightarrow \eta\,\eta$	$\frac{1}{3} \times (Z_{\eta_N}^2 w_{\eta_N}^2 \cos\beta_P^2 + Z_{\eta_S}^2 w_{\eta_S}^2 \sin\beta_P^2)^2$
$G_2 \longrightarrow \eta\,\eta'(958)$	$\frac{1}{3} \times ((Z_{\eta_N}^2 w_{\eta_N}^2 - Z_{\eta_S}^2 w_{\eta_S}^2)\cos\beta_P \sin\beta_P)^2$
$G_2 \longrightarrow \eta'(958)\,\eta'(958)$	$\frac{1}{18} \times (Z_{\eta_S}^2 w_{\eta_S}^2 \cos\beta_P^2 + Z_{\eta_N}^2 w_{\eta_N}^2 \sin\beta_P^2)^2$
$G_2 \longrightarrow a_1(1260)\,\pi$	$\frac{1}{2} \times (Z_\pi w_\pi)^2$
$G_2 \longrightarrow f_1(1285)\,\eta$	$\frac{1}{6}(Z_{\eta_S} w_{\eta_S} \sin\beta_{A_1} \sin\beta_P + Z_{\eta_N} w_{\eta_N} \cos\beta_{A_1} \cos\beta_P)^2$
$G_2 \longrightarrow K_{1\,,A}\,K$	$\frac{2}{3} \times (Z_k w_k)^2$
$G_2 \longrightarrow f_1(1420)\,\eta'(958)$	$\frac{1}{6}(Z_{\eta_N} w_{\eta_N} \sin\beta_{A_1} \sin\beta_P + Z_{\eta_S} w_{\eta_S} \cos\beta_{A_1} \cos\beta_P)^2$
$G_2 \longrightarrow f_1(1285)\,\eta'(958)$	$\frac{1}{6}(Z_{\eta_S} w_{\eta_S} \sin\beta_{A_1} \cos\beta_P - Z_{\eta_N} w_{\eta_N} \cos\beta_{A_1} \sin\beta_P)^2$
$G_2 \longrightarrow f_2(1270)\,\eta$	$\frac{1}{24}\left(\phi_N \cos\beta_p \cos\beta_T + \phi_S \sin\beta_p \sin\beta_T\right)^2$
$G_2 \longrightarrow a_2(1320)\,\pi$	$\frac{\phi_N^2}{8}$
$G_2 \longrightarrow K^*(892)\,K + \text{c.c.}$	$\frac{1}{48}\left(\sqrt{2}\phi_N - 2\phi_S\right)^2$

Table 5.1: Coefficients for the decay channel $G_2 \longrightarrow A + B$.

Branching Ratio	theory	Branching Ratio	theory	Branching Ratio	theory
$\frac{G_2(2210)\longrightarrow \bar{K}\,K}{G_2(2210)\longrightarrow \pi\,\pi}$	0.4	$\frac{G_2(2210)\longrightarrow \rho(770)\,\rho(770)}{G_2(2210)\longrightarrow \pi\,\pi}$	55	$\frac{G_2(2210)\longrightarrow a_1(1260)\,\pi}{G_2(2210)\longrightarrow \pi\,\pi}$	0.24
$\frac{G_2(2210)\longrightarrow \eta\,\eta}{G_2(2210)\longrightarrow \pi\,\pi}$	0.1	$\frac{G_2(2210)\longrightarrow \bar{K}^*(892)\,\bar{K}^*(892)}{G_2(2210)\longrightarrow \pi\,\pi}$	46	$\frac{G_2(2210)\longrightarrow K_{1\,,A}\,K}{G_2(2210)\longrightarrow \pi\,\pi}$	0.08
$\frac{G_2(2210)\longrightarrow \eta\,\eta'}{G_2(2210)\longrightarrow \pi\,\pi}$	0.004	$\frac{G_2(2210)\longrightarrow \omega(782)\,\omega(782)}{G_2(2210)\longrightarrow \pi\,\pi}$	18	$\frac{G_2(2210)\longrightarrow f_1(1285)\,\eta}{G_2(2210)\longrightarrow \pi\,\pi}$	0.02
$\frac{G_2(2210)\longrightarrow \eta'\,\eta'}{G_2(2210)\longrightarrow \pi\,\pi}$	0.006	$\frac{G_2(2210)\longrightarrow \phi(1020)\,\phi(1020)}{G_2(2210)\longrightarrow \pi\,\pi}$	6	$\frac{G_2(2210)\longrightarrow f_1(1285)\,\eta}{G_2(2210)\longrightarrow \pi\,\pi}$	0.02
				$\frac{G_2(2210)\longrightarrow f_1(1420)\,\eta}{G_2(2210)\longrightarrow \pi\,\pi}$	0.01

Table 5.2: Branching ratios of G_2 w.r.t. $\pi\pi$. The columns are sorted as PP on the left, VV in the middle, and AP on the right.

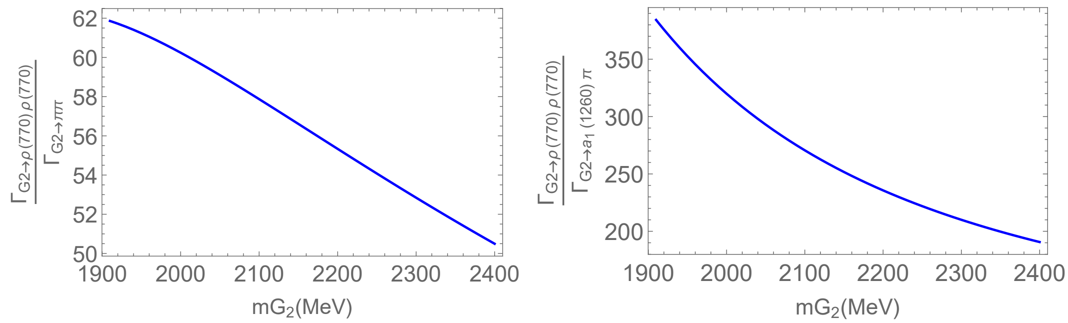

Figure 5.1: Decay ratios $\rho\rho/\pi\pi$ (left) and $\rho\rho/a1(1260)\pi$ (right) given as a function of the tensor glueball mass.

which is that the 2 vector channel, and particularly the ratio $\rho\rho$-$\pi\pi$, is expected to be large. Some decay ratios as a function of the tensor glueball mass are also shown in figure 5.1. In general the $\rho\rho$ dominance will decrease with a higher tensor glueball mass.

A similar dominance of $\rho\rho$ and K^*K^* decay products was found in [77] in a holographic model, but to a somewhat lesser extent (with a ratio of around 10, depending on the parameters).

We cannot compare with the nucleon decay width without knowing the value of g_{NN}. We can relate this to the pion coupling constant assuming tensor meson dominance [175]. This implies certain relations between couplings of different channels for the tensor meson decays. In this case, we will assume these for the tensor glueball as well. The Lagrangian for the decay of the tensor glueball to 2 pions can be rewritten to the form

$$\mathcal{L}_{G\pi\pi} = \frac{g_{\pi\pi}}{M} G_{\mu\nu} \partial^\mu \vec{\pi} \partial^\nu \vec{\pi}, \tag{5.3.1}$$

where $\vec{\pi} = (\pi^1, \pi^2, \pi^3)$ refers to the isospin triplet, and this $g_{\pi\pi}$ includes the $\kappa_{g\pi\pi}$ as well as λ. In this way the pion pion decay width can be written in the form

$$\Gamma_{G\pi\pi} = 6 \left(\frac{g_{\pi\pi}}{M}\right)^2 \frac{\left(\frac{M^2}{4} - m^2\right)^{5/2}}{60\pi M^2}, \tag{5.3.2}$$

where the factor 6 counts the isospin and identical particle factors. Tensor meson dominance (TMD) states that the dominant contribution to the hadron energy momentum tensor $\Theta^{\mu\nu}$ is the tensor mesons $T^{\mu\nu}$. Then, assuming tensor meson dominance leads to the following identity [175]

$$\frac{2g_{NN}}{m} = \frac{g_{\pi\pi}}{M}, \tag{5.3.3}$$

which we will assume is also a valid approximation for the tensor glueball. This allows us to calculate the decay ratio of $G \to N\bar{N}/G \to \pi\pi$ as

$$\frac{\Gamma_{GN\bar{N}}}{\Gamma_{G\pi\pi}} \approx 5.3. \tag{5.3.4}$$

The decay ratio is large enough to be a relevant factor in the search for a tensor glueball. In comparison to a chiral hadronic model [15] or a holographic model [159], the decay width is lower than the 2-vector channel widths, but larger than the other channels. For example compared to the dominant $\rho\rho$ channel, the ratio is $\Gamma_{G\rho\rho}/\Gamma_{GN\bar{N}} \approx 9.6$. The applicability of tensor meson dominance to the tensor glueball is not completely clear, so it is at best an approximate result. However, as an order of magnitude estimation, the outcome can

Resonances	Masses (MeV)	Decay Widths (MeV)	Decay Channels
$f_2(1910)$	1900 ± 9	167 ± 21	$\pi\pi$, KK, $\eta\eta$, $\omega\omega$, $\eta\eta'$, $\eta'\eta'$, $\rho\rho$, $a_2(1320)\pi$, $f_2(1270)\eta$
$f_2(1950)$	1936 ± 12	464 ± 24	$\pi\pi$, KK, $\eta\eta$, K^*K^*, 4π
$f_2(2010)$	2011^{+60}_{-80}	202 ± 60	KK, $\phi\phi$
$f_2(2150)$	2157 ± 12	152 ± 30	$\pi\pi$, $\eta\eta$, KK, $a_2(1320)\pi$, $f_2(1270)\eta$
$f_J(2220)$	2231.1 ± 3.5	23^{+8}_{-7}	$\eta\eta'$
$f_2(2300)$	2297 ± 28	149 ± 41	KK, $\phi\phi$
$f_2(2340)$	2345^{+50}_{-40}	322^{+70}_{-60}	$\eta\eta$, $\phi\phi$

Table 5.3: Spin-2 resonances heavier than 1.9 GeV listed in PDG [2].

be useful.

Next, we compare our theoretical results with relevant data on potential glueball candidates. The candidate resonances are summarized in Table 5.3 and in Figure 5.2. While the mass value in table 5.2 is not in line with every glueball candidate, it gives an overall picture on the decay ratios. One should also keep in mind that lattice determinations still have sizable errors (of the order of 100-200 MeV) and do not include the role of meson-meson loops, which can be quite relevant if the tensor glueball turns out to be broad (this being our favored scenario). In the comparison with data, we shall directly use the mass of the resonance for the decay ratios. Below we discuss each tensor glueball candidate separately. The experimental data and theoretical predictions used for this discussion are shown in table 5.4.

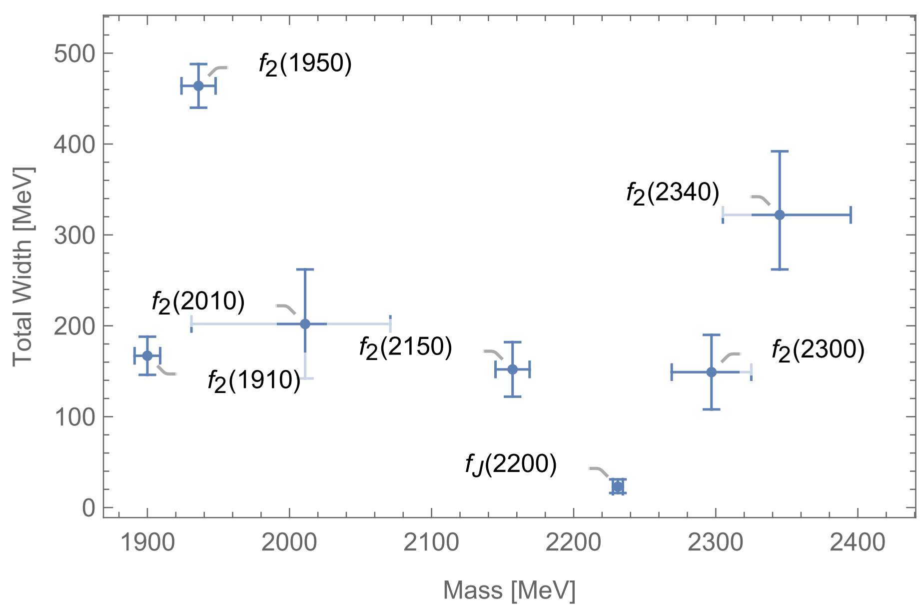

Figure 5.2: Masses and widths of isoscalar-tensor resonances heavier than 1.9 GeV [2].

Resonances	Branching Ratios	PDG	Model Prediction
$f_2(1910)$	$\rho(770)\rho(770)/\omega(782)\omega(782)$	2.6 ± 0.4	3.1
$f_2(1910)$	$f_2(1270)\eta/a_2(1320)\pi$	0.09 ± 0.05	0.07
$f_2(1910)$	$\eta\eta/\eta\eta'(958)$	< 0.05	~ 8
$f_2(1910)$	$\omega(782)\omega(782)/\eta\eta\prime(958)$	2.6 ± 0.6	~ 200
$f_2(1950)$	$\eta\eta/\pi\pi$	0.14 ± 0.05	0.081
$f_2(1950)$	$K\overline{K}/\pi\pi$	~ 0.8	0.32
$f_2(1950)$	$4\pi/\eta\eta$	> 200	> 700
$f_2(2150)$	$f_2(1270)\eta/a_2(1320)\pi$	0.79 ± 0.11	0.1
$f_2(2150)$	$K\overline{K}/\eta\eta$	1.28 ± 0.23	~ 4
$f_2(2150)$	$\pi\pi/\eta\eta$	< 0.33	~ 10
$f_J(2220)$	$\pi\pi/K\overline{K}$	1.0 ± 0.5	~ 2.5

Table 5.4: Decay ratios for the decay channels with available data.

- The $f_2(1910)$ has a width of 167 ± 21 MeV. The decay ratio $\rho(770)\rho(770)/\omega(782)\omega(782)$ of 2.6 ± 0.4 is not far from the theoretical result of 3.1, and the data on the decay ratio of $f_2(1270)\eta/a_2(1320)\pi$ also agrees with the theory. However, the data on the ratio $\eta\eta/\eta\eta'(958)$ gives a value less than 0.05, while the theoretical result is around 8. Furthermore, the ratio of $\omega\omega$ to $\eta\eta\prime$ is very large in theory, but only 2.6 ± 0.6 in data. Both of these involves the $\eta\eta'(958)$ mode, which we can conclude is much stronger in experiment than in theory. The $\eta\eta'$ decay mode for the glueball is small because of flavor symmetry. In exact flavor symmetry it is zero, but in the eLSM it is proportional to $\phi_N - \sqrt{2}\phi_S$, which is small. This mode clearly gives a contradiction between theory and experiment and as such the $f_2(1910)$ cannot be mainly gluonic.

- The meson $f_2(1950)$ decays into $\eta\eta$, $\pi\pi$, $K\bar{K}$, as well as K^*K^* and 4π modes. The experimental ratio $\eta\eta/\pi\pi$ of 0.14 ± 0.05 agrees with theory, and the ratio $K\bar{K}/\pi\pi$ shows agreement between experiment and theory as well. In experiment we only have a lower bound for the ratio $4\pi/\eta\eta$. If we assume that $\rho\rho$ decays into 4 pions (and the direct 4-pion production is small enough to not have complete destructive interference), we get a theoretical lower bound ratio of $4\pi/\eta\eta$. Both of these agree that this ratio is large and in the order of ~ 100. While the theory fits the data well, its large total decay width of 460 MeV would imply a broad tensor glueball candidate. Quite interestingly, the decay $J/\psi \to \gamma K^*(892)\bar{K}^*(892)$ shows a relatively large branching ratio of $(7.0 \pm 2.2)\, 10^{-4}$. A strong coupling to J/ψ is an expected feature of a tensor glueball, and the $f_2(1950)$ is the only candidate with measured $K^*\bar{K}^*$ decay products. Recent T-matrix pole analyses found compatible but slightly lower pole decay widths of 350 ± 114 MeV [111] and $237\pm \sim 60$ MeV [177], which are combined in the novel

PDG estimate for the pole width of 330 ± 110 MeV [2]. These values do not change the qualitative outcomes of our discussion. Rather, they are lower than the PDG estimate and further confirm the existence of the resonance $f_2(1950)$, strengthening the case for the $f_2(1950)$ as a tensor glueball.

- The resonance $f_2(2010)$ has a total decay width of 202 ± 60 MeV. Only $K\overline{K}$ and $\phi(1020)\phi(1020)$ decays have been seen. This fact suggests a large strange-antistrange content for this resonance, rather than a predominantly gluonic state.

- The $f_2(2150)$ is also listed in the PDG but is not completely established. Its mass is close to the one predicted by lattice of around 2.2 GeV. However, the ratio $K\overline{K}/\eta\eta$ is 1.28 ± 0.23, compared to the theoretical prediction of about 4. Likewise, the experimental ratio of $\pi\pi/\eta\eta$ is less than 0.33, while the theoretical estimate is about 10. The predicted ratio of 0.1 for $f_2(1270)\eta/a_2(1320)\pi$ also does not fit the data of 0.79 ± 0.11. While this resonance fits the predicted mass, all available decay rates do not show agreement between data and theory.

- The $f_J(2220)$ (with $J = 2$ or 4) was historically treated as a good candidate [155]. However, most of the decays that the theory predicts are not seen experimentally. Moreover, the only channel denoted as 'seen' in the decay modes table of the PDG [178] is the $\eta\eta'(958)$ one, which in theory is expected to be extremely suppressed ($\sim 10^{-3}$ time the $\pi\pi$) for the tensor glueball. the PDG data list also the decay ratio $\pi\pi/K\bar{K}$ of 1.0 ± 0.5 (even though in the 'decay modes' table these channels are marked as not seen), while the theoretical prediction is approximately 2.5. We also note that while in [113] a potential tensor glueball resonance is found at 2210 MeV, the width of the enhancement is an order of magnitude larger than one listed in PDG for $f_J(2220)$, so while the mass fits the width would not. Also, the uncertainty in the mass allows the glueball structure to also fit to other resonances. For these reasons, we conclude that, on the basis of the present evidence, $f_J(2220)$ should not be considered as a good candidate for being a tensor glueball.

- The resonance $f_2(2300)$, with a total width of 149 ± 41 MeV, decays only into $K\overline{K}$ and $\phi\phi$. Like the $f_2(2010)$, this suggests that it is predominantly a strange-antistrange object.

- Finally, the resonance $f_2(2340)$ has known decay channels into $\eta\eta$ and $\phi(1020)\phi(1020)$, which would also imply a large strange-antistrange component. It also has a broad decay width of 322 ± 60 MeV. Due to a lack of data, both of the last two resonances should be investigated in more details in the future, especially for what concerns other possible decay modes of these resonances. We also refer to the discussion in the next subsection for additional discussions.

Summarizing the above, it turns out that the resonance $f_2(1950)$ seems to be the best fit, although this would imply a broad tensor glueball state. All other states seem disfavored for various mismatches between theory and experiment, such as specific branching or decay ratios with available data, ($f_2(1910)$ and the $f_2(2150)$) or decays in strange states only ($f_2(2010)$, $f_2(2300)$, and $f_2(2340)$).
Yet, it still important to monitor the experimental status of the states above in the future. In particular, the analysis for the states $f_J(2220)$, $f_2(2300)$, and $f_2(2340)$ would benefit from more experimental data, with special attention to the latter broad one.

5.4 Discussions

In this subsection, we discuss two additional points. The first one addresses the numerical values of the partial decay widths of the tensor glueball. While a precise treatment is not possible within the eLSM framework, an estimate can be made by using large-N_c arguments and the decays of the conventional ground-state tensor mesons. The second point discusses the assignment of various tensor states as radially and orbitally excited conventional tensor mesons. In this framework, the tensor glueball should be an additional state that does not fit into the quark-antiquark nonet picture, which has a limited number of states for every level.

5.4.1 Large N_c scaling estimate

Consider the conventional mesons

$$f_2 \equiv f_2(1270) \simeq \sqrt{1/2}(\bar{u}u + \bar{d}d)$$
$$f_2' \equiv f_2'(1525) \simeq \bar{s}s,$$

whose decays rates into $\pi\pi$ are given by:

$$\Gamma_{f_2\to\pi\pi} = 157.2 \text{ MeV}$$
$$\Gamma_{f_2'\to\pi\pi} = 0.71 \text{ MeV}.$$

The decay amplitude $A_{f_2\to\pi\pi}$ requires the creation of a single $\bar{q}q$ pair from the vacuum and scales as $1/\sqrt{N_c}$, where N_c is the number of colors. On the other hand, the amplitude $A_{f_2'\to\pi\pi}$ implies that $\bar{s}s$ first converts into two gluons (gg) that subsequently transforms into $\sqrt{1/2}(\bar{u}u + \bar{d}d)$ (the very same mechanism is responsible for a small (about 3°) but nonzero mixing angle of the physical states in the strange-nonstrange basis fitted in the previous chapter). Schematically this process looks like:

$$\bar{s}s \to gg \to \sqrt{1/2}(\bar{u}u + \bar{d}d)\ . \tag{5.4.1}$$

The amplitude $A_{f_2'\to\pi\pi}$ scales as $1/N_c^{3/2}$ and is OZI [179, 180, 181] suppressed with respect to the previous one. Concretely, let us consider the transition Hamiltonian

$$H_{int} = \lambda\left(|\bar{u}u\rangle\langle gg| + |\bar{d}d\rangle\langle gg| + |\bar{s}s\rangle\langle gg| + h.c.\right), \tag{5.4.2}$$

where λ controls the mixing and therefore scales as $1/\sqrt{N_c}$. Then:

$$A_{f_2'\to\pi\pi} \simeq \sqrt{2}\lambda^2 A_{f_2\to\pi\pi}. \tag{5.4.3}$$

For the decay rates this implies

$$\Gamma_{f_2'\to\pi\pi} \simeq 2\lambda^4\Gamma_{f_2\to\pi\pi}, \tag{5.4.4}$$

which gives $\lambda \simeq 0.22$ by using the experimental values for Γ.

For the tensor glueball decay into $\pi\pi$, it start at an intermediate stage in the chain (5.4.1), since it is

Decay process	Γ_i(MeV)
$G_2 \to \pi\,\pi$	~ 15
$G_2 \to \bar{K}\,K$	~ 6
$G_2 \to \eta\,\eta$	~ 1.6
$G_2 \to \eta\,\eta'(958)$	~ 0.06
$G_2 \to \eta'(958)\,\eta'(958)$	~ 0.08

Table 5.5: Estimations of the decay channel $G_2 \to PP$.

comprised of a gluon-gluon pair. We then have:

$$A_{G_2\to\pi\pi} \simeq \sqrt{2}\lambda A_{f_2\to\pi\pi}, \tag{5.4.5}$$

since it is one extra step compared to the f_2. The decay rates then go as

$$\Gamma_{G_2\to\pi\pi} \simeq 2\lambda^2\Gamma_{f_2\to\pi\pi} \simeq \sqrt{2}\sqrt{\Gamma_{f_2\to\pi\pi}\Gamma_{f_2'\to\pi\pi}} \simeq 15\text{ MeV}. \tag{5.4.6}$$

A similar estimation of the coupling of glueballs to mesons has been done in [182, 183]. By construction, $\Gamma_{G_2\to\pi\pi}$ scales as $1/N_c^2$, which is expected for glueballs, realizing the expectation $\Gamma_{f_2'\to\pi\pi} < \Gamma_{G_2\to\pi\pi} < \Gamma_{f_2\to\pi\pi}$.

The estimate $\Gamma_{G_2\to\pi\pi} \simeq 15$ MeV is only a very rough approximation. It does not take into account phase space or form factors, and it avoids a microscopic evaluation. Still, it gives an order of magnitude idea on how large the $\pi\pi$ mode could be, and by extension how large the other decay rates are. Some of these estimates are shown in Table 5.5.

We note that the $\pi\pi$ decay rate we found is comparable to the one obtained within the Witten-Sakai-Sugimoto model [77], in which

$$\Gamma_{G_2\to\pi\pi}/m_{G(2000)} \simeq 0.014, \longrightarrow \Gamma_{G_2\to\pi\pi} \simeq 28\text{ MeV}. \tag{5.4.7}$$

However, the ratio $\rho\rho/\pi\pi$ we find is a factor of 4 to 5 larger, making it so that while the models agree on $\rho\rho$ dominating, is it substantially larger in the eLSM. This decay width into $\pi\pi$ also implies a large decay width into $\rho\rho \to \pi\pi\pi\pi$.

5.4.2 Classification of tensor meson states

The second point relates to the assignment of quark-antiquark tensor states. Up to now, we have considered all isoscalar f_2 states in the energy region about 2 GeV equally as potential tensor glueball candidates. However, most of them should be interpreted as standard $\bar{q}q$ objects.

For this reason, it is useful look at how to classify them normally, rather than looking at their status as a potential glueball. While the ground-state tensor mesons (with spectroscopic notation 1^3P_2) are well established as $a_2(1320)$, $K_2^*(1430)$, $f_2(1270)$, and $f_2'(1525)$, there is also a nonet of radially excited tensor states (2^3P_2) and a nonet of orbitally excited tensor states (1^3F_2). Based on the quark model [100], the orbitally excited tensor states are thought to be more massive than the radially excited tensor states, just as with the excited vector mesons [116].

The nonet of radially excited tensor mesons consists of the following. The isotriplet state $a_2(1700)$, the isodoublet states $K_2^*(1980)$, and the isoscalar (mostly nonstrange) $f_2(1640)$. The mostly strange $\bar{s}s$ member of the nonet could be assigned to $f_2(1910)$, or $f_2(1950)$, or $f_2(2010)$. The quark model review of the PDG [2] considers $f_2(1950)$ as the radially excited $\bar{s}s$ state. However, the decay of that state does not quite fit with the picture of a predominantly $\bar{s}s$ object. In particular, the experimental $KK/\pi\pi$ ratio is about 0.8 (see Table 5.4), while a $\bar{s}s$ state would imply a ratio larger than one. Furthermore, the mass is very close to that of the tensor isodoublet member $K_2^*(1980)$, which does not support it being a radially excited strange-antistrange state.

For the state $f_2(1910)$, it is currently not clear if it corresponds to a separate resonance or if it is actually the same as the $f_2(1950)$. It is therefore omitted from the PDG summary table. Its mass is even lighter than $K_2^*(1980)$, which makes it unlikely this state is an $\bar{s}s$ state. The decays also do not support it being strange-antistrange. The decay mode $\rho\rho$ should be suppressed, as well as $a_2(1320)\pi$ which should be smaller than $f_2(1270)\eta$. In the data (see Table 5.4), this is not the case.

On the other hand, the state $f_2(2010)$ is well established and is known to decay into $\phi\phi$ and KK. This makes it more likely be include strange contents, thus making it more suitable as the last radially excited tensor meson.

Summarizing the discussion above, we might identify the nonet of radially excited tensor mesons as

$$\{a_2(1700),\ K_2^*(1980),\ f_2(1640),\ f_2(2010)\} \text{ with } 2^3P_2 \text{ and } J^{PC} = 2^{++}. \tag{5.4.8}$$

With the $f_2(1910)$ being less well established, this leaves the $f_2(1950)$ as a potential glueball candidate. In [184] it is also concluded that the $f_2(1950)$ does not fit the 3^3P_2 nonet as the radial excitation of $f_2(1270)$, and the mass is too low to otherwise fit in that nonet according to the Regge trajectory.

The situation for the orbitally excited states is not as clear. There are no well established isotriplet or isodoublet states that could be used to identify the nonet. Possible isoscalar resonances could be the $f_2(2150)$, the $f_2(2300)$ or the $f_2(2340)$. The $f_2(2150)$ could correspond to a nonstrange isoscalar state belonging to the next radially excited nonet 3^3P_2, and the $f_2(2300)$ and the $f_2(2340)$ could be regarded as a single state, which would be the $\bar{s}s$ state of this nonet. However, these resonances are all not well established, and more information is needed to make a definitive statement on this nonet.

5.5 Conclusions

In this chapter, we expanded upon the previous chapter on tensor mesons and adapted it to the study of the tensor glueball. We constructed chirally invariant Lagrangians which describe the tensor glueball decays. From these we could find the decay ratios of certain channels for the tensor glueball. It turns out the dominant decay channels involve two vector decay products. In particular, the channels $\rho\rho$ and $K^*\bar{K}^*$ are large compared to the others.

From the large predicted $\rho\rho/\pi\pi$ ratio, it would follow that the tensor glueball itself is very broad, given the estimate of the $\pi\pi$ mode being of the order of 10 MeV. furthermore, we also predict a very small decay width of the tensor glueball into $K^*(892)K$. This specific decay mode could be useful to exclude potential glueball candidates in the future.

Comparing the theoretical predictions to the experimental data shows that presently the best best match between experimental data and eLSM predictions is for the $f_2(1950)$. This would also imply that the tensor glueball is a relatively broad state. According to lattice QCD, the $f_2(1950)$ might be too light to be the

Resonances	Interpretation status
$f_2(1910)$	Agreement with some data, but excluded by $\eta\eta/\eta\eta'$ and $\omega\omega/\eta\eta\prime$ ratios
$f_2(1950)$	$\eta\eta/\pi\pi$ agrees with data, no contradictions with data, but implies broad tensor glueball Best fit as predominantly glueball among considered resonances
$f_2(2010)$	Likely primarily strange-antistrange content
$f_2(2150)$	All available data contradicts theoretical prediction
$f_J(2220)$	Data on $\pi\pi/K\bar{K}$ disagrees with theory, largest predicted decay channels are not seen
$f_2(2300)$	Likely primarily strange-antistrange content
$f_2(2340)$	Likely primarily strange-antistrange content, would also imply a broad glueball

Table 5.6: Isoscalar tensor resonances and their status as the tensor glueball.

tensor glueball, as it does not fit in the consensus of lattice studies which sets the mass range to 2.2-2.4 GeV. However, an unquenched calculation would include additional meson-meson loop corrections, which would lower the glueball mass. The large width of $f_2(1950)$ can also support the view it is not a conventional quark-antiquark state, and therefore possibly a glueball. The interpretation status of all isoscalar tensor meson resonances that have been considered is summarized in Table 5.6.

In the future, more data on decays of all tensor mesons into vector-vector, pseudoscalar-pseudoscalar, ground-state tensor-pseudoscalar, as well as 2 nucleons would be very helpful to constrain models and falsify different scenarios, since not all resonances considered in this chapter had a great deal of data. In particular, more information about the broad state $f_2(2340)$ could shed light on its nature. Moreover, decays of the J/ψ into tensors as well as radiative (such as photon-photon) decays of tensor states could be of great use to determine aspects of tensor mesons, and the tensor glueball in particular.

In this analysis, the mixing of the tensor glueball with other conventional meson states was not taken into account. Recently, a small mixing of the pseudoscalar glueball and the η was studied on the lattice in [185]. While mixing with the ground state tensor mesons is expected to be small because the tensor glueball is much more massive, the mixing with excited tensor states, which have much more similar masses, could be relevant. Implementing this into the eLSM is in principle possible and can be undertaken once better data, both from experiments and from lattice QCD, is available. Mixing of glueballs with conventional mesons is a crucial part of why they are so difficult to detect, so this could be a significant step towards identifying the tensor glueball. In the next chapter we will discuss a similar mixing of the vector glueball with charmonium states. Because the identification of the vector glueball is not as advanced as for the scalar or tensor glueball, an indirect measurement via the effect of its mixing could be interesting.

Chapter 6

The vector glueball, mixing, and the $\rho\pi$ puzzle

6.1 Introduction

The vector glueball's mass is predicted to be in the range of 3.8 to 4 GeV based on lattice computations [73, 74]. In contrast to the lightest glueball states, potential candidate states are lacking for the vector glueball. However, it shares quantum numbers with the bound charmonium state J/ψ and its excited state, the $\psi(3686)$, which have quantum numbers in the spectroscopic notation $n^{2S+1}L_J$ as 1^3S_1 for the J/ψ and 2^3S_1 for the $\psi(3686)$. These are believed to decay primarily through a 3-gluon channel, already making their decays an interesting avenue in identifying glueballs experimentally. Furthermore, the vector glueball in particular can play a role here, since it can (and in general will) mix with these states with the same quantum numbers.

The J/ψ and $\psi(3686)$ are nonrelativistic bound charm-anticharm states. Their primary decay is through 3 gluons, which in the nonrelativistic limit is proportional to the wave function at the origin. That is, the decay width to some final state h consisting of light hadrons is [186, 187]

$$\Gamma_h = |\psi(\mathbf{r}=0)|^2|\mathcal{M}|^2. \tag{6.1.1}$$

Where $\psi(\mathbf{r})$ is the position wavefunction of the system, and $\mathcal{M}$ is the matrix element associated with the decay channel. This equation, albeit with different $\psi(\mathbf{r})$ and $\mathcal{M}$, holds for both the J/ψ and the $\psi(3686)$. One can then look at the ratio of their decay widths into a specific state. If one chooses to ignore phase space factors –essentially ignoring the mass difference between the J/ψ and the $\psi(3686)$ – only the unknown ratio of wave functions remains. Computing these wave functions is no trivial task, but without knowledge of the wave functions we can already see that the ratio of decay widths is almost independent of the final state h into which it decays. The same argument holds for the decay into e^+e^-, for which this ratio is experimentally well-known. Using PDG data on the e^+e^- channel we can compute this ratio:

$$\frac{\Gamma(\psi(3686) \to h)}{\Gamma(J/\psi \to h)} \approx \frac{\Gamma(\psi(3686) \to e^+e^-)}{\Gamma(J/\psi \to e^+e^-)} = 42.2\%. \tag{6.1.2}$$

Decay channel h	Measured Q_h value
$K^0\bar{K}^{0*}$ + c.c	$2.59 \pm 0.54\%$
K^+K^{-*} + c.c	$0.48 \pm 0.10\%$
$\eta\omega$	$< 6.3\%$
$\omega\eta'$	$16.93^{+13.33}_{-11.23}\%$
$\phi\eta$	$4.19 \pm 0.54\%$
$\phi\eta'$	$3.35 \pm 0.57\%$
$\rho\pi$	$0.19 \pm 0.073\%$
$\eta\rho$	$11.4 \pm 3.39\%$
$\rho\eta'$	$23.46^{+21.12}_{-14.99}\%$
$\omega\pi^0$	$4.67 \pm 1.43\%$

Table 6.1: Q_h values for various VP decay channels from PDG [2]. Taking into account the errors, every channel is consistent with being suppressed compared to the 13% rule.

Usually, branching ratios are more accessible experimentally, formulating this in terms of branching ratios leads us to the 13% rule (historically often called the 12% rule, based on the past value):

$$Q_h = \frac{\mathcal{B}(\psi(3686) \to h)}{\mathcal{B}(J/\psi \to h)} \approx \frac{\mathcal{B}(\psi(3686) \to e^+e^-)}{\mathcal{B}(J/\psi \to e^+e^-)} = 13.3\%. \tag{6.1.3}$$

The 13% rule can also be derived to include an extra phase space factor. We will include this later on, but for a qualitative description we do not need it yet. All measured baryon-antibaryon decay channels are compatible with this rule. Some meson decay channels follow this rule, but some channels severely violate it. The $\rho\pi$ channel is the most prominent channel in which this happens. Hence, the name given to this unexplained behavior is "the $\rho\pi$ puzzle". In Table 6.1 the experimental values for a number of VP channels are shown. Taking into account the uncertainties, all channels are consistent with Q_h being suppressed relative to the 13% rule.

Experimentally, the first indication of the $\rho\pi$ puzzle was observed in 1983 by the Mark II collaboration [188], where the decay of the J/ψ into $\rho\pi$ was substantial, but the decay width for the channel $\psi(3686) \to \rho\pi$ was so small it was only observed decades later by CLEO and BES [189, 190]. Early on it was noticed that the charmonium decays into $\rho\pi$ break hadron helicity conservation [191] which follows from perturbative QCD predictions. Understanding why this rule is broken may have important consequences for the applicability of perturbative QCD to the decay of charmonium states or even other states at a similar mass.
There are many proposed explanations for the $\rho\pi$ puzzle [192, 193]. A non-exhaustive list of explanations not involving the vector glueball include

- Intrinsic charm components in the light mesons such as the ρ, which allow for new diagrams for the decay of the J/ψ, which are suppressed for the $\psi(3686)$ because the excited state is orthogonal to the charm-anticharm component of the ρ [194].
- Suppression of the charm-anticharm wave function at the origin for a component of the $\psi(3686)$ in which the $c\bar{c}$ is in a color-octet ${}^3S_1$ state [195].
- Interference between 3-gluon and electromagnetic decays for the J/ψ decays, while the $\psi(3686)$ decays not through a 3-gluon, but through a specific configuration of 5 gluons [196].
- A large nonvalence gluon or quark-antiquark component present in the wavefunction of the $\psi(3686)$,

which are not significant in the J/ψ since it is the lowest lying state. The valence and nonvalence components then interfere destructively in the $\rho\pi$ channel [197].

- Destructive interference between S-wave and D-wave components of the $\psi(3686)$, which come from mixing with the D-wave charmonium state ψ'' [198].
- Final state interactions, which can be of similar order as tree level amplitudes. In particular, $J/\psi \to \rho\pi$ would be enhanced by the $a_2\rho$ loop diagram, while for the $\psi(3686)$ this can be canceled by the $a_1\rho$ loop diagram [199].
- Cancellation between the amplitudes for the processes $e^+e^- \to \psi(3686) \to \rho\pi$ and the direct decay channel $e^+e^- \to \rho\pi$ [192].

Any such explanation tends to either postulate an enhancement for the decay $J/\psi \to \rho\pi$, or a suppression for the decay $\psi(3686) \to \rho\pi$. The class of explanations we will treat here is that the $\rho\pi$ puzzle is caused by mixing with a vector glueball. In the past a mixing between the vector glueball with the J/ψ [200, 201], as well as the $\psi(3686)$ [202] have been considered. Given recent lattice predictions for the vector glueball mass in the range of about 3.8 to 4 GeV [73, 74], the $\psi(3686)$ is closer in mass to the vector glueball, and so we will initially assume a mixing between the excited charmonium state and the vector glueball, but the calculation can be easily adapted to have mixing between the J/ψ and the vector glueball instead. Aside from the influence of the vector glueball, we will assume the 13% rule holds. This means that mixing of the $\psi(3686)$ with the vector glueball will fall into the category of suppression of the decay $\psi(3686) \to \rho\pi$, and mixing of the J/ψ with the vector glueball will be enhancement of the decay $J/\psi \to \rho\pi$. We will use the framework of the eLSM which we have introduced in Chapter 3 and applied in Chapters 4 and 5, as apply a vector meson dominance (VMD) model, as before.

6.2 Model setup

The central premise of this chapter is the mixing of the excited charmonium state with a three-gluon $J^{PC} = 1^{--}$ vector glueball state. Calling the physical states $\psi(3686)$ as in the PDG listing, and O', the pure charm-anticharm state $\psi_{c\bar{c}}(2S)$, and the pure glueball state O, the mixing is as follows:

$$\begin{pmatrix} \psi(3686) \\ \mathcal{O}' \end{pmatrix} = \begin{pmatrix} \cos(\theta) & \sin(\theta) \\ -\sin(\theta) & \cos(\theta) \end{pmatrix} \begin{pmatrix} \psi_{c\bar{c}}(2S) \\ ggg \equiv \mathcal{O} \end{pmatrix}. \tag{6.2.1}$$

The mixing angle θ is assumed to be small, so $\psi(3686)$ is predominantly charm-anticharm and O' is primarily gluonic. In order to include phase space corrections to the 13% rule consistent with the eLSM, we consider the following interaction for the decay of the J/ψ (or $\psi(2S)$) into an electron-positron pair by the diagram shown in Fig 6.1, which has 2 interaction vertices, found in the Lagrangian terms given by

$$\mathcal{L} = eA_\mu\bar{\psi}\gamma^\mu\psi - \frac{1}{2}\, g_{V_1\gamma}V_{1,\mu\nu}F^{\mu\nu}. \tag{6.2.2}$$

Here $V_{1\mu\nu}$ is the field strength tensor for the initial vector state V_1, which which can be the glueball O, the J/ψ or the $\psi(2S)$, e is the electromagnetic charge, $g_{V_1\gamma}$ is a dimensionless coupling that describes the $V_1\gamma$ transition, and $\psi, \bar{\psi}$ is the (anti)spinor of the electron (positron). We assume that the glueball does not directly couple to photons, so that $g_{O\gamma} = 0$. The resulting matrix element of the decay width depends on

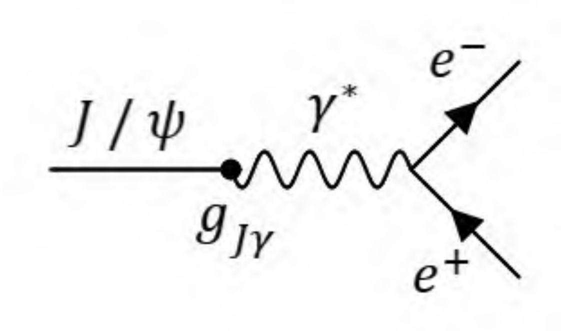

Figure 6.1: Feynman diagram for the decay of the J/ψ into an electron-positron pair.

the phase space as

$$\Gamma_{V_1 e^+ e^-} \propto \left(e^2 g_{V_1\gamma}\right)^2 \frac{|\vec{k}|}{M_{V_1}^2}(M_{V_1}^2 + 2m_e^2), \tag{6.2.3}$$

where we have suppressed some numerical prefactors, as they will be divided out later. By using the experimental result, we can now find the couplings $J/\psi - \gamma$ and $\psi(2S) - \gamma$ transitions, and therefore the ratio r between J/ψ and $\psi(2S)$ couplings, which is more or less the ratio between the wavefunctions at the origin in (6.1.1). Defining r as the ratio between the couplings so that

$$g_{\psi(2S)} = r\, g_{J/\psi} \tag{6.2.4}$$

$$\longrightarrow g_{\psi(3686)} = \cos(\theta)\, g_{\psi(2S)} + \sin(\theta) g_O = r\cos(\theta)\, g_{J/\psi} + \sin(\theta) g_O, \tag{6.2.5}$$

where the $\cos(\theta)$ originates from the mixing with the vector glueball. Since the glueball does not directly couple to the photon, i.e. $g_{O\gamma} = 0$, this gives the following result from the decays into electron-positron:

$$\frac{\mathcal{B}(\psi(2S) \to e^+e^-)}{\mathcal{B}(J/\psi \to e^+e^-)} \approx 13\% \Longrightarrow r^2\cos(\theta)^2 \approx 0.35. \tag{6.2.6}$$

We assume this same ratio r holds for every other coupling too, since it is based on the wavefunctions at the origin.

Now that we have the 13% rule translated to a relation between the coupling constants, we can introduce the interaction Lagrangian terms. We assume that, like the vector glueball, the J/ψ and $\psi_{\bar{c}c}(2S)$ are flavor blind with respect to the 3 light flavors, hence the form of the interaction terms is the same for all 3 states. The Lagrangian for decays into PV is constructed using chiral symmetry, charge conjugation and parity, but dilatation invariance is broken. The strong decay into PV is described by the Lagrangian [98]

$$\mathcal{L}_{PV} = \frac{1}{2} g_{V_1}\, \widetilde{V}_{1,\mu\nu} \mathrm{Tr}[L^\mu \Phi R^\nu \Phi^\dagger] \supset g_{V_1}\, \widetilde{V}_{1,\mu\nu} \mathrm{Tr}[\partial^\mu \mathcal{P} \Phi_0 V^\nu \Phi_0], \tag{6.2.7}$$

where $\widetilde{V}_{1,\mu\nu}$ is the dual field strength tensor for the initial vector state V_1. We remind ourselves that, as with the tensor glueball, each of the V_1 is proportional to the identity matrix for what concerns flavor indices, and so can be taken out of traces.
To include the electromagnetic interactions, we will use a vector meson dominance model [135] as we did in Chapter 4. Equation (6.2.2) included the transition from the J/ψ or $\psi(2S)$ to the photon, which is associated

with a factor

$$-g_{V_1\gamma}, \tag{6.2.8}$$

since in momentum space we have $V_{1,\mu\nu}F^{\mu\nu} \to 2q^2 V_{1,\mu}A^\mu$. The $1/q^2$ cancels with the photon propagator, and the factor 2 cancels with the $\frac{1}{2}$ in (6.2.2). For the light vector mesons, we apply the same shift as before

$$V_{\mu\nu} \to V_{\mu\nu} + \frac{e}{g_\rho}F_{\mu\nu}Q, \tag{6.2.9}$$

which when applied to the kinetic terms gives a vector meson-photon transition like the one of (6.2.2):

$$-\frac{1}{4}V_{\mu\nu}V^{\mu\nu} \to -\frac{1}{4}V_{\mu\nu}V^{\mu\nu} - \frac{e}{2g_\rho}V_{\mu\nu}F^{\mu\nu} + \cdots \tag{6.2.10}$$

At the level of the fields[1] this shift can be realized by

$$V_\mu \to V_\mu + \frac{e}{g_\rho}A_\mu Q. \tag{6.2.11}$$

Next, we introduce a flavor invariant Lagrangian for a PVV interaction

$$\mathcal{L}_{PVV} = g_{PVV}\,\mathrm{Tr}[PV_{\mu\nu}\tilde{V}^{\mu\nu}]. \tag{6.2.12}$$

This Lagrangian initially contains only kinematically impossible decays, but by performing the shift (6.2.9) it generates interactions with the photon relevant to this chapter:

$$\mathcal{L}_{PVV} \to \mathcal{L}_{PVV} + \left(\frac{e}{g_\rho}\right)^2 g_{PVV}F_{\mu\nu}\tilde{F}^{\mu\nu}\mathrm{Tr}[PQQ] + \frac{e}{g_\rho}g_{PVV}\tilde{F}_{\mu\nu}\mathrm{Tr}[P\{Q,V^{\mu\nu}\}]. \tag{6.2.13}$$

Now, we can write down the interactions for the decays of the initial vector states, including electromagnetic decays. The Feynman diagrams for the J/ψ are shown in Fig. 6.2. The same diagrams apply for the $\psi(2S)$, and the vector glueball only decays through channel (i). Each channel separately gives the same phase space factor at the end, but their contributions are all with different coefficients which can either constructively or destructively interfere. The total decay width is thus given by

$$\Gamma = |\sum_i \kappa_i|^2 \frac{|\vec{k}|^3}{12\pi}, \tag{6.2.14}$$

but each with a different κ_i, which contain multiple couplings and constants and moreover depends on which VP particles are the decay product. We will go over the construction of each diagram and how the κ_i follows.

(i) is the strong decay channel described in (6.2.7). It is the only channel through which the vector glueball contributes. The coefficient κ_i follows from the factor

$$g_{V_1}\,\mathrm{Tr}[\partial^\mu\mathcal{P}\Phi_0 V^\nu\Phi_0]. \tag{6.2.15}$$

(ii) follows from the initial vector V_1 converting into a virtual photon by the transition given in (6.2.2),

[1] This is not necessary but is done for clarity. The interaction in (6.2.7) can be rewritten with $V_{\mu\nu}$ so that the previous form can be directly applied. Using the field strength tensors makes gauge invariance more explicit, but in our case the end result is the same.

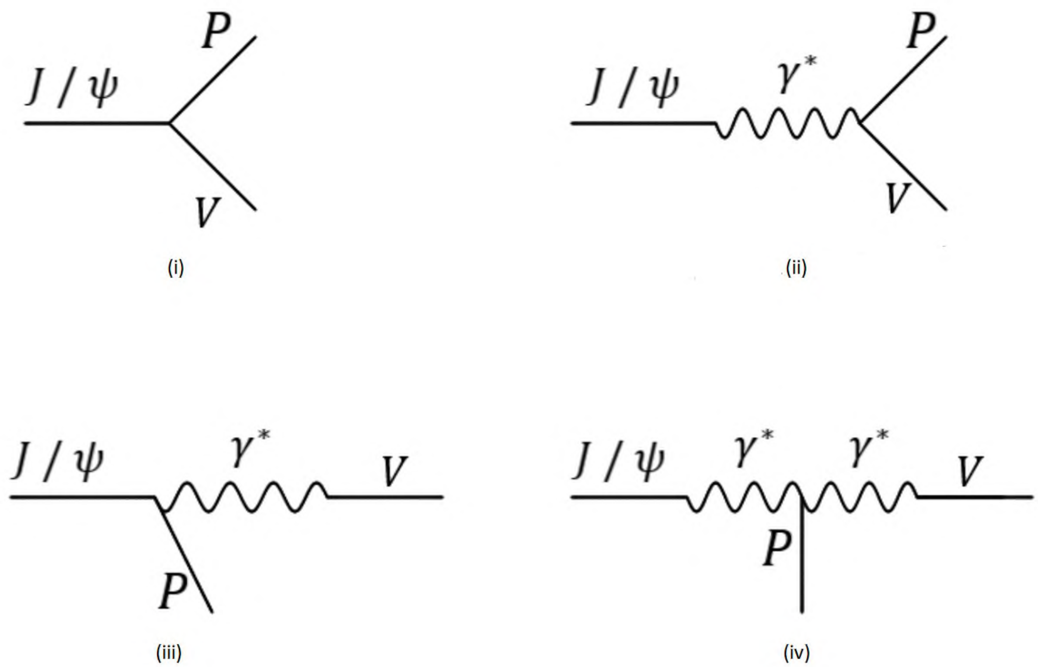

Figure 6.2: Four Feynman diagrams for the decay channels of the J/ψ. Decay channel (i) is a strong decay, while (ii-iv) are through electromagnetic channels.

followed by the virtual photon decaying into a PV pair given by the last term in (6.2.13). Therefore κ_i is given by the following combination

$$-g_{V_1\gamma}g_{PVV}\frac{e}{g_\rho}\mathrm{Tr}[P\{Q,V\}] \tag{6.2.16}$$

(iii) comes from shifting V according to (6.2.11) in the V_1PV vertex of (6.2.7), followed by the virtual photon transitioning to a vector meson as in (6.2.10). The resulting κ_i is thus given by the combination

$$-g_{V_1}(\frac{e}{g_\rho})^2\mathrm{Tr}[\partial\mathcal{P}\Phi_0 Q\Phi_0]\mathrm{Tr}[VQ]. \tag{6.2.17}$$

Note that, similar to in Chapter 4, this is a term with two separate traces, which are expected to be suppressed. We can see firsthand that it has a higher power of (small) coupling constants, so this seems to indeed be the case.

(iv) is generated from the initial V_1 transitioning into a virtual photon by (6.2.2), which proceeds to emit a pseudoscalar by the second term in (6.2.13). The virtual photon then transitions into a vector meson by (6.2.10). Here the factor κ_i is thus given by

$$g_{V_1\gamma}\; g_{PVV}(\frac{e}{g_\rho})^3\;\mathrm{Tr}[PQQ]\mathrm{Tr}[VQ]. \tag{6.2.18}$$

This term also has a double trace structure and a higher power of small coupling constants, in particular the combination $(\frac{e}{g_\rho})^3$, so it is more highly suppressed.

Finally, inspired by [203], we include a form factor for each of the virtual photon propagators

$$F(q^2) = \frac{1}{1 - q^2/\Lambda^2}, \tag{6.2.19}$$

where q is the 4-momentum of the virtual photon and Λ is an energy scale we will fit.

6.3 Results

Now that we have the relevant decay terms and the coefficients κ_i, we can make a fit to the data on Q_h for VP decay channels of the J/ψ and the $\psi(3686)$. While it seems we may have many free parameters, only three independent parameters need to be fitted on the decay of charmonium states. These three will be the strong J/ψ coupling $g_{J/\psi}$, the glueball coupling g_O, and the scale Λ that appears in the form factors (6.2.19). The couplings e and $g_\rho \simeq 5$ are well known and can be taken from literature. The coupling g_{PVV} is fitted to decay of the neutral pion into two photons, which is also discussed in-depth in [204].
The coupling of the $\psi(3686)$ (6.2.5) is a combination of the $\psi(2S)$ and glueball couplings, together with the mixing angle. However, using the 13% rule (6.2.6), this simplifies in the following expression

$$g_{\psi(3686)} = \sqrt{0.35} g_{J/\psi} + \sin(\theta) g_O. \tag{6.3.1}$$

The coupling $g_{\psi(2S)}$ has dropped out, and the glueball coupling and mixing angle only appear in the combination $\sin(\theta)g_O$. Redefining $\sin(\theta)g_O \to g_O$ leaves us with only g_O and $g_{J/\psi}$ as free couplings. The same argument holds for the coupling to the photon, however it is assumed that the glueball does not couple to the photon, and $g_{J/\psi\gamma}$ can be fitted directly from the electron-positron decay of the J/ψ. Various constants that appear in the κ_i are taken from Table 3.3. We will not use any other procedure to fit Λ beforehand, so that leaves with the aforementioned 3 free parameters. These parameters and their numerical values resulting from the fit are shown in Table 6.2.

Parameters	Numerical Values
Strong coupling $g_{J/\psi}$	$-5.4 \cdot 10^{-3}(\mathrm{MeV})^{-2}$
effective glueball coupling $g_O \sin(\theta)$	$5.6 \cdot 10^{-3}(\mathrm{MeV})^{-2}$
Form factor mass scale Λ	$1.6 \cdot 10^3\mathrm{MeV}$

Table 6.2: Fit parameters and their numerical values when fitted to experimental data on Q_h in the VP channels.

We will restrict to describing the ratio Q_h for the VP channel, where the 13% rule is broken most seriously. The results for Q_h, with and without the mixing with a vector glueball, along with experimental data with error bars, are shown in Fig. 6.3. As can be seen, mixing with the vector glueball noticeable improves the agreement with experimental data. When mixing is included, the theory agrees with experiment on all channels except for the $\omega\eta'$, $\rho\eta$ and the $\rho\eta'$, each of which has a large experimental uncertainty. In particular the $\rho\pi$ and charged KK^* channels do not agree with experiment unless the vector glueball is added. Concretely, we find a reduced $\chi^2 \sim 5$ when there is no mixing with the vector glueball, and a reduced $\chi^2 \sim 2$

when we include mixing with the vector glueball. However, since the data and theory with mixing agree on the data points with smaller error, importantly the $\rho\pi$ and the charged KK^*, most of the reduced $\chi^2 \sim 2$ comes from decays with large experimental uncertainties. This is contrary to the unmixed scenario, where there is no agreement within 1 standard deviation between theory and experiment. The glueball coupling $g_O \sin(\theta)$ and the J/ψ coupling found by the fit are of similar order but interfere destructively, so that the model strongly leans into the $\psi(3686)$ suppression hypothesis. Given that the glueball coupling is paired with $\sin(\theta)$ for a small mixing angle θ, coupling of the vector glueball to light VP channels is stronger than that of the J/ψ, which is to be expected. At the current stage, mixing of the $\psi(3686)$ gives slightly better agreement with the data, but it is likely not strong enough to conclude definitively that the glueball mixes with the $\psi(3686)$. Future work to expand the analysis can include higher order strong interaction diagrams, different interaction strengths for mesons with a strange quark, more decay channels and treating the J/ψ and $\psi(3686)$ decays separately, which can help determine the mixing pattern and the mixing angle. If the mixing angle is isolated and determined by the decays of charmonium states, or determined by some other method, we can also give numerical predictions for the partial decay widths of the vector glueball, rather than only having decay ratios as in Chapter 5.

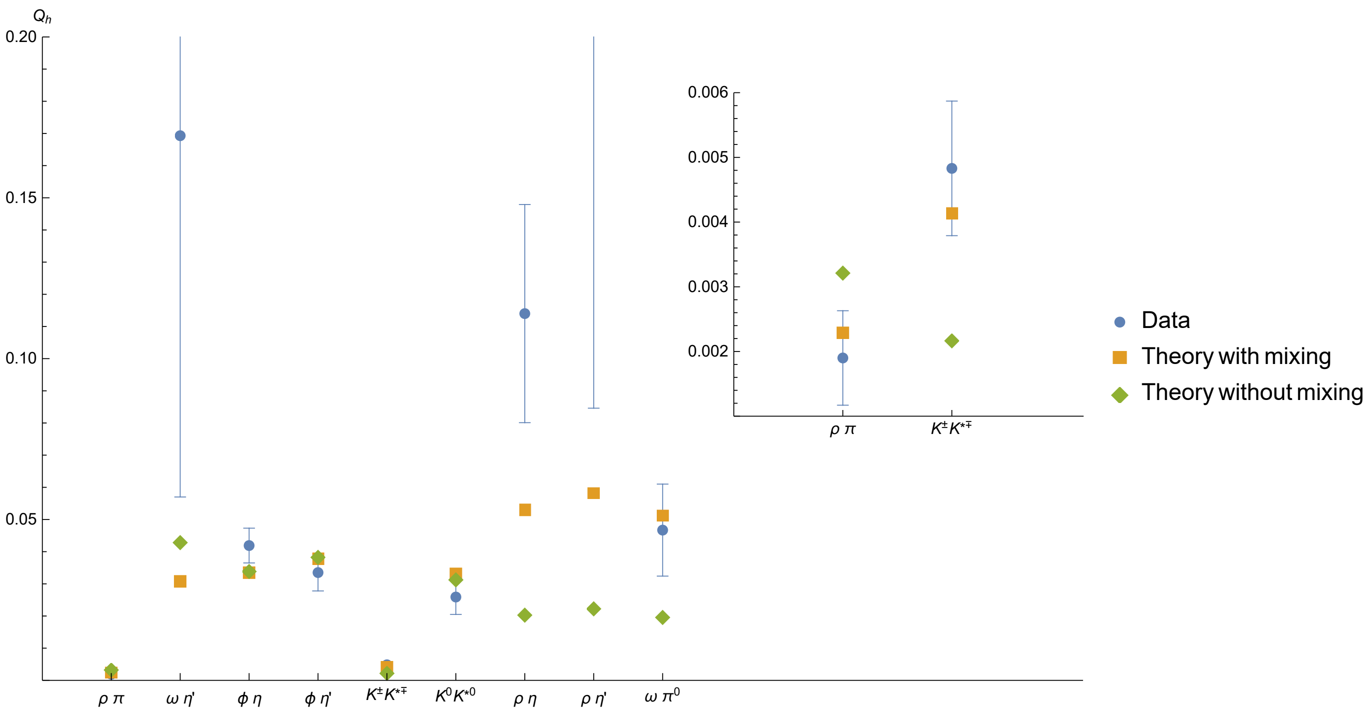

Figure 6.3: Results of the fits – with and without mixing with the vector glueball – for Q_h of the VP decays of charmonium states, together with the experimental data with uncertainties

6.4 Conclusions

In this chapter we studied the decays of charmonium states, in particular in relation to the 13% rule and its unexplained breaking, which is called the $\rho\pi$ puzzle. This puzzle has been an open problem for over 40 years, and its solution could have implications in important aspects of charmonium physics. We attempted to explain the $\rho\pi$ puzzle via mixing of the $\psi(3686)$ with the vector glueball. We have also introduced electromagnetic decay channels through a vector meson dominance model, since these decay channels are also expected to be relevant.

With three free parameters – the glueball coupling, the strong J/ψ coupling, and an energy scale – we manage to make a reasonable description of the experimental data on the Q_h ratio for the available VP channels. The fit shows that, aside from the electromagnetic interactions, including the vector glueball and its mixing with the $\psi(3686)$ significantly improves the matching with experimental data. At the level of this model, including the vector glueball mixing is necessary to satisfy the data. Even with electromagnetic interactions playing a big role, they are by itself not enough. At this point the fit slightly prefers mixing of the glueball with the $\psi(3686)$, but we cannot definitively conclude on way or the other. The analysis can still be expanded further; adding more decay channels, such as those where the 13% rule is not broken, is an obvious extension. One could also include higher order diagrams for the strong interaction, and a different coupling for mesons containing a strange quark as in [205]. Achieving a full description of the J/ψ and $\psi(3686)$ decays separately, rather than the ratio Q_h, would also be a large improvement. One particularly promising outcome of incorporating more decay channels and treating the ground state and excited charmonium decays separately is that it might be possible to find a constraint on the mixing angle. This, in turn, can give us an estimate on vector glueball decays, which can be used in an attempt to discover the vector glueball, or used to compare with experiment in a similar manner as done in Chapter 5.

Chapter 7

Conclusion

In this thesis we have studied the spectroscopy and the decays of mesons of various types in models based on effective Lagrangians, in particular the eLSM.
In chapter 2, we looked at a relatively simple model: a real scalar field coupled to a classical, time independent source. It turns out that there is more to this model than initially meets the eye, and the historical treatment of this model missed those aspects. Historically, the theory was approached as a limit of theories with a time-dependent source, which turns off after some time, where the time when the interaction is turned off is taken to infinity. The standard formalism of the S-matrix was then applied, which said it had to be zero, and no scattering takes place. The main issue, as we have found by solving the model exactly, is that the theory has a nonzero commutator between the Hamiltonian and momentum operator, so that the asymptotically free in- and out-states necessary for the S-matrix formalism do not exist. Whether or not the initial state is a particle number eigenstate or an energy state, which are distinct in the time independent case, can no longer be distinguished in the time dependent case. Which of the two one ends up with then depends on how the limit is taken. In short, the theory has no S-matrix. Hence, approaching the theory by other theories that do have an S-matrix fails. By solving the theory exactly we have computed the decay of the (particle) vacuum and its particle production over time, along with its large volume limits. The resulting behavior is analogous to the Schwinger mechanism, and includes non-exponential decay, saturation at large times, and an explicit realization of the quantum Zeno effect. This theory could potentially be a model for a nonperturbative creation mechanisms of the a scalar particle in the presence of a medium. For example the dilaton, which is seen as the scalar glueball, with a large amount within the $f_0(1710)$ according to the eLSM, which then decays into detectable particles like pions, kaons, etc.

Afterwards, we turned to the extended Linear Sigma Model (eLSM) as the primary theoretical tool to study the interactions of mesons. In Chapter 3 we have introduced the formalism of the eLSM, and in the subsequent chapters we applied this.
In Chapter 4 we extended the eLSM to include the tensor and axial tensor spin 2 mesons. The axial tensor mesons are poorly known at this point, while the tensor mesons are very well established. The match between theory and experiment on the tensor mesons confirms their status as quark-antiquark objects. Using chiral symmetry we use the tensor meson data to make predictions about the interactions of axial tensor mesons, as well as make some predictions for yet unknown decay channels of the tensor mesons. We predict the axial tensor meson masses, which lie around 300 to 400 MeV above the tensor meson masses, and their decays.

The decay widths of the axial tensor mesons turn out to be very large in some channels. This explains why they have not been successfully detected thus far, but also gives a specific direction in which to look for these states.
In Chapter 5 we have included the tensor glueball in the eLSM, and studied its decays. Numerical predictions for the decay widths cannot be made, but we can make estimates of the decay ratios. The dominant decay channel is the decay into two vector mesons, in particular two ρ mesons. By comparing the structure of the decay ratios to those of the plentiful candidate glueball resonances, we conclude that the $f_2(1950)$ is the best candidate to be the tensor glueball, despite its large decay width.
In Chapter 6 we applied the eLSM to the decay of charmonium states. There is a long-standing open problem with these states called the $\rho\pi$ puzzle, which has to do with large breaking of the 13% rule established by perturbative QCD. By incorporating electromagnetic decay channels and mixing with the vector glueball, we drastically improve agreement with experimental values on the ratio of branching ratios, which break the 13% rule. While it does not explain the puzzle entirely, it is clear that including electromagnetic decays is an important part of explaining the $\rho\pi$ puzzle. It also shows that mixing with the vector glueball is potentially a part of the explanation. More experimental data, which might falsify some of the explanations, and theoretical studies, that expand the model and data analysis, are necessary to achieve the full picture of this issue.

The results of this thesis could be interesting for ongoing experiments, such as CLAS, GlueX, and BESIII, and for future ones, such as those taking place at the FAIR facility [206]. The model of Chapter 2 can be used to model interactions of scalar mesons in the presence of a medium in heavy-ion collisions, and the structure of the theory, where we do not have an S-matrix, can teach us about the structure of quantum field theories. The results of Chapter 4 can aid in the discovery of the ground state axial tensor mesons. More experimental data on the isoscalar tensor meson resonances around 2 GeV can lead to a better understanding of the tensor glueball using the analysis of Chapter 5. In particular further studies on the $f_2(1950)$ could tell us more about its status as the potential tensor glueball. The result of Chapter 6 can have implications on the decay of charmonium states and the $\rho\pi$ puzzle, but also on the decays of the vector glueball, which so far has been elusive.

Appendices

Appendix A

The large N_c limit

In a sense the coupling constant of QCD is not really a free parameter, because it is given by the renormalization group flow and the scale of QCD Λ_{QCD}. At high energy scales it does become small so that an expansion in the coupling constant is useful, but it seems then that QCD has no free parameter to be used in an expansion at all energy levels. It turns out that there is a free expansion parameter not immediately obvious, which is the number of colors N_c of the gauge group $\mathrm{SU}(N_c)$. This generalizes the QCD gauge group SU(3) with 3 colors to $\mathrm{SU}(N_c)$. This N_c is then taken to infinity and an expansion in powers of $1/N_c$ follows [131, 132, 133]. In order to retain interesting aspects of the theory, such as keeping the 1-loop contribution to the gluon vacuum polarization finite, a factor of $\sqrt{N_c}$ needs to be included in the coupling constant. This is done by taking the limit in the particular way

$$N_c \to \infty, \qquad \lambda = g^2 N_c \text{ fixed.} \tag{A.1}$$

Here λ is called the 't Hooft coupling, λ being fixed implies that $g \to 0$ in the large N_c limit, but the interactions do not vanish since λ controls the strength of the interaction of the large N_c theory. Due to the combinatorial factors of N_c, the leading order Feynman diagrams are planar diagrams, in which propagators do not cross each other, unless there is an interaction vertex. There are many interesting aspects of large N_c theories, but we will restrict us to the properties of hadrons and as an estimation of which terms are most relevant. The large N_c scaling of relevant hadronic properties goes as follows

- The masses of quark-antiquark states and the masses of glueballs are independent of N_c in the limit of $N_c \to \infty$

$$M_{|q\bar{q}\rangle} \sim N_c^0 \qquad M_{|gg\rangle} \sim N_c^0 \tag{A.2}$$

- The interaction amplitude between n quark-antiquark states scales as

$$A_{|q\bar{q}\rangle\ldots|q\bar{q}\rangle} \sim N_c^{\frac{-(n-2)}{2}}, \tag{A.3}$$

  for $n \geq 2$. In particular, decays are the case $n = 3$, meaning that conventional mesons have a decay width scaling as

$$\Gamma_{|\bar{q}q\rangle} \sim N_c^{-1}, \tag{A.4}$$

so that conventional mesons are very stable in the large N_c limit. Furthermore, mass terms are the case $n = 2$, so the quark-antiquark masses are constant in the large N_c limit.

- The interaction amplitude between n glueball states each consisting of 2 gluons scales as

$$A_{|gg\rangle\ldots|gg\rangle} \sim N_c^{-(n-2)}, \tag{A.5}$$

  which is more strongly suppressed than the interaction amplitude between quarkonia. In particular, two glueball fields $n = 2$ gives a mass term, so glueball masses, like quark-antiquark masses do not depend on N_c.

- The interaction amplitude between n glueballs and m quark-antiquark states scales as

$$A_{(|gg\rangle\ldots|gg\rangle)(|q\bar{q}\ldots q\bar{q}\rangle)} \sim N_c^{-(n+m/2-1)}. \tag{A.6}$$

  Therefore the mixing ($n = 1, m = 1$) of glueballs with quark-antiquark states goes as $N_c^{-1/2}$, and the decay amplitude of glueballs ($n = 1, m \geq 2$) is suppressed by at least a factor of N_c^{-1}, making them more stable than quark-antiquark states in the large N_c limit.

- Baryons, which are made up of N_c quarks, have a mass that scales as

$$M_B \sim N_c. \tag{A.7}$$

For more details on the large N_c limit in the context of hadron physics, see the lecures of [133].

Appendix B

Coherent states

Coherent states are defined as eigenstates of the annihilation operators. For a single annihilation operator a the coherent state $|c\rangle$ then obeys

$$a|c\rangle = c|c\rangle. \tag{B.1}$$

The annihilation operator fulfills the following commutation relationship and action on the n particle states:

$$[a, a^\dagger] = 1, \quad \Rightarrow \quad a|n\rangle = n|n-1\rangle. \tag{B.2}$$

Using this, we can construct a coherent state with the following formal series

$$|0\rangle + \sum_{n=1}^{\infty} \frac{c^n}{\sqrt{n!}}|n\rangle = \left[\sum_{n=0}^{\infty} \frac{\left(c\, a^\dagger\right)^n}{n!}\right]|0\rangle = e^{c\, a^\dagger}|0\rangle, \qquad \Rightarrow \qquad a\left(e^{c\, a^\dagger}|0\rangle\right) = c\left(e^{c\, a^\dagger}|0\rangle\right). \tag{B.3}$$

This is an eigenvector a with with eigenvalue c, which is an arbitrary complex number. In order to be an eigenstate it must be normalized to 1. This can be done straightforwardly using (B.3)

$$\left|e^{c\, a^\dagger}|0\rangle\right|^2 = \left(\langle 0|e^{c^*\, a}\right)\left(e^{c\, a^\dagger}|0\rangle\right) = \langle 0|\left[\sum_{n=0}^{\infty} \frac{\left(c^*\, a\right)^n}{n!}\right]\left(e^{c\, a^\dagger}|0\rangle\right) = \langle 0|0\rangle \sum_{n=0}^{\infty} \frac{\left|\, c\, \right|^{2n}}{n!} = e^{\left|\, c\, \right|^2}. \tag{B.4}$$

Therefore the physical coherent state is given by

$$|c\rangle = e^{-\frac{1}{2}|c|^2}\, e^{c\, a^\dagger}|0\rangle. \tag{B.5}$$

The generalization to the situation with an uncharged scalar field is rather straightforward. We just have to take into account that there are multiple creation and annihilation operators, one for each 3-momentum $\mathbf{p}$, which each have a different eigenvalue, and that the commutation relation is normalized to a distribution rather than the identity. That is, the setup is

$$a_{\mathbf{p}}|\psi\rangle = -h(\mathbf{p})|\psi\rangle, \qquad\qquad [a_{\mathbf{p}}, a^\dagger_{\mathbf{q}}] = (2\pi^3)\delta(\mathbf{p}-\mathbf{q}). \tag{B.6}$$

Furthermore, the action of the annihilation operator is accompanied with a momentum integral instead of a straight multiplication of the creation operators times the eigenvalue

$$\int \frac{d^3p}{(2\pi)^3} \Big(- h(\mathbf{p}) \Big) \; a^\dagger_{\mathbf{p}}. \tag{B.7}$$

The same idea of (B.3) can then be used to find an eigenstate for each $a_{\mathbf{p}}$ with the eigenvalue $-h(\mathbf{p})$:

$$\begin{aligned} &|0\rangle + \left[\sum_{n=1}^{\infty} \frac{1}{n!} \int \frac{d^2p_1 d^3p_2 \cdots d^3p_n}{(2\pi)^{3n}} \Big(- h(\mathbf{p}_1) a^\dagger_{\mathbf{p}_1} \Big) \Big(- h(\mathbf{p}_2) a^\dagger_{\mathbf{p}_2} \Big) \cdots \Big(- h(\mathbf{p}_n) a^\dagger_{\mathbf{p}_n} \Big) \right] |0\rangle = \\ &= \left[\sum_{n=0}^{\infty} \frac{1}{n!} \left(- \int \frac{d^3p}{(2\pi)^3} \, h(\mathbf{p}) \, a^\dagger_{\mathbf{p}} \right)^n \right] |0\rangle = \exp\left\{ - \int \frac{d^3p}{(2\pi)^3} \, h(\mathbf{p}) \, a^\dagger_{\mathbf{p}} \right\} |0\rangle \end{aligned} \tag{B.8}$$

$$\Rightarrow \qquad a_{\mathbf{p}} \exp\left\{ - \int \frac{d^3p}{(2\pi)^3} \, h(\mathbf{p}) \, a^\dagger_{\mathbf{p}} \right\} |0\rangle = -h(\mathbf{p}) \exp\left\{ - \int \frac{d^3p}{(2\pi)^3} \, h(\mathbf{p}) \, a^\dagger_{\mathbf{p}} \right\} |0\rangle.$$

The normalization of the state follows in a very similar way as in the discrete case, again by using the commutation relation of a. The result for the coherent state, which aligns with the relation between the different vacua in 2 reads:

$$\begin{aligned} &|\psi\rangle \quad \text{s.t.} \quad a_{\mathbf{p}} |\psi\rangle = -h(\mathbf{p}) |\psi\rangle, \\ \Rightarrow \quad &|\psi\rangle = \exp\left\{ -\frac{1}{2} \int \frac{d^3p}{(2\pi)^3} \, |h(\mathbf{p})|^2 \right\} \exp\left\{ - \int \frac{d^3p}{(2\pi)^3} \, h(\mathbf{p}) \, a^\dagger_{\mathbf{p}} \right\} |0\rangle. \end{aligned} \tag{B.9}$$

Bibliography

[1] A. K. Cyrol, L. Fister, M. Mitter, J. M. Pawlowski, and N. Strodthoff, "Landau gauge Yang-Mills correlation functions," *Phys. Rev. D* **94** no. 5, (2016) 054005, arXiv:1605.01856 [hep-ph].

[2] **Particle Data Group** Collaboration, S. Navas *et al.*, "Review of particle physics," *Phys. Rev. D* **110** no. 3, (2024) 030001.

[3] **Hadron Spectrum** Collaboration, C. T. Johnson and J. J. Dudek, "Excited J^{--} meson resonances at the SU(3) flavor point from lattice QCD," *Phys. Rev. D* **103** no. 7, (2021) 074502, arXiv:2012.00518 [hep-lat].

[4] M. Gell-Mann, "Symmetries of baryons and mesons," *Phys. Rev.* **125** (1962) 1067–1084.

[5] A. A. Migdal and M. A. Shifman, "Dilaton Effective Lagrangian in Gluodynamics," *Phys. Lett. B* **114** (1982) 445–449.

[6] P. A. Baikov, K. G. Chetyrkin, and J. H. Kühn, "Five-Loop Running of the QCD Coupling Constant," *Phys. Rev. Lett.* **118** no. 8, (2017) 082002, arXiv:1606.08659 [hep-ph].

[7] F. Herzog, B. Ruijl, T. Ueda, J. A. M. Vermaseren, and A. Vogt, "The five-loop beta function of Yang-Mills theory with fermions," *JHEP* **02** (2017) 090, arXiv:1701.01404 [hep-ph].

[8] N. Dupuis, L. Canet, A. Eichhorn, W. Metzner, J. M. Pawlowski, M. Tissier, and N. Wschebor, "The nonperturbative functional renormalization group and its applications," *Phys. Rept.* **910** (2021) 1–114, arXiv:2006.04853 [cond-mat.stat-mech].

[9] A. Deur, S. J. Brodsky, and G. F. de Teramond, "The QCD Running Coupling," *Nucl. Phys.* **90** (2016) 1, arXiv:1604.08082 [hep-ph].

[10] M. Shifman, "Anomalies in gauge theories," *Physics Reports* **209** no. 6, (1991) 341–378.

[11] M. Dine, "TASI lectures on the strong CP problem," in *Theoretical Advanced Study Institute in Elementary Particle Physics (TASI 2000): Flavor Physics for the Millennium*, pp. 349–369. 6, 2000. arXiv:hep-ph/0011376.

[12] G. 't Hooft, "How instantons solve the $U(1)$ problem," *Phys. Rept.* **142** no. 6, (9, 1986) 357–387.

[13] L. Tinti, A. Vereijken, S. Jafarzade, and F. Giacosa, "Scalar field with a time-independent classical source is not trivial after all: From vacuum decay to scattering," *Phys. Rev. D* **110** no. 11, (2024) 116004, arXiv:2403.15531 [hep-th].

[14] S. Jafarzade, A. Vereijken, M. Piotrowska, and F. Giacosa, "From well-known tensor mesons to yet unknown axial-tensor mesons," *Phys. Rev. D* **106** no. 3, (2022) 036008, `arXiv:2203.16585 [hep-ph]`.

[15] A. Vereijken, S. Jafarzade, M. Piotrowska, and F. Giacosa, "Is f2(1950) the tensor glueball?," *Phys. Rev. D* **108** no. 1, (2023) 014023, `arXiv:2304.05225 [hep-ph]`.

[16] A. Vereijken, "Tensor glueball decay into nucleon-antinucleon," *Nuovo Cim. C* **47** no. 4, (2024) 188, `arXiv:2310.10273 [hep-ph]`.

[17] A. Vereijken, "Decays of the tensor glueball in a chiral approach," *EPJ Web Conf.* **291** (2024) 02005, `arXiv:2310.09608 [hep-ph]`.

[18] A. Vereijken, "The rho-pi puzzle and vector glueball mixing," in *8th FAIR next generation scientists workshop 2024*. 2, 2025. `arXiv:2502.21042 [hep-ph]`.

[19] M. E. Peskin and D. V. Schroeder, *An Introduction to quantum field theory*. Addison-Wesley, Reading, USA, 1995.

[20] S. Coleman, *Lectures of Sidney Coleman on Quantum Field Theory*. WSP, Hackensack, 12, 2018.

[21] G. Wentzel, *Quantum theory of fields*. Interscience, New York, 1949.

[22] R. Ticciati, *Quantum field theory for mathematicians*. 1999.

[23] S. R. Coleman, "The Fate of the False Vacuum. 1. Semiclassical Theory," *Phys. Rev. D* **15** (1977) 2929–2936. [Erratum: Phys.Rev.D 16, 1248 (1977)].

[24] F. S. Accetta and P. Romanelli, "SCALAR - TENSOR GRAVITATIONAL EFFECTS ON VACUUM DECAY," *Phys. Rev. D* **41** (1990) 3024.

[25] D. A. Samuel and W. A. Hiscock, "'Thin wall' approximations to vacuum decay rates," *Phys. Lett. B* **261** (1991) 251–256.

[26] T. Hamazaki, M. Sasaki, T. Tanaka, and K. Yamamoto, "Selfexcitation of the tunneling scalar field in false vacuum decay," *Phys. Rev. D* **53** (1996) 2045–2061, `arXiv:gr-qc/9507006`.

[27] M. A. Bezuglov and A. I. Onishchenko, "Two-loop corrections to false vacuum decay in scalar field theory," *Phys. Lett. B* **788** (2019) 122–130, `arXiv:1805.06482 [hep-ph]`.

[28] A. Ivanov, M. Matteini, M. Nemevšek, and L. Ubaldi, "Analytic thin wall false vacuum decay rate," *JHEP* **03** (2022) 209, `arXiv:2202.04498 [hep-th]`. [Erratum: JHEP 07, 085 (2022), Erratum: JHEP 11, 157 (2022)].

[29] A. R. Brown, "Thin-wall approximation in vacuum decay: A lemma," *Phys. Rev. D* **97** no. 10, (2018) 105002, `arXiv:1711.07712 [hep-th]`.

[30] W.-Y. Ai and M. Drewes, "Schwinger effect and false vacuum decay as quantum-mechanical tunneling of a relativistic particle," *Phys. Rev. D* **102** no. 7, (2020) 076015, `arXiv:2005.14163 [hep-th]`.

[31] O. Fialko, B. Opanchuk, A. I. Sidorov, P. D. Drummond, and J. Brand, "Fate of the false vacuum: towards realization with ultra-cold atoms," *EPL* **110** no. 5, (2015) 56001, `arXiv:1408.1163 [cond-mat.quant-gas]`.

[32] O. Fialko, B. Opanchuk, A. I. Sidorov, P. D. Drummond, and J. Brand, "The universe on a table top: engineering quantum decay of a relativistic scalar field from a metastable vacuum," *J. Phys. B* **50** no. 2, (2017) 024003, `arXiv:1607.01460 [cond-mat.quant-gas]`.

[33] G. Isidori, G. Ridolfi, and A. Strumia, "On the metastability of the standard model vacuum," *Nuclear Physics B* **609** no. 3, (2001) 387–409. `https://www.sciencedirect.com/science/article/pii/S0550321301003029`.

[34] D. Buttazzo, G. Degrassi, P. P. Giardino, G. F. Giudice, F. Sala, A. Salvio, and A. Strumia, "Investigating the near-criticality of the Higgs boson," *JHEP* **12** (2013) 089, `arXiv:1307.3536 [hep-ph]`.

[35] F. Devoto, S. Devoto, L. Di Luzio, and G. Ridolfi, "False vacuum decay: an introductory review," *J. Phys. G* **49** no. 10, (2022) 103001, `arXiv:2205.03140 [hep-ph]`.

[36] A. Andreassen, W. Frost, and M. D. Schwartz, "Scale Invariant Instantons and the Complete Lifetime of the Standard Model," *Phys. Rev. D* **97** no. 5, (2018) 056006, `arXiv:1707.08124 [hep-ph]`.

[37] V. F. Guada Escalona, *False Vacuum Decay with Multiple Scalar Fields*. PhD thesis, Ljubljana U., 2021.

[38] A. Salvio, A. Strumia, N. Tetradis, and A. Urbano, "On gravitational and thermal corrections to vacuum decay," *JHEP* **09** (2016) 054, `arXiv:1608.02555 [hep-ph]`.

[39] A. Khvedelidze, G. V. Lavrelashvili, and T. Tanaka, "On cosmological perturbations in closed FRW model with scalar field and false vacuum decay," *Phys. Rev. D* **62** (2000) 083501, `arXiv:gr-qc/0001041`.

[40] J. S. Heyl and A. Loeb, "Vacuum decay constraints on a cosmological scalar field," *Phys. Rev. Lett.* **88** (2002) 121302, `arXiv:astro-ph/0111570`.

[41] A. Higuchi, "Decay of the free-theory vacuum of scalar field theory in de Sitter spacetime in the interaction picture," *Class. Quant. Grav.* **26** (2009) 072001, `arXiv:0809.1255 [gr-qc]`.

[42] S. V. Akkelin, "Quasi equilibrium state of expanding quantum fields and two-pion Bose-Einstein correlations in *pp* collisions at the LHC," *Eur. Phys. J. A* **55** no. 5, (2019) 78, `arXiv:1812.03905 [hep-ph]`.

[43] D. Rindori, L. Tinti, F. Becattini, and D. H. Rischke, "Relativistic quantum fluid with boost invariance," *Phys. Rev. D* **105** no. 5, (2022) 056003, `arXiv:2102.09016 [hep-th]`.

[44] F. Becattini and D. Roselli, "Quantum field corrections to the equation of state of freely streaming matter in the Friedman–Lemaître–Robertson–Walker space-time," *Class. Quant. Grav.* **40** no. 17, (2023) 175007, `arXiv:2212.05518 [gr-qc]`.

[45] F. Becattini and D. Roselli, "Negative pressure as a quantum effect in free-streaming in the cosmological background." 2024.

[46] S. V. Akkelin, "Cosmological particle creation in the little bang," *Phys. Rev. D* **103** no. 11, (2021) 116014, `arXiv:2008.13606 [hep-ph]`.

[47] J. S. Schwinger, "On gauge invariance and vacuum polarization," *Phys. Rev.* **82** (1951) 664–679.

[48] W. Greiner, "Quantum electrodynamics of strong fields," *Lect. Notes Phys.* **231** (1985) 95–226.

[49] F. Gelis and N. Tanji, "Schwinger mechanism revisited," *Prog. Part. Nucl. Phys.* **87** (2016) 1–49, `arXiv:1510.05451 [hep-ph]`.

[50] B. Misra and E. C. G. Sudarshan, "The Zeno's Paradox in Quantum Theory," *J. Math. Phys.* **18** (1977) 756.

[51] L. Fonda, G. C. Ghirardi, and A. Rimini, "Decay Theory of Unstable Quantum Systems," *Rept. Prog. Phys.* **41** (1978) 587–631.

[52] W. M. Itano, D. J. Heinzen, J. J. Bollinger, and D. J. Wineland, "Quantum Zeno effect," *Phys. Rev. A* **41** (1990) 2295–2300.

[53] K. Koshino and A. Shimizu, "Quantum Zeno effect by general measurements," *Phys. Rept.* **412** (2005) 191–275, `arXiv:quant-ph/0411145`.

[54] F. Giacosa, "Non-exponential decay in quantum field theory and in quantum mechanics: the case of two (or more) decay channels," *Found. Phys.* **42** (2012) 1262–1299, `arXiv:1110.5923 [nucl-th]`.

[55] S. Haroche, "Controlling photons in a box and exploring the quantum to classical boundary," *Int. J. Mod. Phys. A* **29** (2014) 1430026.

[56] J. Bernu, S. Deléglise, C. Sayrin, S. Kuhr, I. Dotsenko, M. Brune, J. M. Raimond, and S. Haroche, "Freezing Coherent Field Growth in a Cavity by the Quantum Zeno Effect," *Phys. Rev. Lett.* **101** no. 18, (Oct., 2008) 180402, `arXiv:0809.4388 [quant-ph]`.

[57] H. Nikolić, "Suppressing Hawking radiation by quantum Zeno effect," *Phys. Lett. B* **733** (2014) 6–10, `arXiv:1311.4363 [hep-th]`.

[58] P. Facchi, H. Nakazato, and S. Pascazio, "From the quantum zeno to the inverse quantum zeno effect," *Phys. Rev. Lett.* **86** (Mar, 2001) 2699–2703. `https://link.aps.org/doi/10.1103/PhysRevLett.86.2699`.

[59] M. C. Fischer, B. Gutiérrez-Medina, and M. G. Raizen, "Observation of the quantum zeno and anti-zeno effects in an unstable system," *Phys. Rev. Lett.* **87** (Jul, 2001) 040402. `https://link.aps.org/doi/10.1103/PhysRevLett.87.040402`.

[60] J. J. Sakurai and J. Napolitano, *Modern Quantum Mechanics*. Quantum physics, quantum information and quantum computation. Cambridge University Press, 10, 2020.

[61] M. Blasone, A. Capolupo, O. Romei, and G. Vitiello, "Quantum field theory of boson mixing," *Phys. Rev. D* **63** (2001) 125015, `arXiv:hep-ph/0102048`.

[62] M. Blasone, F. Giacosa, L. Smaldone, and G. Torrieri, "Neutrino oscillations in the interaction picture," *Eur. Phys. J. C* **83** no. 8, (2023) 736, `arXiv:2305.07107 [hep-ph]`.

[63] L. Smaldone and G. Vitiello, "Neutrino Mixing and Oscillations in Quantum Field Theory: A Comprehensive Introduction," *Universe* **7** no. 12, (2021) 504, arXiv:2111.11809 [hep-th].

[64] P. Bicudo, F. Giacosa, and E. Seel, "Computation of Pion and Kaon Heavy Ion Multiplicities in a Gluon-Meson Model," *Phys. Rev. C* **86** (2012) 034907, arXiv:1202.1640 [hep-ph].

[65] A. Schmitt *et al.*, "Mesoscopic Klein-Schwinger effect in graphene," *Nature Phys.* **19** no. 6, (2023) 830–835, arXiv:2207.13400 [cond-mat.mes-hall].

[66] P. Romatschke, "Quantum Field Theory in Large-N Wonderland: Three Lectures," *Acta Phys. Polon. B* **55** no. 4, (2024) 4–A2, arXiv:2310.00048 [hep-th].

[67] F. Giacosa, "Mesons beyond the quark-antiquark picture," *Acta Phys. Polon. B* **47** (2016) 7, arXiv:1511.04605 [hep-ph].

[68] F. Giacosa, P. Kovács, and S. Jafarzade, "Ordinary and exotic mesons in the extended Linear Sigma Model," *Prog. Part. Nucl. Phys.* **143** (2025) 104176, arXiv:2407.18348 [hep-ph].

[69] M. Gell-Mann and M. M. Levy, "The axial vector current in beta decay," *Nuovo Cim.* **16** no. 3, (5, 1960) 705–726.

[70] J. R. Ellis and J. Lanik, "IS SCALAR GLUONIUM OBSERVABLE?," *Phys. Lett. B* **150** (1985) 289–294.

[71] R. Gomm, P. Jain, R. Johnson, and J. Schechter, "Scale Anomaly and the Scalars," *Phys. Rev. D* **33** (1986) 801.

[72] C. J. Morningstar and M. J. Peardon, "The glueball spectrum from an anisotropic lattice study," *Phys. Rev. D* **60** (1999) 034509, arXiv:hep-lat/9901004.

[73] Y. Chen *et al.*, "Glueball spectrum and matrix elements on anisotropic lattices," *Phys. Rev. D* **73** (1, 2006) 014516, arXiv:hep-lat/0510074.

[74] A. Athenodorou and M. Teper, "The glueball spectrum of SU(3) gauge theory in $3 + 1$ dimensions," *JHEP* **11** (2020) 172, arXiv:2007.06422 [hep-lat].

[75] M. Q. Huber, C. S. Fischer, and H. Sanchis-Alepuz, "Higher spin glueballs from functional methods," *Eur. Phys. J. C* **81** no. 12, (2021) 1083, arXiv:2110.09180 [hep-ph].

[76] S. Narison, "Masses, decays and mixings of gluonia in QCD," *Nucl. Phys. B* **509** (1998) 312–356, arXiv:hep-ph/9612457.

[77] F. Brünner, D. Parganlija, and A. Rebhan, "Glueball Decay Rates in the Witten-Sakai-Sugimoto Model," *Phys. Rev. D* **91** no. 10, (2015) 106002, arXiv:1501.07906 [hep-ph]. [Erratum: Phys.Rev.D 93, 109903 (2016)].

[78] F. Brünner and A. Rebhan, "Nonchiral enhancement of scalar glueball decay in the Witten-Sakai-Sugimoto model," *Phys. Rev. Lett.* **115** no. 13, (2015) 131601, arXiv:1504.05815 [hep-ph].

[79] S. Janowski, F. Giacosa, and D. H. Rischke, "Is $f_0(1710)$ a glueball?," *Phys. Rev. D* **90** no. 11, (12, 2014) 114005, arXiv:1408.4921 [hep-ph].

[80] **BESIII** Collaboration, M. Ablikim *et al.*, "Observation of an a0-like State with Mass of 1.817 GeV in the Study of Ds+→KS0K+π0 Decays," *Phys. Rev. Lett.* **129** no. 18, (2022) 182001, `arXiv:2204.09614 [hep-ex]`.

[81] D. Guo, W. Chen, H.-X. Chen, X. Liu, and S.-L. Zhu, "Newly observed a0(1817) as the scaling point of constructing the scalar meson spectroscopy," *Phys. Rev. D* **105** no. 11, (2022) 114014, `arXiv:2204.13092 [hep-ph]`.

[82] E. Oset, L.-R. Dai, and L.-S. Geng, "Repercussion of the a0(1710) [a0(1817)] resonance and future developments," *Sci. Bull.* **68** (2023) 243–246, `arXiv:2301.08532 [hep-ph]`.

[83] A. Di Giacomo, H. G. Dosch, V. I. Shevchenko, and Y. A. Simonov, "Field correlators in QCD: Theory and applications," *Phys. Rept.* **372** (2002) 319–368, `arXiv:hep-ph/0007223`.

[84] B. L. Ioffe, "QCD at low energies," *Prog. Part. Nucl. Phys.* **56** (2006) 232–277, `arXiv:hep-ph/0502148`.

[85] S. Narison, "Mini-review on QCD spectral sum rules," *Nucl. Part. Phys. Proc.* **258-259** (2015) 189–194, `arXiv:1409.8148 [hep-ph]`.

[86] F. Giacosa, A. Koenigstein, and R. D. Pisarski, "How the axial anomaly controls flavor mixing among mesons," *Phys. Rev. D* **97** no. 9, (5, 2018) 091901, `arXiv:1709.07454 [hep-ph]`.

[87] F. Giacosa, S. Jafarzade, and R. D. Pisarski, "Anomalous interactions between mesons with nonzero spin and glueballs," *Phys. Rev. D* **109** no. 7, (2024) L071502, `arXiv:2309.00086 [hep-ph]`.

[88] J. R. Pelaez, "From controversy to precision on the sigma meson: a review on the status of the non-ordinary $f_0(500)$ resonance," *Phys. Rept.* **658** (2016) 1, `arXiv:1510.00653 [hep-ph]`.

[89] G. Amelino-Camelia *et al.*, "Physics with the KLOE-2 experiment at the upgraded DAϕNE," *Eur. Phys. J. C* **68** (2010) 619–681, `arXiv:1003.3868 [hep-ex]`.

[90] T. Feldmann, P. Kroll, and B. Stech, "Mixing and decay constants of pseudoscalar mesons," *Phys. Rev. D* **58** (1998) 114006, `arXiv:hep-ph/9802409`.

[91] F. J. Llanes-Estrada, "Glueballs as the Ithaca of meson spectroscopy: From simple theory to challenging detection," *Eur. Phys. J. ST* **230** no. 6, (2021) 1575–1592, `arXiv:2101.05366 [hep-ph]`.

[92] H.-Y. Cheng, C.-K. Chua, and K.-F. Liu, "Scalar glueball, scalar quarkonia, and their mixing," *Phys. Rev. D* **74** (11, 2006) 094005, `arXiv:hep-ph/0607206`.

[93] F. Giacosa, T. Gutsche, V. E. Lyubovitskij, and A. Faessler, "Scalar nonet quarkonia and the scalar glueball: Mixing and decays in an effective chiral approach," *Phys. Rev. D* **72** (11, 2005) 094006, `arXiv:hep-ph/0509247`.

[94] C. Amsler and F. E. Close, "Is $f_0(1500)$ a scalar glueball?," *Phys. Rev. D* **53** (1, 1996) 295–311, `arXiv:hep-ph/9507326`.

[95] C. Amsler and F. E. Close, "Evidence for a scalar glueball," *Phys. Lett. B* **353** no. 2–3, (6, 1995) 385–390, `arXiv:hep-ph/9505219`.

[96] F. Divotgey, L. Olbrich, and F. Giacosa, "Phenomenology of axial-vector and pseudovector mesons: decays and mixing in the kaonic sector," *Eur. Phys. J. A* **49** (10, 2013) 135, arXiv:1306.1193 [hep-ph].

[97] H. Hatanaka and K.-C. Yang, "$K_1(1270) - K_1(1400)$ mixing angle and new-physics effects in $B \to K_1 l^+ l^-$ decays," *Phys. Rev. D* **78** (10, 2008) 074007, arXiv:0808.3731 [hep-ph].

[98] F. Giacosa, J. Sammet, and S. Janowski, "Decays of the vector glueball," *Phys. Rev. D* **95** no. 11, (6, 2017) 114004, arXiv:1607.03640 [hep-ph].

[99] W. I. Eshraim, C. S. Fischer, F. Giacosa, and D. Parganlija, "Hybrid phenomenology in a chiral approach," *Eur. Phys. J. Plus* **135** no. 12, (12, 2020) 945, arXiv:2001.06106 [hep-ph].

[100] S. Godfrey and N. Isgur, "Mesons in a relativized quark model with chromodynamics," *Phys. Rev. D* **32** (Jul, 1985) 189–231.

[101] F. Giacosa, T. Gutsche, V. E. Lyubovitskij, and A. Faessler, "Decays of tensor mesons and the tensor glueball in an effective field approach," *Phys. Rev. D* **72** (12, 2005) 114021, arXiv:hep-ph/0511171.

[102] L. Burakovsky and T. J. Goldman, "Regarding the enigmas of P-wave meson spectroscopy," *Phys. Rev. D* **57** (3, 1998) 2879–2888, arXiv:hep-ph/9703271.

[103] D. Guo, C.-Q. Pang, Z.-W. Liu, and X. Liu, "Study of unflavored light mesons with $J^{PC} = 2^{--}$," *Phys. Rev. D* **99** no. 5, (2019) 056001, arXiv:1901.03518 [hep-ph].

[104] L. M. Abreu, F. M. da Costa Júnior, and A. G. Favero, "Revisiting the tensor $J^{PC} = 2^{--}$ meson spectrum," *Phys. Rev. D* **101** no. 11, (2020) 116016, arXiv:2004.10736 [hep-ph].

[105] A. Türkan, H. Dağ, J. Y. Süngü, and E. V. Veliev, "Hot medium effects on pseudotensor $\mathrm{K}_2(1820)$ meson," *EPJ Web Conf.* **199** (2019) 03007.

[106] J. Y. Süngü, A. Türkan, E. Sertbakan, and E. V. Veliev, "Axial-tensor Meson family at $T \neq 0$," *Eur. Phys. J. C* **80** no. 10, (2020) 943, arXiv:2005.11526 [hep-ph].

[107] D. Parganlija, P. Kovacs, G. Wolf, F. Giacosa, and D. H. Rischke, "Meson vacuum phenomenology in a three-flavor linear sigma model with (axial-)vector mesons," *Phys. Rev. D* **87** no. 1, (1, 2013) 014011, arXiv:1208.0585 [hep-ph].

[108] D. Parganlija and F. Giacosa, "Excited Scalar and Pseudoscalar Mesons in the Extended Linear Sigma Model," *Eur. Phys. J. C* **77** no. 7, (2017) 450, arXiv:1612.09218 [hep-ph].

[109] C. S. Fischer, S. Kubrak, and R. Williams, "Mass spectra and Regge trajectories of light mesons in the Bethe-Salpeter approach," *Eur. Phys. J. A* **50** (2014) 126, arXiv:1406.4370 [hep-ph].

[110] A. V. Sarantsev, I. Denisenko, U. Thoma, and E. Klempt, "Scalar isoscalar mesons and the scalar glueball from radiative J/ψ decays," *Phys. Lett. B* **816** (2021) 136227, arXiv:2103.09680 [hep-ph].

[111] **Joint Physics Analysis Center** Collaboration, A. Rodas, A. Pilloni, M. Albaladejo, C. Fernandez-Ramirez, V. Mathieu, and A. P. Szczepaniak, "Scalar and tensor resonances in J/ψ radiative decays," *Eur. Phys. J. C* **82** no. 1, (2022) 80, arXiv:2110.00027 [hep-ph].

[112] D. Binosi, A. Pilloni, and R.-A. Tripolt, "Study for a model-independent pole determination of overlapping resonances," *Phys. Lett. B* **839** (2023) 137809, `arXiv:2205.02690 [hep-ph]`.

[113] E. Klempt, K. V. Nikonov, A. V. Sarantsev, and I. Denisenko, "Search for the tensor glueball," *Phys. Lett. B* **830** (2022) 137171, `arXiv:2205.07239 [hep-ph]`.

[114] E. Klempt, "Scalar mesons and the fragmented glueball," *Phys. Lett. B* **820** (2021) 136512, `arXiv:2104.09922 [hep-ph]`.

[115] E. Klempt and A. V. Sarantsev, "Singlet-octet-glueball mixing of scalar mesons," *Phys. Lett. B* **826** (2022) 136906, `arXiv:2112.04348 [hep-ph]`.

[116] M. Piotrowska, C. Reisinger, and F. Giacosa, "Strong and radiative decays of excited vector mesons and predictions for a new $\phi(1930)$ resonance," *Phys. Rev. D* **96** no. 5, (9, 2017) 054033, `arXiv:1708.02593 [hep-ph]`.

[117] A. Koenigstein and F. Giacosa, "Phenomenology of pseudotensor mesons and the pseudotensor glueball," *Eur. Phys. J. A* **52** no. 12, (12, 2016) 356, `arXiv:1608.08777 [hep-ph]`.

[118] V. Shastry, E. Trotti, and F. Giacosa, "Constraints imposed by the partial wave amplitudes on the decays of J=1, 2 mesons," *Phys. Rev. D* **105** no. 5, (2022) 054022, `arXiv:2107.13501 [hep-ph]`.

[119] J. R. Pelaez, "Light Meson Resonances," `arXiv:2509.08648 [hep-ph]`.

[120] G. Mezzadri, "Light hadron spectroscopy at BESIII," *PoS* **234** (3, 2015) 423. The European Physical Society Conference on High Energy Physics (EPS-HEP2015).

[121] **BESIII** Collaboration, S. Marcello, "Hadron Physics from BESIII," *JPS Conf. Proc.* **10** (2016) 010009. Proceedings of the 10th International Workshop on the Physics of Excited Nucleons (NSTAR2015).

[122] **CLAS** Collaboration, A. Rizzo, "The meson spectroscopy program with CLAS12 at Jefferson Laboratory," *PoS* **253** (2, 2016) 8. The 8th International Workshop on Chiral Dynamics.

[123] **CLAS** Collaboration, M. Carver *et al.*, "Photoproduction of the $f_2(1270)$ meson using the CLAS detector," *Phys. Rev. Lett.* **126** no. 8, (2021) 082002, `arXiv:2010.16006 [nucl-ex]`.

[124] **VES group, COMPASS** Collaboration, D. Ryabchikov, "Meson spectroscopy at VES and COMPASS," *EPJ Web Conf.* **212** (6, 2019) 03010. The 12th International Workshop on $e^+ e^-$ Collisions from Phi to Psi (PhiPsi 2019).

[125] **GlueX** Collaboration, H. Al Ghoul *et al.*, "First results from the GlueX experiment," *AIP Conf. Proc.* **1735** no. 1, (5, 2016) 020001, `arXiv:1512.03699 [nucl-ex]`.

[126] **GlueX** Collaboration, B. Zihlmann, "GlueX a new facility to search for gluonic degrees of freedom in mesons," *AIP Conf. Proc.* **1257** no. 1, (8, 2010) 116–120.

[127] **GlueX** Collaboration, M. Shepherd, "GlueX at Jefferson Lab: a search for exotic states ofmatter in photon-proton collisions," *PoS* **212** (10, 2014) 12. 52nd International Winter Meeting on Nuclear Physics.

[128] **PANDA** Collaboration, M. F. M. Lutz *et al.*, "Physics Performance Report for PANDA: Strong Interaction Studies with Antiprotons." 3, 2009.

[129] **NA61/SHINE** Collaboration, H. Adhikary *et al.*, "Evidence of isospin-symmetry violation in high-energy collisions of atomic nuclei," *Nature Commun.* **16** no. 1, (2025) 2849, `arXiv:2312.06572 [nucl-ex]`.

[130] W. Brylinski, M. Gazdzicki, F. Giacosa, M. Gorenstein, R. Poberezhnyuk, and S. Samanta, "Evidence of isospin-symmetry violation in high-energy collisions of atomic nuclei – Supplementary Information," `arXiv:2312.07176 [nucl-th]`.

[131] G. 't Hooft, "A planar diagram theory for strong interactions," *Nucl. Phys. B* **72** no. 3, (4, 1974) 461–473.

[132] E. Witten, "Baryons in the $1/N$ expansion," *Nucl. Phys. B* **160** no. 1, (11, 1979) 57–115.

[133] F. Giacosa, "Introductory Visual Lecture on QCD at Large N_c: Bound States, Chiral Models, and Phase Diagram," *Acta Phys. Polon. B* **55** no. 4, (2024) 4–A1, `arXiv:2402.14097 [hep-ph]`.

[134] L. Kopke and N. Wermes, "J/psi Decays," *Phys. Rept.* **174** (1989) 67.

[135] H. B. O'Connell, B. C. Pearce, A. W. Thomas, and A. G. Williams, "$\rho - \omega$ mixing, vector meson dominance and the pion form-factor," *Prog. Part. Nucl. Phys.* **39** (1997) 201–252, `arXiv:hep-ph/9501251`.

[136] F. Giacosa, A. Okopińska, and V. Shastry, "A simple alternative to the relativistic Breit–Wigner distribution," *Eur. Phys. J. A* **57** no. 12, (2021) 336, `arXiv:2106.03749 [hep-ph]`.

[137] **JPAC** Collaboration, V. Mathieu, A. Pilloni, M. Albaladejo, L. Bibrzycki, A. Celentano, C. Fernández-Ramírez, and A. P. Szczepaniak, "Exclusive tensor meson photoproduction," *Phys. Rev. D* **102** no. 1, (2020) 014003, `arXiv:2005.01617 [hep-ph]`.

[138] **JPAC** Collaboration, J. Nys, A. N. Hiller Blin, V. Mathieu, C. Fernández-Ramírez, A. Jackura, A. Pilloni, J. Ryckebusch, A. P. Szczepaniak, and G. Fox, "Global analysis of charge exchange meson production at high energies," *Phys. Rev. D* **98** no. 3, (2018) 034020, `arXiv:1806.01891 [hep-ph]`.

[139] L. Bibrzycki and R. Kaminski, "Tensor meson photoproduction as a final state interaction effect," *Phys. Rev. D* **87** no. 11, (2013) 114010, `arXiv:1306.4882 [hep-ph]`.

[140] F. Gross *et al.*, "50 Years of Quantum Chromodynamics," (12, 2022) , `arXiv:2212.11107 [hep-ph]`.

[141] V. Mathieu, N. Kochelev, and V. Vento, "The physics of glueballs," *Int. J. Mod. Phys. E* **18** no. 1, (1, 2009) 1–49, `arXiv:0810.4453 [hep-ph]`.

[142] V. Crede and C. A. Meyer, "The experimental status of glueballs," *Prog. Part. Nucl. Phys.* **63** no. 1, (7, 2009) 74–116, `arXiv:0812.0600 [hep-ex]`.

[143] H.-X. Chen, W. Chen, X. Liu, Y.-R. Liu, and S.-L. Zhu, "An updated review of the new hadron states," (4, 2022) , `arXiv:2204.02649 [hep-ph]`.

[144] H. B. Meyer, "Glueball Regge trajectories," phd thesis, University of Oxford, 2004.

[145] K. Sakai and S. Sasaki, "Glueball spectroscopy in lattice QCD using gradient flow," *Phys. Rev. D* **107** no. 3, (2023) 034510, `arXiv:2211.15176 [hep-lat]`.

[146] F. Chen, X. Jiang, Y. Chen, K.-F. Liu, W. Sun, and Y.-B. Yang, "Glueballs at Physical Pion Mass," (11, 2021) , `arXiv:2111.11929 [hep-lat]`.

[147] C. Bonanno, M. D'Elia, B. Lucini, and D. Vadacchino, "Towards glueball masses of large-N SU(N) pure-gauge theories without topological freezing," *Phys. Lett. B* **833** (2022) 137281, `arXiv:2205.06190 [hep-lat]`.

[148] E. B. Gregory, A. C. Irving, B. Lucini, C. C. McNeile, A. Rago, C. Richards, and E. Rinaldi, "Towards the glueball spectrum from unquenched lattice QCD," *JHEP* **10** (10, 2012) 170, `arXiv:1208.1858 [hep-lat]`.

[149] E. Trotti, S. Jafarzade, and F. Giacosa, "Thermodynamics of the glueball resonance gas," *Eur. Phys. J. C* **83** no. 5, (2023) 390, `arXiv:2212.03272 [hep-ph]`.

[150] J. M. Pawlowski, C. S. Schneider, J. Turnwald, J. M. Urban, and N. Wink, "Yang-Mills glueball masses from spectral reconstruction," (12, 2022) , `arXiv:2212.01113 [hep-ph]`.

[151] M. Q. Huber, C. S. Fischer, and H. Sanchis-Alepuz, "Apparent convergence in functional glueball calculations," *Eur. Phys. J. C* **85** no. 8, (2025) 859, `arXiv:2503.03821 [hep-ph]`.

[152] E. Bennett, J. Holligan, D. K. Hong, J.-W. Lee, C. J. D. Lin, B. Lucini, M. Piai, and D. Vadacchino, "Color dependence of tensor and scalar glueball masses in Yang-Mills theories," *Phys. Rev. D* **102** no. 1, (2020) 011501, `arXiv:2004.11063 [hep-lat]`.

[153] J. Turnau, "IS THERE A 2++ GLUEBALL AT 1410-MeV?," *Z. Phys. C* **25** (1984) 299–302.

[154] E. Klempt, "Meson spectroscopy: Glueballs, hybrids and Q anti-Q mesons," in *Zuoz Summer School on Phenomenology of Gauge Interactions*, pp. 61–126. 8, 2000. `arXiv:hep-ex/0101031`.

[155] V. V. Anisovich and A. V. Sarantsev, "Observation of tensor glueball in the reactions p anti-p —> pi pi, eta eta, eta eta-prime," *JETP Lett.* **81** (2005) 417–423, `arXiv:hep-ph/0504106`.

[156] V. V. Anisovich, "Systematization of tensor mesons and the determination of the 2++ glueball," *JETP Lett.* **80** (2004) 715–720, `arXiv:hep-ph/0412093`.

[157] S. Narison, "QCD spectral sum rules 2022," in *12th High-Energy International Conference in Madagascar*. 11, 2022. `arXiv:2211.14536 [hep-ph]`.

[158] Y. Chen, D. Li, and M. Huang, "The dynamical holographic QCD method for hadron physics and QCD matter," *Commun. Theor. Phys.* **74** no. 9, (2022) 097201, `arXiv:2206.00917 [hep-ph]`.

[159] F. Hechenberger, J. Leutgeb, and A. Rebhan, "Radiative Meson and Glueball Decays in the Witten-Sakai-Sugimoto Model," (2, 2023) , `arXiv:2302.13379 [hep-ph]`.

[160] R. C. Brower, S. D. Mathur, and C.-I. Tan, "Glueball spectrum for QCD from AdS supergravity duality," *Nucl. Phys. B* **587** (2000) 249–276, `arXiv:hep-th/0003115`.

[161] Y. Chen and M. Huang, "Two-gluon and trigluon glueballs from dynamical holography QCD," *Chin. Phys. C* **40** no. 12, (2016) 123101, `arXiv:1511.07018 [hep-ph]`.

[162] M. Rinaldi and V. Vento, "Glueballs at high temperature within the hard-wall holographic model," *Eur. Phys. J. C* **82** no. 2, (2022) 140, arXiv:2112.11307 [hep-ph].

[163] M. Rinaldi, "Meson and glueball spectroscopy within the graviton soft-wall model," *Rev. Mex. Fis. Suppl.* **3** no. 3, (2022) 0308019, arXiv:2204.05187 [hep-ph].

[164] D. Elander, M. Piai, and J. Roughley, "Holographic glueballs from the circle reduction of Romans supergravity," *JHEP* **02** (2019) 101, arXiv:1811.01010 [hep-th].

[165] B. A. Li, "2^{++} Glueball," *Phys. Rev. D* **86** (2012) 017501, arXiv:1109.0938 [hep-ph].

[166] R. S. Longacre and S. J. Lindenbaum, "Evidence for a 4th state related to the three J**(PC) = 2++, pi- p —> phi phi n states explainable by 2++ glueball production," *Phys. Rev. D* **70** (2004) 094041, arXiv:hep-ex/0407054.

[167] A. V. Sarantsev and E. Klempt, "Scalar and tensor mesons in $d\bar{d}$, $s\bar{s}$ and $gg \to f_0, f_2$," (11, 2022) , arXiv:2211.08791 [hep-ph].

[168] E. Klempt, "Glueballs, a fulfilled promise of QCD?," (11, 2022) , arXiv:2211.12901 [hep-ph].

[169] N. Kivel and M. Vanderhaeghen, "Production of a tensor glueball in the reaction $\gamma\gamma \to G_2\pi^0$ at large momentum transfer," *Phys. Lett. B* **781** (2018) 169–173, arXiv:1712.04285 [hep-ph].

[170] W. Kou and X. Chen, "Production of Tensor Glueball in Ultraperipheral pp, $AuAu$ and $PbPb$ Collisions," (8, 2022) , arXiv:2208.14222 [hep-ph].

[171] S. Janowski, D. Parganlija, F. Giacosa, and D. H. Rischke, "The Glueball in a Chiral Linear Sigma Model with Vector Mesons," *Phys. Rev. D* **84** (2011) 054007, arXiv:1103.3238 [hep-ph].

[172] W. I. Eshraim, S. Janowski, F. Giacosa, and D. H. Rischke, "Decay of the pseudoscalar glueball into scalar and pseudoscalar mesons," *Phys. Rev. D* **87** no. 5, (3, 2013) 054036, arXiv:1208.6474 [hep-ph].

[173] W. I. Eshraim, "Decay of the pseudoscalar glueball into vector, axial-vector, scalar and pseudoscalar mesons," *Eur. Phys. J. C* **83** no. 3, (2023) 262, arXiv:2005.11321 [hep-ph].

[174] Z.-G. Wang and Z.-Y. Di, "Masses and decay constants of the heavy tensor mesons with QCD sum rules," *Eur. Phys. J. A* **50** (2014) 143, arXiv:1405.5092 [hep-ph].

[175] B. G. Yu, T. K. Choi, and W. Kim, "Regge phenomenology of pion photoproduction off the nucleon at forward angles," *Phys. Rev. C* **83** (2011) 025208, arXiv:1103.1203 [nucl-th].

[176] F. Giacosa and G. Pagliara, "Spectral function of a scalar boson coupled to fermions," *Phys. Rev. D* **88** no. 2, (2013) 025010, arXiv:1210.4192 [hep-ph].

[177] **Crystal Barrel** Collaboration, M. Albrecht *et al.*, "Coupled channel analysis of $\bar{p}p \to \pi^0\pi^0\eta$, $\pi^0\eta\eta$ and $K^+K^-\pi^0$ at 900 MeV/c and of $\pi\pi$-scattering data," *Eur. Phys. J. C* **80** no. 5, (2020) 453, arXiv:1909.07091 [hep-ex].

[178] **Particle Data Group** Collaboration, R. L. Workman and Others, "Review of Particle Physics," *PTEP* **2022** (2022 and 2023 update) 083C01.

[179] S. Okubo, "Phi meson and unitary symmetry model," *Physics Letters* **5** no. 2, (1963) 165–168. https://www.sciencedirect.com/science/article/pii/S0375960163925489.

[180] G. Zweig, *An SU(3) model for strong interaction symmetry and its breaking. Version 2*, pp. 22–101. 2, 1964.

[181] J. Iizuka, K. Okada, and O. Shito, "Systematics and phenomenology of boson mass levels. 3.," *Prog. Theor. Phys.* **35** (1966) 1061–1073.

[182] W. Toki, "Search for Glueballs," in *24th Annual SLAC Summer Institute on Particle Physics: The Strong Interaction, From Hadrons to Protons*, pp. 141–169. 1996.

[183] F. Giacosa, "Heavy Glueballs: Status and Large-N_c Widths Estimate," *Acta Phys. Polon. Supp.* **10** (2017) 1021–1027, arXiv:1708.03755 [hep-ph].

[184] Z.-C. Ye, X. Wang, X. Liu, and Q. Zhao, "The mass spectrum and strong decays of isoscalar tensor mesons," *Phys. Rev. D* **86** (2012) 054025, arXiv:1206.0097 [hep-ph].

[185] X. Jiang, W. Sun, F. Chen, Y. Chen, M. Gong, Z. Liu, and R. Zhang, "η-glueball mixing from $N_f = 2$ lattice QCD," (5, 2022) , arXiv:2205.12541 [hep-lat].

[186] T. Appelquist and H. D. Politzer, "Orthocharmonium and e+ e- Annihilation," *Phys. Rev. Lett.* **34** (1975) 43.

[187] T. Appelquist and H. D. Politzer, "Heavy Quarks and Longlived Hadrons," *Phys. Rev. D* **12** (1975) 1404.

[188] M. E. B. Franklin *et al.*, "Measurement of $\psi(3097)$ and ψ' (3686) Decays Into Selected Hadronic Modes," *Phys. Rev. Lett.* **51** (1983) 963–966.

[189] **CLEO** Collaboration, N. E. Adam *et al.*, "Observation of 1-0- final states from psi(2S) decays and e+ e- annihilation," *Phys. Rev. Lett.* **94** (2005) 012005, arXiv:hep-ex/0407028.

[190] **BES** Collaboration, M. Ablikim *et al.*, "Observation of psi prime decays to rho(770) pi and rho(2150) pi," arXiv:hep-ex/0408047.

[191] S. J. Brodsky and G. P. Lepage, "Helicity Selection Rules and Tests of Gluon Spin in Exclusive QCD Processes," *Phys. Rev. D* **24** (1981) 2848.

[192] **Quarkonium Working Group** Collaboration, N. Brambilla *et al.*, "Heavy quarkonium physics," arXiv:hep-ph/0412158.

[193] X.-H. Mo, C.-Z. Yuan, and P. Wang, "Study of the Rho-pi Puzzle in Charmonium Decays," *HEPNP* **31** (2007) 686–701, arXiv:hep-ph/0611214.

[194] S. J. Brodsky and M. Karliner, "Intrinsic charm of vector mesons: A Possible solution of the 'rho pi puzzle'," *Phys. Rev. Lett.* **78** (1997) 4682–4685, arXiv:hep-ph/9704379.

[195] Y.-Q. Chen and E. Braaten, "An Explanation for the rho pi puzzle of J / psi and psi-prime decays," *Phys. Rev. Lett.* **80** (1998) 5060–5063, arXiv:hep-ph/9801226.

[196] J. M. Gerard and J. Weyers, "Phases and amplitudes in inclusive psi and psi-prime decays," *Phys. Lett. B* **462** (1999) 324–328, arXiv:hep-ph/9906357.

[197] V. L. Chernyak and A. R. Zhitnitsky, "Asymptotic Behavior of Exclusive Processes in QCD," *Phys. Rept.* **112** (1984) 173.

[198] J. L. Rosner, "Charmless final states and S D wave mixing in the psi-prime- prime," *Phys. Rev. D* **64** (2001) 094002, arXiv:hep-ph/0105327.

[199] X.-Q. Li, D. V. Bugg, and B.-S. Zou, "A Possible explanation of the 'rho pi puzzle' in J / psi, psi-prime decays," *Phys. Rev. D* **55** (1997) 1421–1424.

[200] S. J. Brodsky, G. P. Lepage, and S. F. Tuan, "Exclusive Charmonium Decays: The $J/\psi(\psi') \to \rho\pi$, $K^*\bar{K}$ Puzzle," *Phys. Rev. Lett.* **59** (1987) 621.

[201] W.-S. Hou and A. Soni, "Vector Gluonium as a Possible Explanation for Anomalous psi Decays," *Phys. Rev. Lett.* **50** (1983) 569.

[202] M. Suzuki, "Elusive vector glueball," *Phys. Rev. D* **65** (2002) 097507, arXiv:hep-ph/0203012.

[203] Q. Zhao, G. Li, and C.-H. Chang, "Study of electromagnetic decay of J / psi and psi-prime to vector and pseudoscalar," *Phys. Lett. B* **645** (2007) 173–179, arXiv:hep-ph/0610223.

[204] S. Weinberg, *The quantum theory of fields: Modern applications*, vol. 2. Cambridge University Press, 1996.

[205] R. Escribano, "J/psi —> VP decays and the quark and gluon content of the eta and eta-prime," *Eur. Phys. J. C* **65** (2010) 467–473, arXiv:0807.4201 [hep-ph].

[206] J. G. Messchendorp *et al.*, "Hadron Physics Opportunities at FAIR," arXiv:2512.15986 [hep-ex].

Acknowledgement

This final page is dedicated to thanking all the people who have either helped bring forth this thesis, supported me, or have just made things more pleasant in the years working on this thesis.

First of all I want to thank my supervisors Francesco Giacosa and Leonardo Tinti, for guiding and supporting me through this process. For sharing their knowledge in many discussions, from physics, mathematics and academia, to the obscure knowledge Leonardo had on any topic the conservation turned to.

I also want to thank the professors from the university, for their teaching, support and discussions. Thank you Stanislaw Mrówczyski, Wojciech Broniowski, Maciej Rybczyński and all the others.

Thank you Shahriyar Jafarzade and Enrico Trotti, Shahriyar being my most frequent collaborator and Enrico my office mate, and both my travel buddies. It was a pleasure discussing and working on physics with you two, or talking about whatever else. We have made some wonderful memories in conferences and PhD schools together.

A thank you to the rest of the physics institute, students or otherwise, for making this a pleasant time along with nice discussions and collaborations. Thank you Krzysztof Kyziol, Milena Piotrowska, Anna Kolbus, Magdalena Plodowska, Karol Szary, Sylwia Bazak, Vanamali Shastry, Haradhan Adhikary, Ali Bazgir, Uzair Shah, Regina Stachura and all the others.

I also want to thank Adrian Königstein and Dirk Rischke for the opportunity to visit Frankfurt and Jena and their hospitality. Thank you to Keiwan Jamaly, Marc Winstel everyone else who warmly welcomed me in Frankfurt and allowed me to visit their meetings.

I am grateful to Anton Rebhan and Jonas Mager for allowing me to visit them in Vienna and discuss glueballs. These were some wonderful weeks and you were very welcoming to me.

I want to thank all my friends and family, for making these times more pleasant and taking my mind off of physics when it needed to.

The very last thank you is dedicated to my parents. Margot and Johan, even through a string of difficult times, you always gave me your unwavering support and understanding. Thank you.